An investigation of the role of mitochondrial STAT3 and modulation of Reactive Oxygen Species in adipocyte differentiation

A dissertation submitted in fulfilment of the requirement for the degree

of

MASTER OF SCIENCE

in Biotechnology

of

RHODES UNIVERSITY

by

ADAM HILDYARD KRAMER

January 2014

Declaration

I declare that this thesis is my own, unaided work. It is being submitted for the degree of Master of Science of Rhodes University. It has not been submitted before for any degree or examination at any other university.

……

Mr Adam Kramer

Abstract

Stem cells have the ability to differentiate into a myriad of different cell types. The understanding of the differentiation process is of paramount importance if we are to use these cells in the lab as well as in therapeutics. Here, the levels and localization of the signal transducer and activator of transcription 3 (STAT3), with particular attention focused on the mitochondrial serine 727 phosphorylated form of STAT3 (pSTAT3S727) during differentiation, was investigated. Using the murine preadipocyte progenitor cell line 3T3-L1, as well as adipose derived human mesenchymal stem cells (HMSC-ad) as differentiation models, the relative levels of Reactive Oxygen Species (ROS) and the levels and localization of STAT3 were investigated during the differentiation process. ROS is known to play an important signalling role during differentiation and is well reported during the events of adipogenesis. ROS are generated as a by-product in the Electron Transport Chain (ETC), and it has recently been reported that pSTAT3S727 plays an important role at complex I of the ETC. Various techniques including fluorescence confocal microscopy, flow cytometry and Western blots were utilized to investigate the non-canonical role STAT3 plays during adipogenesis. Mitochondrial isolations were performed to investigate the levels of STAT3 in the mitochondria during differentiation. Further to this, an impedance based real time differentiation assay was developed using the xCELLigence Real Time Cell Analyser to monitor differentiation and the affects various compounds, including a STAT3 inhibitor, have on differentiation. Results indicate that upon induction of differentiation, levels of mitochondrial pSTAT3S727 dramatically decrease and leave the mitochondria. This corresponds to increasing levels of ROS. The canonical active form of STAT3 following phosphorylation on tyrosine 705 (pSTAT3Y705) was found to decrease and lose its nuclear localization. These initial results indicate that STAT3 plays an important non-canonical role in the mitochondria during differentiation.

Acknowledgements

I wish to thank firstly my parents, Debby and David, for both their emotional and financial support, without whom I would not have been able to complete this work. I could not ask for better, more supportive parents. I also wish to thank my amazing supervisor, Dr Earl Prinsloo, for all his hard work, expertise and friendship over the last few years; Dr Adrienne Edkins for always being eager to help; my sister Rachel for always being there for me; my lab mates and great friends, Morgan, Lara, Claire, Dustin, Lance, Jason, Karim, Cindy, Lorraine, Stefan, Julia, Rose and my #sciencebuddy Nina; everyone in BioBRU and the Department of Biochemistry, Microbiology and Biotechnology for such a great work environment; my digsmates, past and present. Finally I would like to thank the National Research Foundation for financial support.

Outputs

Kramer, A. H., Joos-Vandewalle, J., Edkins, A. L., Frost, C. L., & Prinsloo, E. (2014). Real-time monitoring of 3T3-L1 preadipocyte differentiation using a commercially available electric cell-substrate impedance sensor system. *Biochemical and biophysical research* communications, 1–6. doi:10.1016/j.bbrc.2013.12.123

Kadye, R., Kramer, A. H., Joos-Vandewalle, J., Parsons, M., Njengele, Z., Hoppe, H., & Prinsloo, E. (2013). Guardian of the Furnace: Mitochondria, TRAP1, ROS and stem cell maintenance. *IUBMB life*, (21), 1–4. doi:10.1002/iub.1234

Table of Contents

List of Figures

List of Tables

List of Abbreviations

AFM	Atomic Force Microscopy
ATP	Adenosine 5´-triphosphate
ATP	Adenosine Triphosphate
BMP	Bone Morphogenetic Proteins
BSA	Bovine Serum Albumin
C/EBP	CCAAT/enhancer binding proteins
cAMP	cyclic Adenosine Monophosphate
cdks	cyclin dependant kinases
CI	Cell Index
COX (I-IV)	Complex (I-IV)
DCF-DA	Dichloro-dihydro-Fluorescein Diacetate
DEX	Dexamethasone
DMEM	Dulbecco's modified Eagle's medium
DMSO	Dimethyl Sulfoxide
DNA	Deoxyribose Nucleic Acid
Dvl	Dishevelled
ECIS	Electric Cell-Substrate Impedance Sensor
ECM	Extracellular Matrix
ERK	Extracellular signal regulated kinase
ES	Embryonic stem (cell)
ETC	Electron Transport Chain (ETC)
EtOH	Ethanol
FCS	Foetal calf serum
Fz	Frizzled
gp130	Glycoprotein 130
GRIM-19	Genes associated with Retinoid-IFN-induced Mortality-19
GSK-3β	Glycogen Synthase Kinase 3β
HBMSCs	Bone Marrow Derived Human Mesenchymal Stem Cells
HMSC-ad	Human adipose Derived Mesenchymal Stem Cells
Hsp	Heat shock protein
IBMX	3-isobutyl-1-methylxanthine
ICA	Intensity Correlation Analysis
ICQ	Intensity Correlation Quotient
IGF-1	Insulin-like Growth Factor receptor 1
IL-6	Interleukin 6
INS	Insulin
iPCS	Induced Pluripotent Stem Cells
JAK	Janus Kinase
LAMP1	Lysosomal-associated membrane protein 1
LIF	Leukaemia Inhibitory Factor

MAPK/MEK	Mitogen Activated protein kinase kinase
MCE	Mitotic Clonal Expansion
NADH	Nicotinamide Adenine Dinucleotide
PBS	Phosphate Buffered Saline
PDM	Product of the Differences from the Mean
PHB	Prohibitin
PPAR	Peroxisome Proliferator-Activated Receptor
ROS	Reactive Oxygen Species
ROSI	Rosiglitazone
RTCA	Real Time Cell Analysis
SCNT	Somatic Cell Nuclear Transfer
SP	Single Plate
STAT3	Signal Transducers and Activators of Transcription factor 3
TGF-β2	Transforming Growth Factor
TRAP1	Tumor Necrosis Factor Receptor Associated Protein 1
VDAC	Voltage Dependant Anion Channels
WAT	White Adipose Tissue

List of symbols

%	percent or g/100 ml
°C	degree Celsius
g	grams
g	centrifugal force of gravity
kDa	kilo Daltons
L	litres
M	Molar
mg	milligrams
min	minutes
ml	millilitre
mM	millimolar
mol	mole
nM	nanomolar
rpm	revolutions per minute
U	units
V	volts
α	Alpha
β	Beta
γ	Gamma
δ	Delta
µg	micrograms
µl	microlitres

Chapter 1

An investigation on the role of mitochondrial STAT3 and modulation of reactive oxygen species in 3T3-L1 adipocyte differentiation

1: Introduction

1.1 Stem cells

The properties of stem cells which separate them from normal cells include characteristics such as an indefinite capacity to self-renew as well as the ability to become cells of different lineages (Liras, 2010). The ability of pluripotent stem cells to differentiate into any cell type means that, in the future, they will become extremely important tools in both medicine and research, and, for this reason, the understanding of these cells is of utmost importance (Thiede, 2009). Stem cells have possible applications not only in the lab as a potentially unlimited source of model cells, but in regenerative medicine where cell treatments may be used in therapy for multiple human diseases (Sullivan *et al.,* 2010).

Stem cell based treatments for Amyotrophic Lateral Sclerosis, a neurological disease, entered a phase one trial after successful human trials utilizing mesenchymal stem cells were performed (Mazzini *et al.,* 2008) and it has been reported that all participants have coped well (Mazzini *et al.,* 2012), while treatments for macular degeneration using human embryonic stem cells, the first of its kind, was given the go ahead after a successful long term safety study *(*Lu *et al.,* 2009). Preliminary findings of this clinical trial have been promising with the eyesight of one patient with dry-age related macular degeneration improving (Schwartz *et al.*, 2012) Other conditions which could potentially be treated using stem cells are illustrated in Figure 1.1.

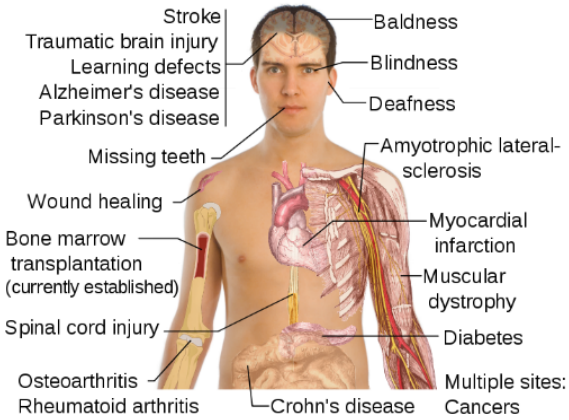

Figure 1.1. The potential therapeutic uses of stem cells (Haggstrom, 2011). Image is in the public domain.

1.1.1 Asymmetric and symmetric stem cell division

Stem cells undergo either asymmetric or symmetric cell division. Symmetric division results in two daughter stem cells displaying identical properties of the parent stem cell, while asymmetric division results in the formation of a single daughter stem cell and a daughter cell that undergoes differentiation (a progenitor cell), resulting in the loss of stem cell pluripotency, with the potential to generate numerous mature cells as illustrated in Figure 1. 2 (Reya & Clevers, 2005).

1.1.2 Cell potency

Stem cells are able to self-renew (the ability to produce identical stem cells) and produce differentiated, mature cells which have specific characteristics and functions as illustrated in Figure 1.2. These specialized cells differentiate in response to certain physiological stimuli. There are different types of stem cells and are distinguished based on differentiation potential and source (Aflatoonian & Moore, 2005). Examples of specific types of stem cells include *pluripotent* (able to turn into any cell of the three germ layers) embryonic stem cells which are able to differentiate into any cell type, with the exception of embryonic structures such as the placenta and umbilical cord. These cells however, are unable to form a complete organism. Only the fertilized oocyte and the descendants of the first two cell divisions are termed *totipotent* (able to turn into any differentiated cell type in the organism) and are able to form the embryo and the trophoblasts of the placenta (Alison & Islam, 2009). *Multipotent* adult stem cells (such as hematopoietic cells) are specialized cells able to differentiate into multiple, but limited number of cell types. *Unipotent* cells are only able to differentiate into a

single cell type and are found within different body tissues. Both multipotent and unipotent cells act as cell reservoirs in the different tissues (reviewed in Liras, 2010).

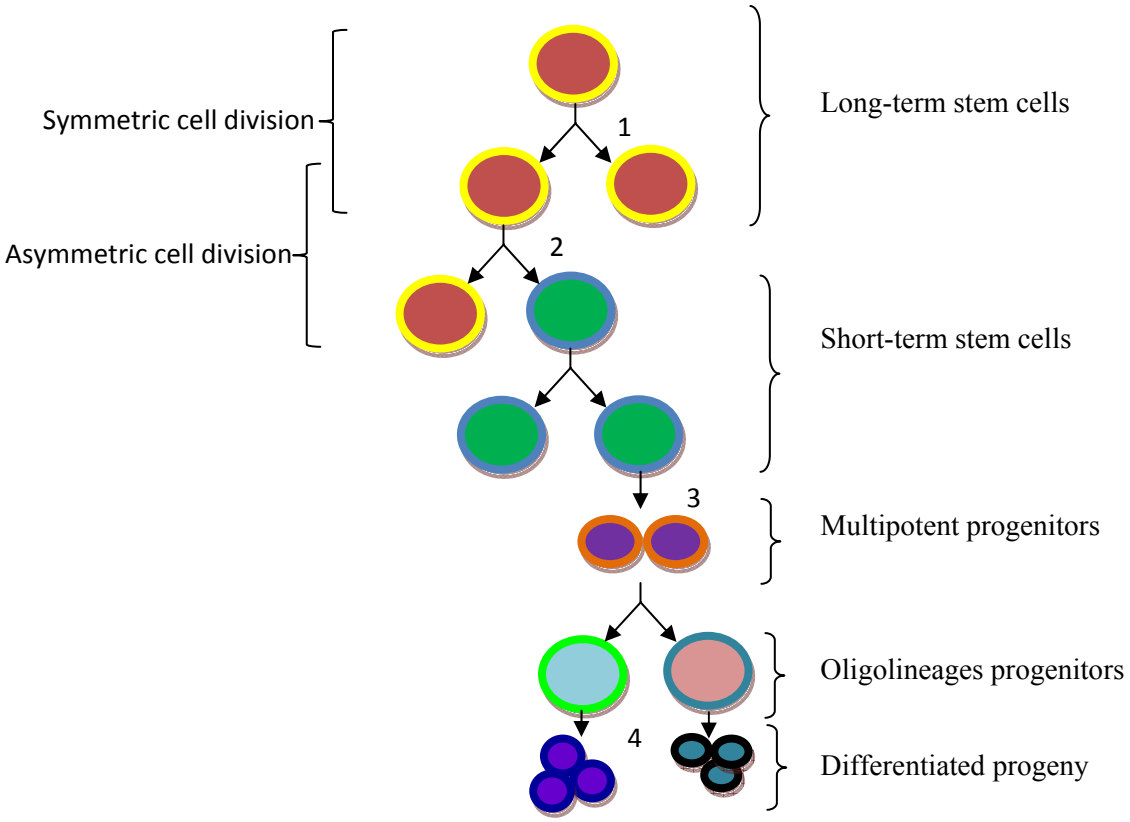

Figure 1.2. Stem cell division and differentiation. 1: Symmetric stem cell division; 2: Asymmetric stem cell division; 3: Progenitor division; 4: Terminal differentiation (Modified from Weissman, 2000)

Embryonic stem cells

Embryonic stem cell lines are undifferentiated pluripotent cells derived from early embryos. These cells are harvested from the inner cell mass of pre-implantation blastocysts. Embryonic stem cell lines have been established from rodents (Martin, 1981), primates (Thomson *et al.,* 1995) and humans (Thomson *et al.,* 1998). These cells are able to self-renew indefinitely and have the potential to differentiate into specialized cells.

The first embryonic stem cell line was derived from blastocysts of mice at day 3.5 of mouse development (Martin, 1981). Mouse ES cells remain undifferentiated in the presence of myeloid leukaemia inhibitory factor (LIF); however, this is not the case for human ES cells

which require alternative culturing methods to remain undifferentiated *in vitro,* such as conditioned media or the presence of feeder cells such as mouse fibroblasts. The feeder cells provide a variety of growth factors (Thomson *et al.,* 1998) such as transforming growth factor β2 (TGF-β2) (Che *et al.,* 2006) extracellular matrix (ECM) proteins (Alitalo *et al*., 1982) activin, Wnts, and antagonists of bone morphogenetic proteins (BMPs) (Prowse *et al.*, 2007). These factors activate or inhibit specific pathways which results in the maintenance of pluripotency.

One of the most important pathways involved in maintaining pluripotency in mouse embryonic stem cells is the Janus Kinase-Signal Transducers and Activators of Transcription factor 3 (JAK-STAT3) signalling pathway (Takeda *et al.,* 1997; Matsuda *et al.*, 1999; Raz *et al.,*1999). The JAK-STAT3 pathway transmits information from extracellular polypeptide signals through trans-membrane receptors (Zhong *et al.*, 1994). This pathway is activated in the culture of mouse embryonic stem cells by the addition of interleukin 6 type cytokines such as Leukaemia Inhibitory Factor (LIF), for example (Raz *et al.*, 1999). Other signalling pathways that are fundamental to self-renewal in mouse and human cells include the Wnt/β-catenin pathway (Kléber & Sommer, 2004). This complex pathway involves 19 highly conserved Wnt glycoproteins. The pathway is activated when Wnt ligands bind to receptors belonging to the Frizzeled family of surface receptors (Komiya & Habas, 2008). Downstream signalling of this receptor results in the inactivation of glycogen synthase kinase 3 (GSK-3β). Inhibition of GSK-3β via a GSK-3β specific inhibitor was shown to maintain the undifferentiated phenotype of both mouse and human embryonic stem cells and sustain levels of pluripotent state-specific factors such as Oct-3/4, Rex-1 and Nanog (Sato *et al.*, 2004). In the absence of specific self-renewal signals, pluripotent stem cells differentiate uncontrollably into cells which make up the three germ layers, namely the endo-, ecto-, and mesoderm (Mitalipov & Wolf, 2008).

Induced Pluripotent Stem (iPS) cells

Recently protocols have been developed to induce pluripotency in adult somatic cells. These induced pluripotent stem cells (iPSC) are adult somatic cells which have been reprogrammed to a pluripotent state (Takahashi & Yamanaka, 2006; Takahashi *et al.,* 2007; Yu *et al.,* 2007). This can be done through a number of methods including the introduction of certain transcription factors, somatic cell nuclear transfer (SCNT) and cell fusion (Kléber &

Sommer, 2004; Sullivan *et al.,* 2010). Induced PSCs have a huge potential as experimental, diagnostic and therapeutic tools, but still require extensive research before their potential can be realized (reviewed in Sullivan *et al.* 2010). Recently the world's first clinical study investigating the use of iPS cells to treat eye disorders started in Japan after a study showed that the cells elicited no immune response (Araki *et al*., 2013)

Adult stem cells

Adult stem cells are reservoir stem cells which are involved in the continuous maintenance and repair of tissues and organs throughout the life span on an organism (Young & Black, 2004). These undifferentiated somatic cells are slow cycling and divide much less frequently than normal cells (Young & Black, 2004). For this reason, somatic stem cells are incredibly rare. In the small intestine there are about 10 stem cells for every 300 + cells while in the bone marrow, multipotent haematopoietic stem cells occur with a frequency of about 1 in every 10 000 (Alison & Islam, 2009) The use of adult stem cells in transplants hold much promise, and, adult hematopoietic stem cells from bone marrow, and more recently, from blood, have been used in transplants for more than 40 years (Körbling & Freireich, 2011).

Mesenchymal stem cells are a type of adult stem cell which hold much promise in cell treatments as previously mentioned. Mesenchymal stem cells are multipotent adult progenitor cells with the capability of differentiating into a multitude of cell types including adipocytes, osteoblasts and chrondocytes, myotubes, astrocytes, tenocytes, and hematopoietic-supporting stroma (Hass *et al.,* 2011; Tremain *et al.*, 2001) and therefore provide model systems to study cellular differentiation. They are most commonly isolated from bone marrow and adipose tissue, however they are found in nearly all tissues (Hass *et al.,* 2011) and do slightly differ depending on their location and niche environment (Jansen *et al.*, 2010).

Stem cell niches and *in vitro* culture of stem cells

Stem cell niches are defined as specific anatomic locations where stem cells reside. These niches regulate how the stem cells participate in tissue generation, maintenance and repair. By providing regulatory signals to the stem cell population, the niche environment saves stem cells from deletion and protects the host against excess stem cell proliferation (Scadden, 2006). *In vitro,* it has been attempted to recreate these specialized environments through number of approaches including the use of specialized media, the introduction of specialized growth factors, 3D culturing and the use of specific growth surfaces.

Stem cell maintenance media provides the cells with the nutrients and specific factors required to maintain their pluripotent state. Most stem cell maintenance media still require undefined ingredients. The culturing of embryonic stem cells *in vitro,* for example requires 'conditioned' medium containing a variety of undefined biological substances. Conditioned medium is medium which contains secretions from feeder cells. Alternatively, and most commonly, stem cells are cultured alongside a feeder cell line such as mouse embryonic fibroblasts. Feeder cells are cells (typically mouse embryonic fibroblasts) that have either been irradiated or chemically treated inhibiting the ability of the cells to divide. These cells secrete a complex matrix of proteins which maintain the health of the stem cell population and are directly associated in maintaining the self-renewal ability of stem cells in culture (Villa-Diaz *et al.*, 2009). As mentioned previously, a number of protein mediators and pathways need to either remain active or dormant within the cell and it is these pathways and proteins which can be exploited to maintain pluripotency by induction *in vitro.* Stem cells require a very specific set of conditions to remain in a pluripotent state or differentiate to a specific lineage and the medium they are grown in is but one important factor.

The surfaces which stem cells are grown on are also important as stem cells usually grow best when attached to other cells or to an extracellular matrix. Surfaces can be separated into three main groups: synthetic coatings, synthetic biomolecules and recombinant biomolecules. These coatings are required to allow stem cells to attach to the surface. There is an increasing belief that surfaces can play a major role in directing the differentiation of stem cells *in vitro* as surfaces are easy to control and are able to mimic the microenvironment and niches in which stem cells differentiate (Baker, 2011). Novel culturing techniques such as 3D culturing are becoming increasingly popular. This method makes use of cell scaffolds when growing cells *in vitro* and is a technique required if stem cells are ever to be used to regenerate tissue *in vitro*. Three dimensional matrices have been shown to play a role in directing differentiation in stem cells. Battista *et al.* (2005) investigated the role of material composition and structure in promoting mouse embryonic stem cell growth and differentiation and found that both the composition and strength of the supportive matrix play a critical role in development. The group showed that it is possible to direct differentiation to endothelial cell types by changing the physical and biochemical properties of the scaffold.

1.2 Mitochondria and Reactive Oxygen Species (ROS) production in stem cells

Mitochondria are cytoplasmic organelles found in all eukaryotic cells. These organelles are responsible for converting nutrients into adenosine triphosphate (ATP), the molecule which provides energy for all cellular activities. This process, known as aerobic respiration, is why mitochondria are so important within all eukaryotic cells. This important organelle also plays an essential role in processes such as steroid metabolism, calcium homeostasis, apoptosis and cellular proliferation (McBride *et al.,* 2006; Nesti *et al.,* 2007).

1.2.1 The electron transport chain and Reactive Oxygen Species (ROS) production

Reactive Oxygen Species (ROS) are generated as a by-product in the electron transport chain, located in the membrane of mitochondria, which is essential in energy production. The electron transport chain transfers electron from electron donor such as nicotinamide adenine dinucleotide (NADH) to an accepter to O_2 while transferring H^+ ions across the inner membrane of the mitochondria.

The mitochondrial electron transport chain is made up of a series of electron carriers which are arranged spatially into four complexes, namely complex I, II, III and IV. Through the glycolysis of carbohydrates, acetate in the form of acetyl-CoA is produced from pyruvate (which enters into the mitochondria by means of intermembrane proteins such as Voltage Dependant Anion Channels (VDAC) and Pyruvate carries, reviewed in Schell & Rutter, (2013)); this fuels the Citric acid cycle which produces NADH and $FADH_2$. Electrons derived from the metabolic reduction of these molecules are fed through the electron transport chain and eventually pass to molecular oxygen where water is formed at complex IV. The transfer of electrons releases energy which is used to create a proton gradient. At each complex, using the energy released during the transfer of electrons, protons are pumped from the mitochondrial matrix into the intermembrane space creating an electrochemical proton gradient. This gradient is used to generate ATP by ATP synthase, as illustrated in Figure 1.3.

The NADH dehydrogenase complex, more commonly known as complex I, is the largest complex of the ETC, made up of at least 40 polypeptide chains. Complex I accepts electrons from NADH and passes them through flavin to ubiquinone. Additional electrons are derived from Complex II (succinate dehydrogenase) which delivers electrons originating from the reduction of succinate in the citric acid cycle, to the ubquinone pool. The electrons are then transferred to cytochrome the b-c_1 complex, complex III. From here, electrons are passed to

cytochrome C and finally to cytochrome C oxidase (complex IV) which uses the electrons and hydrogen ions to reduce molecular oxygen to water. As electrons are passed through the chain, energy is released and used to pump protons into the intermembrane space at each complex (Alberts *et al*., 2002).

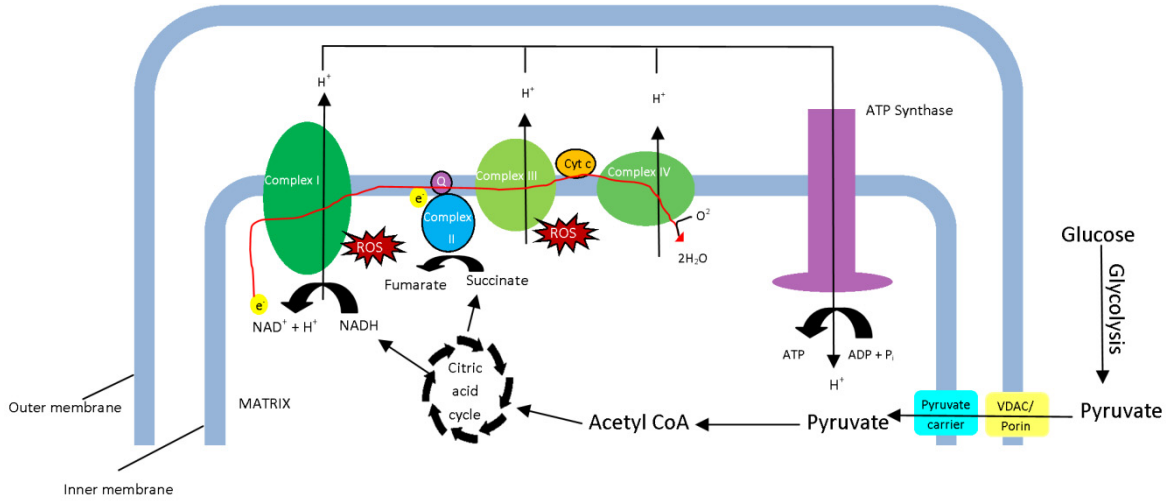

Figure 1.3. The general mechanism of oxidative phosphorylation. As high energy electrons are passed along the electron transport chain, the energy released at each complex is used to create a H^+ gradient which is used to generate ATP by ATP synthase. Leaked electrons result in ROS being produced at two potential sites at complex I and at the ubiquinone site at complex III.

During the transfer of electrons through the ETC, electrons occasionally leak out of the system to molecular oxygen creating superoxide ($O_2^{\cdot -}$). Superoxide (a free radical ROS) is converted to H_2O_2 (a non-radical ROS) by spontaneous dismutation or by superoxide dismutase (SOD). Studies have shown that the main ROS production happens at two main sites in the electron transport chain, namely the ubiqinone site at complex III (Boveris, Cadenas, & Stoppani, 1976) and at two sites in complex I (Hirst *et al.,* 2008). There is growing evidence that the majority of ROS production occurs at complex I of the ETC (McLennan & Esposti, 2000; Liu *et al.*, 2002)

ROS damage the cell and therefore dedicated enzymes (such as superoxide dismutase) exist to protect the cell (Brookes, 2005). Oxidative stress is defined as a disturbance of the equilibrium between free radicals and ROS, and endogenous antioxidant defence mechanisms (Reya *et al.,* 2001). Oxidative stress causes damage to the cell and has a detrimental effect of

the self-renewal ability of stem cells (Vieira *et al.*, 2011; Wang *et al*., 2013). It also causes senescence in normal cells. This may be the reason for the stem cell niche propensity towards hypoxia (Danet *et al.,* 2003) and the Warburg effect in stem cells. The Warburg effect is thought to provide the resources required by the rapidly proliferating cells while protecting mitochondria from ROS-induced membrane damage and apoptosis. This effect has been observed in rapidly proliferating cancer, cancer stem cells and normal stem cells (Ruckenstuhl *et al.*, 2009; Gogvadze, Zhivotovsky, & Orrenius, 2010; Menendez *et al*., 2013; Wang *et al*., 2013).

1.2.2 The Warburg effect

It has been shown that mouse ES cells have a high glycolytic rate and therefore display the Warburg effect (Kondoh *et al.,* 2007). Glycolysis is the anaerobic metabolic pathway which converts glucose into pyruvate. The Warburg effect was described over seven decades ago by Otto Warburg. Warburg noticed that cancer cells maintain high levels of glycolysis under aerobic conditions. This is unusual as glycolysis in normal cells is subdued by the presence of oxygen because of the energy efficiency with which mitochondria convert pyruvate to CO_2 and water. The Warburg effect may be the way in which tumour and ES cells counteract the effects of oxidative stress by reducing the accumulation of ROS. ROS production is an unavoidable consequence of normal cellular metabolism and is the cause of cellular senescence (Kondoh *et al.,* 2005a). Enhanced glycolysis has been shown to protect cells from oxidative stress and, therefore, senescence (Kondoh *et al.,* 2005b). Increased glycolysis could work as, or activate radical scavengers; this could account for the Warburg effect in mouse ES cells as a mechanism to reduce oxidative damage and intrinsic production of ROS, sustaining the immortal phenotype of ES cells. The Warburg effect in ES cells can be reverted, explaining why differentiated cells do not present enhanced glycolysis (Kondoh, 2008).

Interestingly, activated STAT3 has been implicated in cancer by activating the Warburg effect. It has been shown that constitutively activated, tyrosine phosphorylated STAT3 leads to an induction of aerobic glycolysis and decreased mitochondrial respiration (Demaria *et al.*, 2010). Further to this it has recently been hypothesized that a member of the Heat shock protein 90 (Hsp90) family, Tumor Necrosis Factor Receptor Associated Protein 1 (TRAP1) may play a role in the modulation of mitochondrial activity, survival and differentiation of stem cells (Kadye *et al*., 2013). This hypothesis is particularly interesting as Hsp90 has been shown to directly interact with STAT3 (Kramer *et al.*, 2012).

1.2.3 Roles of Reactive Oxygen Species (ROS) in signalling

Stem cells must balance self-renewal, maintenance and differentiation events and it has been shown that bioenergetics plays a crucial role in regulating stem cell fate (Vieira *et al.*, 2011; Wang *et al.*, 2013). Mitochondria have been shown to potentially play important roles in stem cell differentiation and apoptosis (reviewed in Parker *et al.,* 2009). Research has shown that mitochondria play a role in cell differentiation for a number of reasons, one of the most important involving oxidative stress of the cell. The volume and efficacy of mitochondria within cells determine a cells ability to regulate ROS and respond to oxidative stress conditions (Lyu *et al.,* 2008). High ROS levels have been suggested to play a crucial role in cell signalling, proliferation and differentiation (Sauer *et al.,* 2001) indicating that mitochondria potentially play important roles in stem cell self-renewal and differentiation. Studies show that the levels of ROS in stem cells such as Hematopoietic Stem Cells (HSC) are relatively lower than those of their progeny (Lyu *et al.,* 2008), which is interesting to note as HSCs are found to be enriched in regions of bone marrow of a hypoxic environment (Parmar *et al.,* 2007). Embryonic stem cells contain a relatively large number of competent active mitochondria and are able to resist oxidative stress better than differentiated cells (Saretzki *et al.,* 2004). This however requires further investigation.

It has been suggested that stem cell stability and pluripotency can be verified using functional mitochondrial characteristics (Lonergan *et al.* 2006). Mitochondrial properties such as subcellular localization and metabolic activity of stem cells have been shown to change dramatically with increasing passage number in culture and can therefore be used as a marker of the *stemness* of stem cells (Lonergan *et al.* 2006). Differentiated cell types can be characterized by the number of mitochondria they possess and the copies of mitochondrial genome per organelle (St John *et al.,* 2006). The increase in mitochondrial mass in differentiated cells is accompanied by an increased ATP production and therefore higher ROS levels. The role of ROS in the differentiation of stem cells has been shown to play a vital role in both maintaining self-renewal and differentiation (Dayem *et al.,* 2010; Le Belle *et al*., 2011). ROS contributing factors need to be understood in order to elucidate the potential role of mitochondria in stem cell self-renewal and differentiation.

1.3 Adipocyte differentiation

Specialized cells known as adipocytes accumulate triacylglycerols and make up what is known as white adipose tissue (WAT). Adipogenesis occurs in an organism during periods of an excess of energy. This energy is stored in the form of triacylglycerols which are stored

in adipocytes and are available to the organism during times of deprivation (Otto & Lane, 2005). During the process of adipogenesis, fibroblast like unipotent preadipocytes differentiate into mature adipocytes containing large lipid droplets made up of triacylglycerols. This differentiation process is regulated by multiple signalling proteins, including the CCAAT/enhancer binding proteins (C/EPBs), and peroxisome proliferator-activated receptors (PPARs) (Gregoire *et al.,* 1998; Otto & Lane, 2005)

1.3.1 Models of adipogenesis

There are a handful of established cell lines used to study adipogenesis such as the 3T3-L1 and 3T3-F442A murine preadipocyte lines (Green & Kehinde, 1974). The 3T3-L1 preadipocyte line is viewed as the gold standard to monitor unipotent cell differentiation to mature adipocytes. Human mesenchymal stem cells have been used to investigate adipogenesis, however as 3T3-L1 differentiation processes have remained the subject of choice for studying adipogenesis, a summary of what has been discovered thus far with respect to this line will be reviewed in greater detail.

1.3.2 In vitro adipogenesis

In vitro, 3T3-L1 cells are grown to post-confluence prior to inducing differentiation. Confluence induces growth arrest and cell-cell contact induces expression of lipoprotein lipase and type VI collagen genes which are important in accumulation of fatty acids (Cornelius *et al.,* 1988). Growing cells to post confluence causes cells to enter the G_0 phase of the cell cycle, which is required for optimum differentiation, as cells must synchronously re-enter the cell cycle to achieve efficient differentiation.

Once post-confluent, a differentiation cocktail is introduced into the cell culture. This cocktail is made up of insulin (Green & Kehinde, 1975), dexamethasone (Chem *et al.,* 1978) and IBMX (Russell, 1976). This cocktail kick-starts adipogenesis, causing growth-arrested 3T3-L1 preadipocytes synchronously re-enter the cell cycle and undergo what is known as mitotic clonal expansion (MCE), the first major event in adipogenesis. Each component plays a role in activation of the factors that are required for adipogenesis: Insulin acts through the insulin-like growth factor receptor (IGF-1) and IGF can replace insulin. Activation of IGF-1 results in an increase of cyclic adenosine monophosphate (cAMP). Levels of cAMP are further increased through the activation of glucocorticoid pathways by glucocorticoids such as dexamethasone, which also increases levels of intracellular Ca^{+} (MacDougald & Lane, 2003). The cAMP phosphodiesterase inhibitor, 3-isobutyl-1-methylxanthine (IBMX) is used to

further increase levels of cAMP. Both cAMP and IBMX decrease levels of Specificity protein 1 (Sp1), a transcription factor which represses the C/EBPα promoter and delays the DNA binding activity of C/EBPβ and C/EBPδ (Otto & Lane, 2005). The insulin sensitizer and PPARγ agonist rosiglitazone has been included in the cocktail and is reported to increase differentiation efficiency (Zebisch *et al.*, 2012). A summation of the effect of each of these components is illustrated in Figure 1.4.

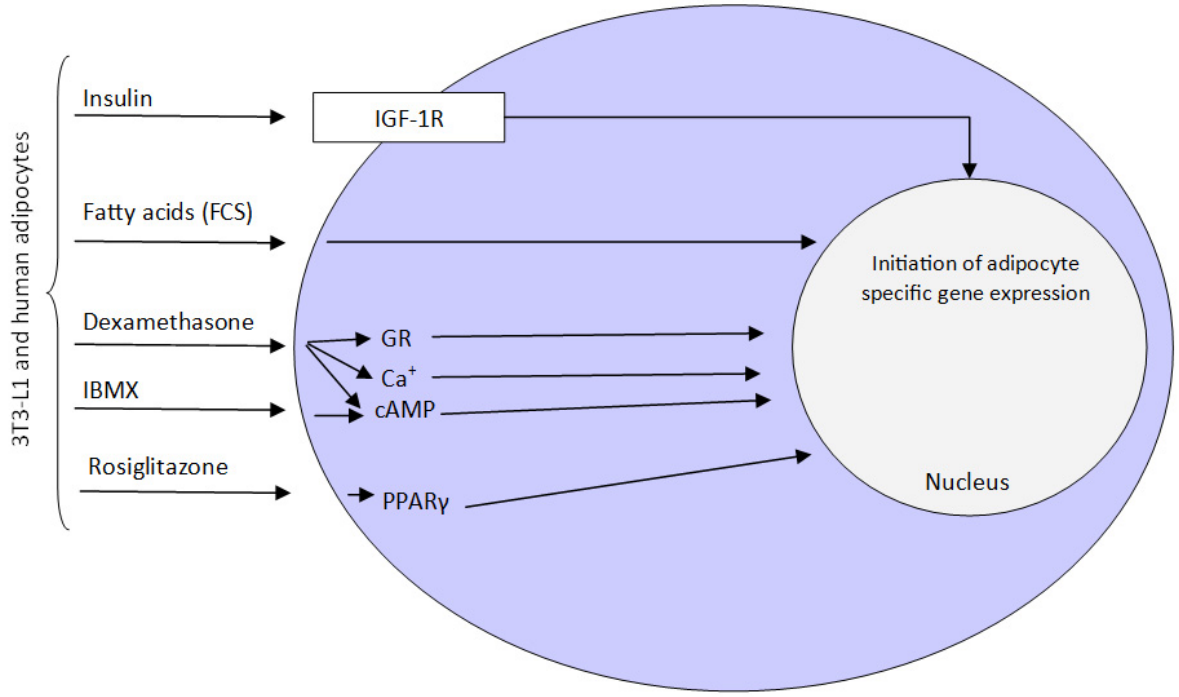

Figure 1.4. Induction of 3T3-L1 preadipocyte differentiation: highlighting the effects of insulin, dexamethasone, IBMX and rosiglitazone have on preadipocytes and how differentiation is induced. (Modified from Stankov *et al.* (2009))

MCE is the process of growth arrested cells re-entering the cell cycle and mitotically dividing twice to four times before the differentiation into adipocytes. The DNA replication process during growth is hypothesized to be required to make the promoter/enhancer elements available for the transcription of genes important for adipocyte differentiation (Cornelius *et al.,* 1994a), and is followed by expression of genes that produce the adipocyte phenotype (Ntambi & Kim, 2000).

MCE is initiated through the expression of genes such as *c-fos, c-jun, c-myc*, C/EBPβ and C/EBPδ (Cornelius *et al*., 1994). The C/EBP family of transcription factors was one of the

first shown to be important in adipocyte differentiation. CCAAT/enhancer binding proteins (C/EBP) have a basic transcriptional activation domain and an adjoining leucine zipper motif allowing for homo- and heterodimerization. Isoforms of C/EBP are found in tissues which metabolize lipid and cholesterol related compounds at high rates (Christy *et al.,* 1989), such as the liver and have been shown to be particularly important in adipose differentiation. These genes are expressed during the first few hours after the introduction of the differentiation cocktail and cause the cells to re-enter the cell cycle, and progress to the G_1 phase (Patel & Lane, 2000). Interestingly, it has been shown that in bone marrow derived human mesenchymal stem cells (HBMSCs), contact inhibition does not occur and during adipocyte differentiation of these cells, mitotic clonal expansion was not observed (Qian *et al.*, 2010). It was shown in the same research that the transcription factors of both the C/EBP and PPAR family were crucial in HBMSC adipocyte differentiation.

Various isoforms of C/EBP exist, however they are not all adipose specific, despite their importance in adipogenesis. C/EBPα for example is not adipose specific, however is expressed before the transcription of most adipocyte-specific genes has started, and in some instances is sufficient to induce differentiation of preadipocytes. The isoforms C/EBPα, C/EBPβ, and C/EBPδ each have distinct sequential and spatial expression during adipocyte differentiation. C/EBPα is expressed relatively late in the differentiation process, while the β and δ isoforms are present in preadipocytes. Their levels significantly increase during preadipocyte differentiation into adipocytes (Cao *et al.*, 1991)

C/EBPβ is a particularly important transcription factor for differentiation and is expressed within two hours of hormonal stimulation. However, at this point C/EBPβ lacks DNA binding potential (Tang & Lane, 1999). CEPB/β only gains DNA binding potential 14 hours after induction, and with DNA binding ability transcriptionally activates genes coding for C/EBPα and PPARγ through C/EPB regulatory elements in their proximal promoters (Tang *et al*, 2003). Interestingly it has been shown that the DNA binding efficiency of C/EPBβ is significantly increased in the presence of high levels of ROS (Lee *et al.,* 2009)

Peroxisome proliferator-activated receptor (PPAR) is another early adipocyte transcription factor required for adipocyte differentiation although the role this molecule plays in adipogenesis is not completely understood. PPARs forms heterodimers with the retinoid X receptor (RXR) and regulates transcription through this binding. The PPARγ isoforms is the

most adipose specific and is able to induce growth arrest and initiation of adipogenesis. The expression of PPARγ is controlled by the expression of C/EBP-β and δ, and levels of PPARγ increases significantly during differentiation. The activation of these transcription factors leads to full adipocyte differentiation (Gregoire *et al.*, 1998)

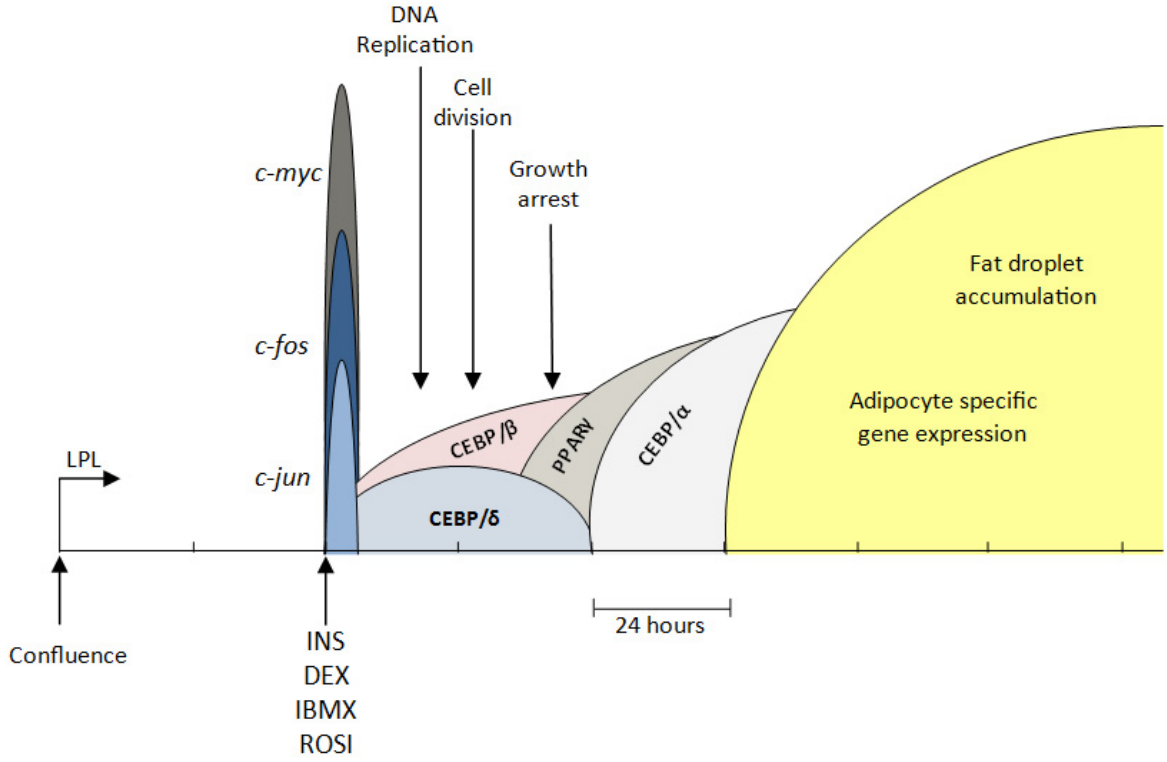

Figure 1.5. Progression of 3T3-L1 preadipocyte differentiation, highlighting the major events and expression of important transcription factors during differentiation (Modified from Ntambi & Kim, (2000))

The use of human mesenchymal cells to monitor adipogenesis has become popular as well (Janderová *et al*., 2003; Qian *et al*., 2010; Scott *et al.,* 2011). The molecular mechanisms that govern adipocyte differentiation have not been as rigorously investigated as murine models, however multiple similarities between the systems are evident. Janderová *et al.* (2003) found that the pattern of adipogenic genes expressed, such as those of the PPAR and CEBP families, during the induction of adipogenesis in primary human mesenchymal cells was similar as those found in established adipogenesis models, such as the 3T3-L1 cell line. Further to this, the use of the same differentiation cocktail, that is insulin, dexamethasone, IBMX and an insulin sensitizer such as rosiglitazone used to induce murine adipogenesis *ex vivo* has been used extensively in human mesenchymal models to study human adipogenesis (Scott *et al.*, 2011). One key difference in the differentiation of murine 3T3-L1 cells and human mesenchymal cells is the requirement of contact inhibition and mitotic clonal

expansion. Qian *et al.*, (2010) reported that in isolated bone marrow derived human primary mesenchymal cells, both contact inhibition and mitotic clonal expansion were not observed.

1.4 Signal transducer and activator of transcription 3 (STAT3)

Signal transducers and activators of transcription (STATs) are a class of proteins which mediate cellular differentiation, proliferation, survival and immune function within the cell (Levy *et al.,* 2002). In mammals there are seven STAT genes which code for the STAT family including STAT1, STAT2, STAT3 STAT4, STAT5a, STAT5b and STAT6. These proteins are inactive as transcription factors in the absence of specific receptor stimulations; STATs are localized in the cytoplasm when inactive, but are targeted to the nucleus once a stimulus has been encountered (Aaronson and Horvath, 2002).

1.4.1 The functional domains of the STAT3 molecule

Various methods such as sequence comparisons, biochemical assays and mutagenesis have resulted in the identification of distinct functional domains within STAT3 molecules (Figure 1.6). The 130 N-terminal amino acid residues aid in the binding of the molecule to multiple DNA sites (Xu *et al.,* 1996). Residues 400-500 do not bind DNA but do confer DNA binding specificity (Horvath *et al.,* 1995) while residues 600-700, which share homologies with the Src-homology-2 (SH2) domains, mediate dimerization as a response to phosphotyrosine recognition at position 705 (Shuai *et al.,* 1994). The C terminus of STAT3 proteins is important in transcriptional activation and can be controlled via serine phosphorylation at position 727 (Wen *et al.,* 1995). However it has been shown that serine phosphorylation of STAT3 has no influence on DNA binding of STAT3 (Wen & Darnell, 1997). Serine phosphorylation has recently been implicated as an important modification for mitochondrial STAT3 (Wegrzyn *et al.*, 2009; Gough *et al*., 2009; Tammineni *et al*., 2013). The C terminus may also play an important role in regulating the differential properties of STAT3 isoforms (Park *et al.,* 2000).

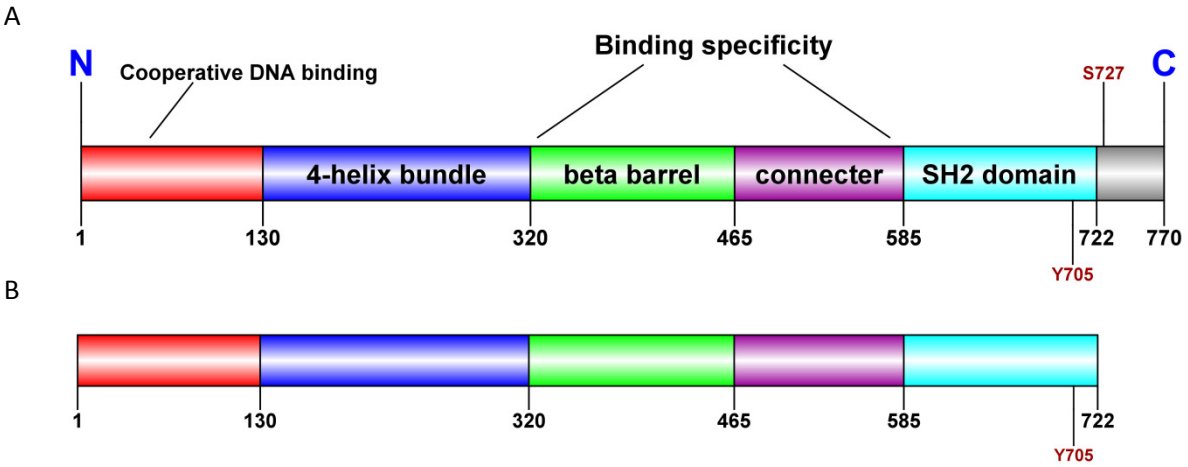

Figure 1.6. The domain structure of STAT3α and STAT3β. The domain structure of the two major isoforms of STAT3, (A) illustrating the both tyrosine and serine phosphorylation sites on the α isoform, and the (B) tyrosine phosphorylation site on the β isoform (Modified from (Becker *et al*., 1998)

The full length STAT3 protein is ideally 770 amino acids in length but post-transcriptional processing results in multiple C-terminal truncated isoforms. The two major isoforms STAT3α and the post-transcriptionally modified STAT3β are the 91 kDa and 89 kDa respectively. STAT3β is shorter than STAT3α, where 55 amino acid residues of STAT3α are replaced by 7 residues in STAT3β on the C terminus (Schaefer *et al.,* 1997). The properties of the two isoforms have been shown to differ with respect to DNA binding activities both *in vitro* (Park *et al.,* 1996) and *in vivo* (Schaefer *et al.,* 1997). STAT3α and STAT3β show no difference in terms of DNA binding strength but it has been shown that STAT3β dimers are more stable and this plays a critical role in determining the DNA binding activity of the STAT3 isoforms (Park *et al.,* 2000). It has been reported that STAT3β has a longer nuclear retention time that STATα (Huang *et al.*, 2007) and it was speculated by Huang *et al.*, (2007) that the difference in nuclear retention time of the two isoforms may contribute to the distinct functions of each isoform. Further research by Ng *et al.*, (2012) showed that there is sustained nuclear translocation and phosphorylation of STAT3β.

The DNA binding domains of STAT molecules are highly conserved. Small differences in the amino acid sequence in this domain do occur between the different STAT molecules. These differences determine the binding and transcription of distinct genes by each STAT (Boucheron *et al.,* 1998). This domain is also thought to be involved in the nuclear translocation of activated STAT1 and STAT3 dimers (Boucheron *et al.,* 1998).

1.4.2 The canonical JAK-STAT signalling pathway

The Janus kinase-signal transducers and activators of transcription (JAK-STAT) pathway transmits information from extracellular polypeptide signals through transmembrane receptors (Darnell, 1997). This results in the targeting of STAT proteins to specific DNA sequences in the nucleus which in turn activates gene transcription (Aaronson and Horvath 2002, Gough *et al.,* 2009), such as those which code for proteins such as γ-interferon-responsive cell cycle regulator p21 (Chin *et al.,* 1996, Ouchi *et al.,* 2000) and the interleukin 6 (IL6)-responsive acute phase response protein (Zhang and Darnell Jr., 2001). Proteins such as p21 are inhibitors of cell cycle regulators such as cyclin dependant kinases (CDKs) (Chin *et al.,* 1996) while IL6- responsive acute phase response protein plays a central role in inflammation and tissue injury (Ridker *et al.,* 2000). The pathway is highly adapted and ligand specific; regulated by a vast array of both intrinsic and environmental stimuli (Darnell, 1997; Aaronson and Horvath, 2002).

STATs are activated in response to receptor-ligand coupling such as the binding of cytokines and growth factors like the Interleukin-6 family (IL-6, IL-11), ciliary neurotrophic factor, and oncostatin M all of which bind to a common receptor subunit, gp130, for example when activating STAT3 (Kaptein *et al.,* 1996). There are more than 40 known different polypeptide ligands which cause STAT phosphorylation through cytokine receptors plus JAK kinases or growth factors (Bromberg *et al.,* 1999)

STAT proteins are recruited to the intracellular domain of the receptor through binding between STAT Src-homlogy (SH2) domains and receptor phosphotyrosine residues. The interactions between the SH2 and phosphotyrosine residues are highly specific and critical in determining the specificity of the receptor mediated STAT activation (Aaronson and Horvath 2002). STAT activating cytokines generally do not have a tyrosine kinase activity. This activity is provided by receptor associated cytoplasmic proteins known as the Janus kinase (JAKs) family (Chin *et al.,* 1996; Aaronson and Horvath, 2002). These proteins are highly conserved and play a fundamental role in the signalling pathway. JAKs bind specifically to the intracellular domains of the cytokine receptors and catalyse ligand induced self-phosphorylation and of tyrosine residues on the receptor, thereby creating STAT docking sites (Chin *et al.,* 1996).

STATs are phosphorylated on designated tyrosine residues and results in STAT homo- and heterodimerization (Ehret *et al.,* 2001). STAT dimers are transported from the cytoplasm to

the nucleus where they bind to specific sequences of DNA and initiate transcription (Zhang and Darnell Jr., 2001; Aaronson and Horvath, 2002) as illustrated in Figure 1.7. The translocation of STAT3 to the nucleus has been shown to be mediated by Hsp90 (Shah *et al.*, 2002; Sato *et al.*, 2003; Kramer *et al.*, 2012).

The ligand-dependent activation of STAT molecules is associated with differentiation and growth regulation of cells while that of constitutive activation of STATs is a trait of growth dysregulation. Mice lacking STAT1, for example, form chemically induced tumors of the skin much more easily than those of normal, wild type mice (Kaplan *et al.,* 1998). Many tumor derived cell lines as well as cells derived from human cancers have been shown to contain constitutively activated STAT proteins, especially STAT3 (Garcia and Jove, 1998)

STAT3 has been shown to mediate responses to growth factors and cytokines such as interleukin-6 family of cytokines, and has been linked to cancer development (Bromberg *et al.,* 1999). Interferon signalling to the cell nucleus is thought to be achieved through the phosphorylation of the single tyrosine residue 705 on STAT3 in the DNA binding domain (Zhong *et al.,* 1994; Bromberg *et al.,* 1999) via the JAK-STAT pathway which results in the expression of a variety of target genes (Ouchi *et al.,* 2000).

The dimer conformation of STAT3 allows the molecule to bind to consensus DNA targets and induce gene expression. It has been shown that STAT3 has alternative functions which are independent of STAT3 being phosphorylated or DNA binding. Non-canonical STAT3 activity occurs when unphosphorylated STAT3 enters the nucleus and binds to non-canonical regions of DNA based entirely on structural features (Timofeeva *et al*., 2012). Unphosphorylated STAT3, for example, can stimulate the expression of pro-inflammatory and pro-oncogenic genes either dependently or independently of binding to nuclear factor-κB (Yang *et al.,* 2007). Further to this is has been reported that STAT3 can form stable dimers in the presence of divalent cations independently of serine or tyrosine phosphorylation (Novak *et al*, 1998).

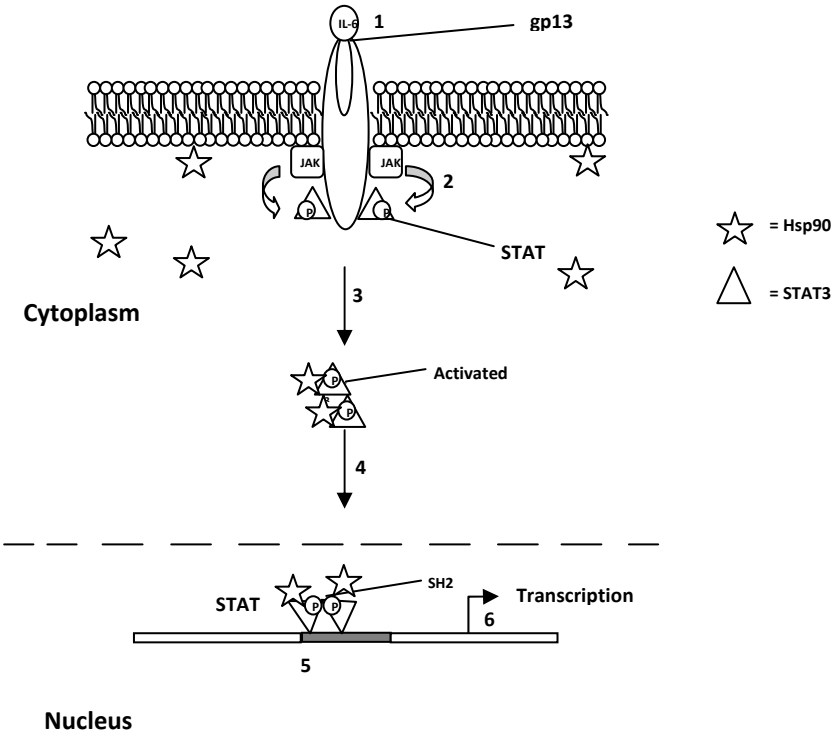

Figure 1. 7. Activation of transcription via the JAK-STAT3 signalling pathway mediated by Hsp90. Activation of STAT3, a cytokine such as IL-6 (1) causes STAT3 recruitment to receptor tyrosine phosphopeptides, in this case gp130 where it is phosphorylated on tyrosine 705 by JAK kinase (2). STAT3 dissociates from the receptor, and, mediated by Hsp90, forms dimers (3), migrates to the nucleus (4) where it binds response elements in target genes (5) which are then transcribed (6) (Modified from (Kaptein *et al.,* 1996)).

Nuclear trafficking of STAT3 is therefore a key regulatory mechanism of STAT3 transcriptional activity, and may be irrespective of tyrosine phosphorylation (Cimica *et al.,* 2011).

Proteins being transported into or out of the nucleus require either a nuclear localization signal (NLS) or a nuclear export signal (NES). These signal sequences interact with the karyophein-b family of proteins (importins and exportins) which interact with nuclear pore complexes (NPC) to facilitate transport. The direction of protein transport is controlled by a gradient of RanGTP, a protein which controls the conformation of the NPC, either allowing for the import or export of proteins, into or out of the nucleus (Cimica *et al.,* 2011).

As the regulation of transcription factor access to the nucleus is a means to control the transcription of certain genes, the nuclear trafficking of STAT3 is essential to its function as a transcription factor. It has been shown that STAT3 possesses a constitutive nuclear

localization signal and that import of STAT3 is independent of tyrosine phosphorylation but is dependent on the action of RanGTP and importin β1 (Cimica *et al.,* 2011).

As mentioned previously, it has been shown that STAT3 plays a role in activating the Warburg effect (Demaria *et al.*, 2010) and may explain the STAT3 'addiction' observed in cancer. The role of STAT3 in the development of malignant tumours varies depending the type of cancer, but it has been shown that pSTAT3Y705 is highly active in most cancers (Hodge *et al.,* 2005). Demaria & Poli (2011) showed that canonically activated STAT3 (pSTAT3Y705) acts a master regulator of the Warburg effect in cancer, by inhibiting mitochondrial respiration and activating glycolysis, a characteristic of many cancers. This is achieved by STAT3 up regulating the Hypoxia Inducible Factor α (HIFα) gene leading to a HIFα mediated glycolysis and glucose metabolism as well as STAT3 directly or indirectly down regulating the transcription of mitochondrial genes. This could have potential implications for the role of STAT3 in stem cells, by reducing levels of ROS and further contributing to the maintenance of potency.

1.4.3 STAT3 in the mitochondria

STAT3 has recently been shown to localize to the mitochondria where it is thought play a non-canonical role (Wegrzyn *et al.*, 2009 Reich, 2009). The role STAT3 plays in the mitochondria is still not fully understood however it has been reported that it appears to maintain electron transport chain basal activity (Wegrzyn *et al.,* 2009) and it has been suggested that it may be a negative regulator of the Mitochondrial Permeability Transition Pore (MPTP) (Boengler *et al.*, 2010). The role of STAT3 in the mitochondria is thought to be mediated by Genes associated with Retinoid-IFN-induced Mortality-19 (GRIM-19) (Tammineni *et al*., 2013).

GRIM-19 was originally identified as an apoptosis-related gene in human cancer cell lines (Angell *et al.*, 2000). It has been shown to be a critical subunit of complex I of the electron transport chain located in the inner membrane of mitochondria (Angell *et al.,* 2000). Interestingly, GRIM-19 has also been shown to be a negative regulator of STAT3 and it has been shown via yeast two hybrid screening that the two proteins directly and specifically interact (Lufei *et al.,* 2003; Zhang *et al.,* 2003)

Wegrzyn *et al.,* (2009) showed that STAT3 is found in the mitochondria after hypothesizing that because GRIM-19 is important in the assembly of complex I of the electron transport

chain (Huang *et al*., 2004) and the fact that that GRIM-19 and STAT3 directly interact (Lufei *et al.,* 2003), STAT3 should be found in the mitochondria. Wegrzyn *et al.,* (2009) showed that STAT3 does not adhere to the outer mitochondrial membrane non-specifically. Recently it has been shown that GRIM-19 acts as a chaperone to recruit STAT3 into mitochondria and that GRIM-19 actively enhances the incorporation of STAT3 into complex I (Tammineni *et al.,* 2013).

Mitochondrial STAT3 has also been shown to play an important role in ischemic pre- and post- conditioning in myocardial cells. STAT3 had been shown to be important in reducing myocardial injury by pre- and post-ischemic conditioning by Fuglesteg *et al.* (2008). The importance of STAT3 in the mitochondria after an ischemic event was demonstrated by Boengler *et al.* (2010) who also showed that STAT3 was present in cardiomyocyte mitochondria. The study found that mitochondrial STAT3 is associated with reduced cell death after ischemia. The group suggests that STAT3 is imported into the mitochondria via the mitochondrial presequence receptor Tom20, as the two proteins were shown to co-immunoprecipitate.

Experiments conducted by Gough *et al.,* (2009) have shown that STAT3 plays a role in the mitochondria which is dependant not on the canonical Tyrosine 705 phosphorylation of STAT3, but rather the phosphorylation of the Serine 727 residue of the STAT3 molecule. The study showed that the promotion of cellular transformation by the H-Ras oncogene is promoted by mitochondrial STAT3 sustaining altered glycolytic and oxidative phosphorylation, suggesting that STAT3 regulates a metabolic function in the mitochondria.

Recently the importance of the phosphorylation of the Serine 727 residue in the function of mitochondrial STAT3 has further been noted. Zhang *et al.,* (2013) have shown that mitochondrial STAT3 plays a crucial role in breast cancer. Through site directed mutagenesis experiments the group showed that the phosphorylation of Serine 727 of mitochondrial STAT3 has dramatic effects on tumour growth, the activity of complex I of the electron transport chain and the accumulation of ROS in the cell. In addition to the this, site directed mutagenesis experiments conducted by Tammineni *et al.,* (2013) showed that a S727A mutation reduced the import and assembly into complex I of STAT3 by GRIM-19. These studies highlight the potential role mitochondrial STAT3 plays in regulating ROS. Given that STAT3 has been implicated in activating the Warburg effect as well as its potential role in the

mitochondrial ETC, it can be speculated that activated STAT3, both canonically active pSTAT3Y705 and non-canonically active pSTAT3S727 play a role in mediating ROS signalling.

Despite the large amount of evidence suggesting a role for STAT3 in mitochondria, whether STAT3 plays a role in the mitochondria remains a controversial topic. Khan *et al*, (2013) were unable to detect a co-localization signal between 3 fluorescently tagged recombinant STAT3 molecules, namely, STAT3-GFP, STAT3-DsRed and STAT3-Flag with the mitochondrial protein COXIV in human Hep3B hepatocytes. It may be that co-localisation signals between the two proteins was low as STAT3 may not directly interact with COXIV, and may be interacting with other proteins within the mitochondria. The team were however able to detect a strong co-localization signal between STAT6 and COXIV suggesting that STAT family proteins may indeed play an important role in mitochondria.

1.5 The role of STAT3 in adipogenesis

STAT3 is known to be expressed in both 3T3-L1 preadipocytes and differentiated adipocytes. The involvement of STAT3 in adipogenesis was first investigated by Stephans *et al.* (1996). The study found that levels of STAT3 were elevated during adipogenesis and this up-regulation was unaffected when adipogenesis was inhibited by TNFα (a cytokine known to inhibit differentiation) suggesting that STAT3 was not tightly regulated during the events of adipogenesis.

Deng *et al.,* (2000) investigated the role of STAT3 during both growth of 3T3-L1 preadipocytes and during adipogenesis. Results of the study indicated that in proliferating preadipocytes STAT3 was highly tyrosine phosphorylated. However, in growth arrested preadipocytes and adipocytes levels of pSTATY705 were significantly lower. In addition to this, Deng and colleagues showed that induction of differentiation with IBMX, dexamethasone and insulin led to a delayed 3 day increase in pSTAT3Y705 that coincided with mitotic clonal expansion. These results indicated the tyrosine phosphorylation of STAT3 is important in proliferation of 3T3-L1 cells, but not necessarily in differentiation. Later, Deng and colleagues showed that the protein inhibitor of activated STAT3 (PIAS3) could inhibit adipogenic gene expression (Deng *et al.,* 2006). Wang *et al.,* (2010) confirmed this with results indicating that STAT3 regulated the expression of PPARγ. STAT3 was also recently shown to directly regulate the transcription of CEBP/β by binding to the distal region

of its promoter (Zhang *et al.,* 2011). The same study indicated that JAK2 acted upstream of STAT3. This research concluded that the JAK/STAT3 pathway is involved in the early stages of 3T3-L1 differentiation by regulating the expression of CEBP/β.

The importance of the phosphorylation of STAT on the Serine 727 residue in adipogenesis is unknown. There are reports that serine and tyrosine phosphorylation negatively regulate each other (Chung *et al.,* 1997) and it has been shown that insulin reduces tyrosine phosphorylation and increases serine phosphorylation, reducing the nuclear localization of STAT3 and its transcriptional activity (Andersson *et al.,* 2007)

1.6 Mitochondria, Reactive Oxygen Species (ROS) and Mitotic Clonal Expansion (MCE)

High levels of ROS during adipogenesis are well reported. It has been shown that fat accumulation is correlated with oxidative stress in both mice and humans (Furukawa *et al.,* 2004). Further to this it has been shown that the production of ROS increases selectively in the adipose tissue of obese mice and increased ROS levels have been reported to be a major trigger for insulin resistance (Houstis *et al.,* 2006). Krieger-Brauer & Kather, (1995) proposed that ROS production occurs during adipogenesis as a result of insulin and IGF-1 stimulating NADPH-dependant hydrogen peroxide generation. Tormos *et al.,* (2011) has reported that ROS produced at complex III of the electron transport chain regulates adipogenesis in human mesenchymal stem cells. In the study, mitochondrial targeted antioxidants inhibited adipocyte differentiation and this inhibition was rescued by the addition of exogenous hydrogen peroxide. Further to this, the genetic manipulation of complex III indicated that ROS produced at complex III was required to initiate adipogenic differentiation. The research concluded that ROS generation was not simply a consequence of increased metabolism, but plays an essential role in adipogenesis.

C/EPBβ DNA binding has been shown to be enhanced by oxidation *in vitro* and recently it has been shown that redox-induced C/EBP DNA binding activity, along with the dual phosphorylation of C/EBP, is required for MCE and terminal differentiation of adipocytes in 3T3-L1 cells (H. Lee *et al*., 2009).

Mitotic clonal expansion, as discussed previously, is an essential event during differentiation. It has been shown that ROS accelerate MCE and this results in greater differentiation

efficiency (Lee *et al*., 2009). During MCE, C/EPBβ is activated as cells synchronously re-enter S phase. C/EPBβ is activated by being sequentially phosphorylated by MAPK and GSK3β (nuclear) (Tang *et al.,* 2005). This activation induces C/EPBβ DNA binding and the transcription of adipocyte genes, allowing the differentiation process to progress. ROS may therefore play an important role in activating CEBP/β DNA binding and the induction of adipogenic events.

C/EBPβ is thought to mediate the expression of PPARγ. Genes activated by PPARγ regulate fatty acid uptake and glucose metabolism. Rosiglitazone is a potent agonist of the PPARγ and is marketed as an insulin sensitizer anti-diabetic drug. It has also been shown to induce mitochondrial biogenesis (Wilson-fritch *et al.,* 2003). The concentration of mitochondrial proteins increases by between 20 and 30 fold during adipogenesis, suggesting that mitochondrial biogenesis is a crucial aspect of adipocyte differentiation. Wilson-fritch and company (2003) showed that 3T3-L1 cells treated with rosiglitazone had greater mitochondrial density and resulted in qualitative changes in mitochondria. The thiazolidinedione class of drug has been added to the 3T3-L1 differentiation cocktail to increase the efficiency of preadipocytes differentiation, by potentially increasing ROS levels further as a result of increased glucose metabolism and increased mitochondrial biogenesis.

Given that STAT3 has been found to localise to mitochondria and has been shown to potentially play a role in within the electron transport chain, STAT3 may play a role in regulating differentiation events in a non-canonical manner by regulating ROS production. Further to this, as it has been shown that a prerequisite for STAT3 to localise to the mitochondria is phosphorylation of it serine 727 residue, mitochondrial STAT3 must be the longer α isoform of the STAT3 molecule, as the β isoform lacks the serine 727 residue. Interestingly, it has been shown that the α isoform has a shorter nuclear retention time than the β isoform, and it can be speculated that this could be an indication of non-conical functions this isoform may play, for example, within mitochondria.

1.7 Problem Statement

STAT3 has recently been shown to localize to mitochondria and play a role in the electron transport chain where it mediates ROS production. ROS play important role during cell differentiation. An understanding of how STAT3 mediates ROS production is required to further understand the complex events that occur during cell differentiation.

1.8 Hypothesis

As the role of STAT3 in differentiation processes is known to be important, it is hypothesized that mitochondrial STAT3 may further contribute to the potency of multipotent cells and play an important role in the mitochondria.

1.9 Aims and objectives

Aim: To monitor and investigate the levels and localization of STAT3 and its phosphorylated forms during adipogenesis of murine 3T3-L1 preadipocytes and adipose derived human mesenchymal stem cells and to compare and contrast the two models.

Broad objectives:

- Culture the 3T3-L1 murine preadipocyte line and adipose derived human mesenchymal stem cells (HMSC-ad)
- To successfully induce adipogenesis in both models
- To develop a real time differentiation assay utilizing the ACEA xCELLigence RTCA.
- To investigate the levels and localization of both unphosphorylated and phosphorylated forms of STAT3
- To investigate the levels of Reactive Oxygen Species during adipogenesis
- To investigate the levels and co-localization of STAT3 within the mitochondria of differentiating 3T3-L1 and HMSC-ad cells.

Chapter 2: Material and methods

Materials

All chemicals, culture media, molecular biology reagents, suppliers, catalogue numbers and equipment are listed in Appendix A5-8. The antibodies used in this study are listed below (Table 2.1-2.3). Unless stated otherwise, all reagents were of the highest grade and purity.

Table 2.1: List of primary antibodies used for Western blotting and immunofluorescence microscopy

Antibody	Company	Catalogue number	Dilution for Western blotting	Dilution for immunofluorescence microscopy
rabbit anti-pSTAT3 (Ser 727) polyclonal IgG	Santa Cruz (USA)	sc-8001	1:2000	1:200
rabbit anti-pSTAT3 polyclonal IgG	Santa Cruz (USA)	sc-7993	1:1500	1:200
rabbit anti C/EBPβ polyclonal IgG	Santa Cruz (USA)	sc-150	1:1500	1:200
rabbit anti-Prohibitin polyclonal IgG	Santa Cruz (USA)	sc-28259	1:2000	-
rabbit anti-Actin polyclonal IgG	Sigma Aldrich (USA)	A2103	1:2000	-
rabbit anti-Histone H3 polyclonal IgG	Cell Signalling Technologies (USA)	9715L	1:2000	-
rabbit anti-STAT3 polyclonal IgG	Santa Cruz (USA)	sc-7179	-	1:200
goat anti-VDAC polyclonal IgG	Santa Cruz (USA)	sc-8828	-	1:200

Table 2.2: Secondary antibodies for Western detection

Antibody	Company	Catalogue number	Dilution
goat anti-rabbit IgG-HRP	Santa Cruz (USA)	sc-2004	1:4000

Table 2.3: Secondary antibodies for immunofluorescence microscopy

Antibody	Company	Catalogue number	Dilution	Colour
Alexa Fluor® 488 chicken anti-rabbit IgG (H+L)	Invitrogen	A21441	1:500	Green
Alexa Fluor® 546 donkey anti-mouse IgG (H+L)	Invitrogen	A10036	1:500	Red

Methods

2.1 3T3-L1 cell culture

Murine preadipocyte 3T3-L1 cells were received at passage 19 and were a kind gift from Prof. Carmenita Frost (Nelson Mandela Metropolitan University). The cells were maintained in a basal media (Dulbecco's Modified Eagle's Medium (DMEM) (Sigma, USA, Cat. No D 5546) supplemented with 5% Foetal Calf Serum (FCS) (BioWest Cat. No. S1820), 1% L-glutamine (Sigma, Cat. No. 56-85-9)) and 1% penicillin/streptomycin/amphotericin B (PSA) (Sigma, Cat. No. A5955)) in a humidified incubator at 37°C, in a 5% CO_2 atmosphere and subcultured as necessary by routine trypsinisation. Cell viability was determined by trypan blue staining. 3T3-L1 preadipocytes were freshly split 24 hours prior to experimentation and allowed to grow to approximately 80% confluence.

2.2 HMSC-ad cell culture

HMSC-ad (Cat. No. 7510) cells were purchased from ScienCell (CA, USA) and received at passage 1. Complete mesenchymal stem cell media (MSCM) (Cat. No. 7501)) was purchased from ScienCell and prepared as per manufactures instructions (ScienCell MSCM consists of 500 ml of basal medium, 25 ml of foetal bovine serum (FBS, Cat. No. 0025), 5 ml of mesenchymal stem cell growth supplement (MSCGS, Cat. No. 7552) and 5 ml of penicillin/streptomycin solution (P/S, Cat. No. 0503)). A poly-L-lysine coated T75 tissue culture flask was prepared by incubating the flask with a solution of poly-L-lysine (1 mg/mL), (poly-L-lysine stock solution, 10 mg/ml, ScienCell cat. no. 0413) which was incubated overnight in a humidified incubator at 37 °C, in a 5 % CO_2 atmosphere.

After incubation for a minimum of 12 hours the flask was rinsed twice with sterile water and 20 mL of HMSC media added to the flask. The HMSC-ad stock was plated directly into the flask and left undisturbed for a minimum of 16 hours in a humidified incubator at 37 °C, in a

5 % CO_2 atmosphere. Cells were then fed to remove and residual dimethyl sulphoxide (DMSO). Cells were fed every three days until the culture reached 70% confluency, thereafter cells were fed every day and then split when 90% confluency was attained.

Prior to trypsinization, all required components were warmed to room temperature. Media was removed and cells were washed with Ca^{2+} and Mg^{2+} free PBS (Sigma). Next, 8 mL of PBS was added to the flask first and then 2 mL of trypsin/EDTA solution and incubated at 37 ˚C until the cells had completely rounded up. The trypsin solution was transferred to a 50 mL tubes and the flask incubated for a further 2 minutes. 5 mL of MSCM was then added to the flask to resuspended trypsinized cells, this was then added to the same 50 mL tube which was subjected to centrifugation at 1000 rpm for 5 minutes. The supernatant was poured off the pelleted cells, and the cells were resuspended in the residual volume to create a single cell suspension, before more complete media (10 mL) was added. Cells were then counted via trypan blue staining and seeded at 5000 cells/cm^2 onto freshly prepared poly-L-lysine coated tissue culture plastics as required.

2.3 Cryopreservation of mammalian cells

Following trypsinization, cells from one confluent T75 flask were resuspended in complete media, followed by centrifugation at 2000 rpm for 2 minutes (3T3-L1) or 1000 rpm for 5 minutes (HMSC-ad). The pelleted cells were resuspended in 1 mL cryopreservation media (10 % (v/v) DMSO in basal media (for 3T3-L1 cells) or MSC media (for HMSC-ad cells)). The solution was transferred to a cryo vial, kept on ice for about half an hour before being stored at -80 °C or in liquid nitrogen for long term storage.

Cells were routinely checked for *Mycoplasma* contamination (See Appendix A1 for methodology)

2.4 Differentiation of 3T3-L1 preadipocytes

Differentiation of 3T3-L1 cells was based on the protocol by Zebisch *et al.* (2012). Cells were grown to confluence (Day -2) and maintained in normal growth medium for a further 2 days. Two days post confluence (Day 0) cells were washed with PBS and fed using adipocyte differentiation media. Differentiation media was made up of basal media supplemented with 10 µg/mL insulin (NovoRapid), 0.25 µM dexamethasone (Sigma), 0.5 mM 3-Isobutyl 1-methylxanthine (IBMX) (Sigma) and 2 µM rosiglitazone (Sigma). Dexamethasone and IBMX were dissolved in ethanol, and rosiglitazone in DMSO. Two days after induction,

media was aspirated and cells washed with PBS. Cells were fed with maintenance media supplemented with 10 µg/mL insulin for days 3 – 4 and then normal maintenance media thereafter.

2.5 Differentiation of adipose derived human mesenchymal stem cells (HMSC-ad)

Differentiation of HMSC-ad cells was based on the above protocol (Zebisch *et al.*, 2012) for the differentiation of 3T3-L1 preadipocytes to allow for accurate comparisons to be made. As human mesenchymal stem cell growth media (HMSCM) contains a variety of factors to maintain the multipotent potent state of the cells, media was aspirated and cells washed 3x with Dulbecco's Phosphate Buffered Saline (pH 7.4) (Sigma) before the addition of basal media supplemented with INS/DEX/IBMX/ROSI.

2.6 General protocol for Real Time Analysis using the xCELLigence system

The xCELLigence RTCA SP system was initialized, as per manufacturer's instructions, prior to commencement of the experiment by filling all 96 wells of the E-plate View 96 with the basal media (BM) (100 µL) and equilibrated at room temperature for 30 minutes. The plate was placed into the single plate (SP) station cradle (housed in the incubator) to establish a background reading. Both 3T3-L1 cells and HMSC-ad cells were seeded at 5000, 10 000 and 15 000 cells per well to establish what density of cells gave the best results. It was found that 10 000 3T3-L1 cells and 5000 HMSC-ad cells per well resulted in the most accurate *CI* curves. In following experiments, cells were enumerated by trypan blue staining and plated at 10 000 cells per well for experiments on the 3T3-L1 line and 5000 cells per well for HMSC-ad line as determined in optimization experiments, in 50 µL aliquots and in quadruplicate. Cells were allowed to settle for 30 minutes outside the incubator prior to returning the E-plate to the SP Station. Growth was monitored by electrical impedance measurements using the RTCA SP as arbitrary cell index (*CI*) units. Standard differentiation media components, i.e. INS/DEX/IBMX/ROSI were added at 4X strength in 50 µl to account for dilution effects in predetermined wells. Duplicate clear plastic 96 well plates were prepared in the same manner to allow for visualization of the experiments.

2.7 Oil Red O Staining

Following the xCELLigence experiment, plates were stained with Oil Red O (Sigma). A working solution was prepared from a filtered 0.5% (w/v) stock solution with distilled water

(6:1) to a final concentration of 0.3% (w/v). Briefly, medium was discarded and cells washed in phosphate buffered saline (PBS) pH 7.4 for 5 minutes. Cells were then incubated for 5 minutes in 10 % (v/v) formalin at room temperature after which fresh formalin was added and incubated at room temperature for a further hour. The plate was wrapped in parafilm and tinfoil to prevent drying. The formalin was then removed and wells were washed with 60 % isopropanol. Wells were allowed to dry completely before the addition of Oil Red O working solution. The plate was incubated at room temperature for 10 minutes before removing the stain and washing repeatedly with water. Cells were then viewed at 20x magnification (UOP BSZ500X Inverted microscope) under brightfield conditions, ScopePhoto 3.1 (ScopeTek) was used to capture images.

2.8 Cell cycle analysis

Cells were stained with propidium iodide in the presence of RNAse as specified by Nunez (Nunez, 2001). Pre-confluent and 2 days post-confluent 3T3-L1 cells (as judged by light microscopy) were collected via tripsinization. Cells were enumerated by trypan blue staining and 1 x 10^6 cells used per sample. Cells were fixed with 70% EtOH on ice for 15 minutes. Following fixation, cells were pelleted at 1500 rpm for 5 minutes and the supernatant discarded. Pelleted cells were resuspended in 500 µL of propidium iodide solution (15 µL PI, (10 mg/ml), 30 µL RNAse, 30 µL Triton X-100, 2925 µL PBS) and transferred to a 37˚ C incubator for 40 minutes. Following incubation, 3 mL of PBS was added to each sample and cells pelleted at 1500 rpm for 5 minutes and the resulting supernatant discarded. Finally, pelleted cells were resuspended in 500 µL of PBS. After doublet discrimination gating to exclude cell aggregates, DNA content as a measure of PI fluorescence was detected by excitation with the blue laser at 488 nm and emission detected in the 610/20 channel flow cytometry using a Becton Dickson FACS Aria II flow cytometer. Cell cycle analysis was performed using FCSExpress 4 (De Novo Software) using built in cell cycle models.

2.9 Analysis of intracellular levels of Reactive Oxygen Species (ROS)

Reactive oxygen species levels in cells were measured using 5-(and-6)-chloromethyl-2',7'-dichlorodihydrofluorescein diacetate, acetyl ester (DCF-DA) assay. DCF-DA is a stable non-fluorescent reduced dye that becomes fluorescent following cellular oxidation allowing for measurement by flow cytometry

Cells were trypsinzied and resuspended to a density of 1 x 10^6 cells/mL in PBS. 180 µL of the cell suspension was transferred to a micro reaction tube and 20 µL of a 1 mM solution of DCFH-DA was added to the cells (final concentration of 100 µM). The samples were incubated at 37° C for 30 minutes. ROS levels were measure Fluorescence was detected by excitation with the blue laser at 488 nm and emission detected in the 610/20 channel was measured via flow cytometry using the BD FACS Aria II SORP (Fluorescence Activated Cell Sorter Special Order Research Product) Results were analysed using FlowJo v10.

2.10 Immunofluorescence staining

Cells were grown on borosilicate glass cover slips in 6 well culture plates (Nunclon™, Nunc). Following differentiation treatments (for 0-6 days for 3T3-L1 cells or 0-3 days for HMSC-ad cells) and individual compound treatments of 3T3-L1 cells (lasting 3 days), cells were subjected to immunofluorescence staining. Medium was aspirated, and the cells were washed with PBS, before fixation for 30 minutes using a 4% (v/v) formaldehyde solution. Following fixation, cells were washed with PBS. Cells were then permeabilized for 5 minutes with 0.1% Triton X solution which was followed by a set of three 5 minute PBS washes. Coverslips were then blocked for a minimum of 1 hour at room temperature using a 1% (w/v) BSA/PBS solution. Following this, coverslips were incubated with appropriate primary antibodies (1:500 dilution in 1% (w/v) BSA/PBS) overnight at 4 ˚C. The next morning the antibody solutions were aspirated and coverslips washed three times, 10 minutes per wash with a 1% (w/v) BSA/PBS solution. Coverslips were then incubated with appropriate fluorescently tagged secondary antibodies (1:2000 dilution in 1% (w/v) BSA/PBS) in the dark at room temperature for a minimum of one hour before a final set of three 10 minute washes with a 1 (w/v) BSA/PBS solution. Nuclear material was stained by dipping coverslips in a Hoechst 33342 solution (1:1000 in water (v/v)) and cover slips were then allowed to dry before mounting with Dako fluorescent mounting medium (Dako, USA). The same procedure was performed, without primary antibody, as a control. Samples were analysed using the Zeiss AxioVert.A1 Fluorescence Microscope and the Zeiss Meta confocal LSM microscope.

2.11 Isolation of crude mitochondria

Fresh isolation buffer was prepared (0.3 M mannitol (Sigma), 0.1 % BSA, 0.2 mM EDTA, 10 mM HEPES) and the pH adjusted to 7.4 using KOH. The buffer was chilled on ice and protease inhibitor added prior to use (1:100 dilution).

Cells were tripsinized and washed with cold PBS. Cells were counted via trypan blue staining (a minimum of 3 x 10^6 cells were used per isolation). Following the PBS wash, cells were pelleted via centrifugation at 2000 rpm for 2 minutes. The resulting pellets were resuspended in cold isolation buffer (5 times the pellet volume) and transferred to a 1 mL micro reaction tube. The cell suspension was then homogenized on ice using a plastic Dounce homogenizer. When over 70% of cells had been ruptured, as determined by trypan blue staining, the homogenate was subjected to centrifugation at 1000 *g* for 10 minutes to remove whole cells and nuclei. The supernatant was collected and subjected to further centrifugation at 15 000 *g* for 15 minutes. The supernatant, representing the cytosolic fraction was removed and stored, and the pellet, representing the mitochondrial fraction washed in twice in cold isolation buffer prior to being processed for western blot analysis.

2.12 Western analysis

Cells were collected via trypsiniztion and enumerated by trypan blue staining. Cells were then lysed in Laemmli sample buffer supplemented with 5% (v/v) β-mercaptethanol (BioRad) at 95˚ C for 10 minutes. Following SDS-PAGE electrophoresis (Laemmli, 1970) and transfer onto PVDF filter membranes (BioRad), membranes were blocked for 1 hour at room temperature with 5% (w/v) skim milk in a TBS-Tween 20 buffer. Blocking was followed by an overnight incubation at 4˚ C in with the relevant primary. The membrane was then washed and incubated with a HRP linked secondary antibody for 1 h at room temperature. After washing, the membrane was developed with Clarity Western ECL Substrate (BioRad) according to the manufacturer's instructions. Images were captured using the UVTec Prochemilumence System.

Where necessary, actin was used as a loading control as it is commonly used in 3T3-L1 differentiation studies utilizing both Western blot and quantitative real time polymerase chain reactions (qRT-PCR) (Arsenijevic et al., 2012; Gwon et al., 2013).

Chapter 3

Development of an assay to monitor differentiation in real-time using the ACEA xCELLigence Real Time Cell Analyser (RTCA).

Specific objectives:

1. **To successfully induce adipocyte differentiation in murine 3T3-L1 preadipocytes and human HMSC-ad mesenchymal stem cells.**
2. **To confirm adipogenic event in both models utilising molecular techniques such as Western blot analysis and immunofluorescence microscopy as well as Oil RedO staining.**
3. **To develop a real time differentiation assay using the ACEA xCELLigence Real Time Cell Analyser (RTCA).**
4. **To investigate the effect of each compound making up the differentiation compound has on each model**

3: Development of an assay to monitor differentiation in real-time using the ACEA xCELLigence Real Time Cell Analyser (RTCA).

3.1 Introduction

Adipogenesis has classically been monitored through endpoint analysis utilizing the lipid soluble dye, Oil Red O. The method was first described by Kuri-harcuch & Green, (1978) who noted that intracytoplasmic lipid accumulation seemed to be directly proportional to the extent of differentiation, and formally reported to quantify adipose conversion by Ramirez-Zacarias *et al.,* (1992). The method has since become standard in confirming adipocyte differentiation, in both murine preadipocyte (Mehra *et al*, 2007; Zebisch *et al*., 2012) and mesenchymal (Janderová *et al.,* 2003; Jaiswal, 2000; Hass *et al.,* 2011) adipogenesis models.

The assay involves staining intracytoplasmic lipids with the lipid soluble dye, Oil Red O, and requires that cells are fixed using isopropanol, and analysed at a specific end point. Optimization of differentiation protocols through the use of end point assays can be laborious and inaccurate. Although end point analysis, such as Oil Red O staining can confirm that cells have accumulated fat droplets, and Western analysis can confirm adipocyte specific proteins are expressed; real-time analysis may allow for the development of optimal, efficient differentiation protocols. This ultimately leads to more accurate results as a profile of cell growth, arrest or death (Kustermann *et al.*, 2013) at any point during the differentiation process can be monitored.

Multiple novel approaches to monitor adipocyte differentiation of 3T3-L1 cells have been reported. The use of spectroscopic techniques has been reported to monitor adipocyte differentiation in both murine 3T3-L1 preadipocytes and human mesenchymal stem cells. Surface Enhanced Raman spectroscopy has been used to monitor mesenchymal adipogenesis in real-time. Moody and colleauges (2010) used this technique to gather chemical information about cells undergoing adipognenesis in a non-distructive manner. The method involves cells taking up gold nanoparticles which aggregate in cells, allowing for chemical analysis about lipid uptake in real-time. Most recently, the use of Surface Infared spectroscopy has been reported to monitor 3T3-L1 adipogenesis. Aonuma *et al*, (2013) cultured 3T3-L1 cells on a silicon prism and differentiation monitored utilizing infrared spectroscopy. The group was able to detect a C=O stretching band of triacylglycerides before

microscopic confirmation of lipid droplet formation allowing the group to detect early adipogenic events in a real-time, label free manner.

The use of flow cytometry to assess lipid accumulation was reported by Lee *et al.* (2004). The cytoplasmic granularity of 3T3-L1 cells induced to differentiate was found to correlate with increased levels of lipid accumulation. This method is particularly useful because it allows for the identification and collection of live adipocytes with similar lipid properties for down stream analysis. Other techniques to monitor the physical properties of differentiating cells such as atomic force microscopy (AFM) have also been reported. Utililizing AFM, the topography and mechanical properties of cells can be determined. Kwon *et al.* (2012) monitored 3T3-L1 differentiation on a single cell level by measuring the membrane stiffness of cells. The group found that there was a good correlation between the reduction of membrane stiffness with differentiation. Both results form Lee *et al* (2004) and Kwon *et al,* (2012) provide good evidense of the morphological changes that occur during adipogenesis and that these changes can be used to monitor differentiation.

There is an obvious need for the development of simple real-time, label free methods to monitor differentiation, and electric based biosensors have proved incredbly useful in this reagard. The use of electric cell substrate impedance and capacitance based biosensors to monitor adipocyte differentiation of 3T3-L1 preadipocytes in real-time has been reported using a non-commercial prototype biosensor which measured capacitance (Lee *et al.,* 2013) and an impedance based system which was used to monitor the adipocyte differentiation of human mesenchymal cells (Bagnaninchi & Drummond, 2011). In the capacitance based sensor developed by Lee *et al.* (Lee *et al*., 2013) cells were placed between two electrodes and the change in the dielectric constant (ε) was measured. This value is directly proportional to capacitance and is dependent on cell size, cell membrane potential and the contents of the cell (Lee *et al.,* 2012). As capacitance systems are able to detect changes in the composition of cells, they are ideal systems to measure the differentiation of cells where gross cellular accumulation or novel biogenesis occurs; case in point, lipid accumulation during adipogenesis. However, lipid accumulation is but one property that can be measured to monitor adipogenesis. The morphology of cells dramatically changes during differentiation processes (Fan *et al.*, 1983). These changes in morphology can be measured in real-time using commercially available Electric Cell-Substrate Impedance Sensors (ECIS). These impedance based systems measure the alternating current impedance between a small sensing electrode and a large counter electrode while cells are cultured on the gold sensing electrode.

As cells attach and spread on the surface of the sensing electrode, passively blocking the current, the electrical impedance which results is registered by the sensor. Impedance is therefore affected by the shape, adhesion, or mobility of the adherent cells (Pethig, 1984; Tirado *et al*, 2002). Both impedance based and capacitance based biosensors provide insights on what is happening to cells, and ideally an instrument that measures both these parameters would be advantageous.

The development of the real-time biosensors such as the ACEA xCELLigence Real-time Cell Analyser (RTCA) has revolutionised label-free cell biological analysis, giving more reliable medium to high throughput data regarding, amongst others, cell proliferation, migration (Limame *et al.*, 2012), compound toxicity (Kustermann *et al.*, 2013) and viral cytopathic effects (Tang & Stratton, 2013). The use of the ACEA xCELLigence Real-time Cell Analyser Single Plate (SP) system to monitor the primary events of 3T3-L1 and HMSC-ad adipocyte differentiation and illustrate the potential of the system to screen for pro- and anti-differentiation compounds is reported here. The xCELLigence RTCA should theoretically be able to monitor Mitotic Clonal Expansion (MCE) during 3T3-L1 differentiation by potentially monitoring proliferation changes following the induction of differentiation.

Based on published recommendations (Mehra *et al.*, 2007; Zebisch *et al.,* 2012) the ability of the ACEA xCELLigence RTCA SP (single plate) to monitor growth and differentiation of 3T3-L1 preadipocytes in real-time in a 96 well assay format was evaluated. The proprietary 96 well E-plates used in the experiment are designed with gold microelectrode arrays at the base of each well that measure electrical impedance at given time points (Z_i) in relation to a background reading (Z_0) to calculate arbitrary cell index (*CI*) units as:

$$\mathrm{CI} = \frac{\mathrm{Z_i} - \mathrm{Z_0}}{15}$$

The xCELLigence monitoring software records the *CI* values which can be used to calculate theoretical doubling time (as cell density increases, so does *CI*) however as these values are affected by cell properties such as shape, adhesion, and mobility of cells the system can be used to monitor morphological changes. The ability of this technology allows for effective monitoring of cell differentiation.

3.2 Results and Discussion

3.2.1 Confirmation of the induction of adipogenic events

Morphological changes

Adipogenesis was monitored routinely by light microscopy. Upon the induction of differentiation distinct morphological changes were observed. 3T3-L1 cells adopted a highly spindle like morphology for the first two days post induction as indicated by the arrows in panels showing Days 1 and 2 of differentiation (Figure 3.1A), thereafter becoming more rounded. Fat droplets were easily observed from day 3 of differentiation and became more distinct with time as shown by the arrow in Day 5 (Figure 3.1A). The size of 3T3-L1 cells induced to differentiate became much more varied, more clearly seen in fluorescence images in Figure 3.2, with particularly large cells occasionally being observed (Day 2, Figure 3.3)

The human mesenchymal stem cells were induced to differentiate using the same protocol used in 3T3-L1 preadipocyte differentiation to allow for comparisons to be made between the two models of adipogenesis. Reported mesenchymal adipogenesis protocols are similar to 3T3-L1 differentiation protocols (Janderová *et al.*, 2003).

The HMSC-ad cells are much smaller than the murine 3T3-L1 preadipocytes with nuclear diameter of HMSC-ad cells found to be ~5-10 μm while that of 3T3-L1 cells was ~10-20 μm as determined by fluorescence microscopy. The adipose derived HMSC-ad cells interestingly did not exhibit contact inhibition upon reaching confluence. This finding correlates with previous findings by Qian *et al.* (2010). Cells were found to grow in multilayers upon reaching confluence, and as judged by light microscopy, grew much more quickly than the 3T3-L1 preadipocytes. The HMSC-ad cells seemed to differentiate much more readily with lipid droplets (indicated by red arrows in Figure 3.1B) starting to be observed as early as 24 hours post induction. Changes in the morphology of the HMSC-ad cells were also noted. The morphology became much more rounded upon induction and cell size increased dramatically as seen in Figure 3.1B.

Based on light microscopy, it appeared that differentiation protocols were effective in inducing adipocyte differentiation of both 3T3-L1 and HMSC-ad cells. It appeared that HMSC-ad cells were differentiating more quickly than the 3T3-L1 cells, with larger lipid droplets being observed earlier in HMSC-ad cells.

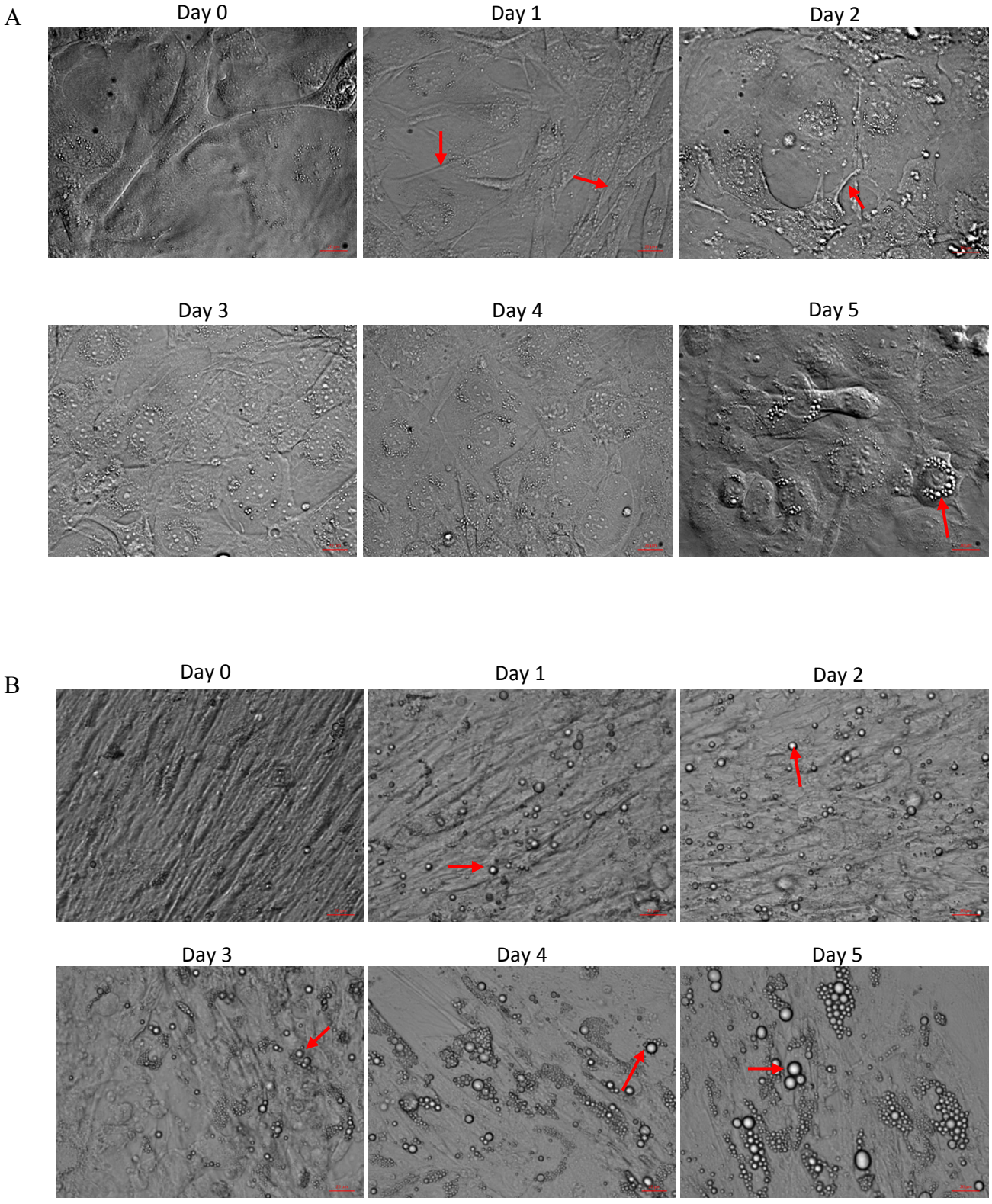

Figure 3.1. Morphological changes during adipogenesis. Adipocyte differentiation of (A) 3T3-L1 murine preadipocytes and (B) adipose derived human mesenchymal stem cells. Images captured through days 0 to 6 of differentiation. Arrows highlight regions of lipid accumulation. Scale bars = 20 µm. Images were captured using a Zeiss AxioVert.A1 FL-LED Fluorescence Microscope at 400x magnification with a Ph 2 filter. Images representative of multiple images (n = 3)

Expression and localisation of C/EBPβ

CCAAT/enhanced binding protein β (C/EBPβ) plays a significant role during adipogenesis (Cornelius *et al.,* 1994; Tang *et al.,* 2003). Tang and Lane (1999) showed that the expression of C/EBPβ in 3T3-L1 cells occurs rapidly after the induction of differentiation with maximum levels being reached 4 hours after induction and maintained for a further 48 hours. Levels of C/EBPβ then slowly start to drop.

C/EBPβ localisation and levels were monitored by fluorescence microscopy and Western blot analysis to confirm that adipogenic events were occurring in 3T3-L1 preadipocytes and HMSC-ad cells upon the introduction of differentiation with IBMX, dexamethasone, insulin and rosiglitazone.

It is important to note that C/EBPβ has two major isoforms. It has been shown that isoform expression is differentially regulated at the translational level (Kim *et al.,* 2008) and both are transcribed from the same mRNA molecule (Tang & Lane, 1999). Isoforms are expected to migrate at around 38 kDa and 18kDa during SDS-PAGE. In 3T3-L1 uninduced preadipocytes were shown to have minimal levels of the transcription factor, with a faint band of the larger isoform being observed in the uninduced lysate as shown in Figure 3.2A. Western blot analysis indicated that expression of C/EBPβ increased upon differentiation with maximum levels being observed in the first 24 hours of differentiation as observed in the Day 1 lysate (Figure 3.2A). These levels were shown to remain relatively constant for 4 days post induction (Days 2-5, Figure 3.2BA), and thereafter slowly started to diminish with minimal levels observed in day 6 (Day 6, Figure 3.2B) of the sample set.

In HMSC-ad cells the expression of C/EBPβ was found to be similar to those of 3T3-L1 preadipocytes with expression of the protein in the mesenchymal cells only observed post induction, although a potential band at 18 kDa was observed in the uninduced lysate. Day 3, interestingly, was found to have highest expression, indicating that C/EBPβ may play a slightly different role in human mesenchymal adipogenesis. The larger isoform of C/EBPβ also ran at a slightly higher size than the murine isoform. Two faint bands which ran at around 30 kDa and 35 kDa respectively were occasionally observed in induced cell lysates, and are most prominent in the Day 3 lysate (Figure 3.2B). These bands could represent isoforms of C/EBPβ present in the human cells. Since it is known that C/EBPβ has multiple isoforms, transcribed from the same mRNA molecule, these bands most probably represent minor isoforms of the protein and are most probably not as a result of non-specific binding.

A

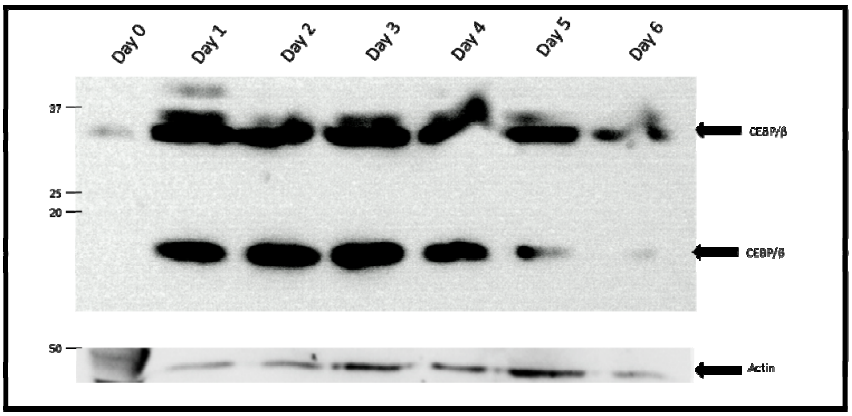

B

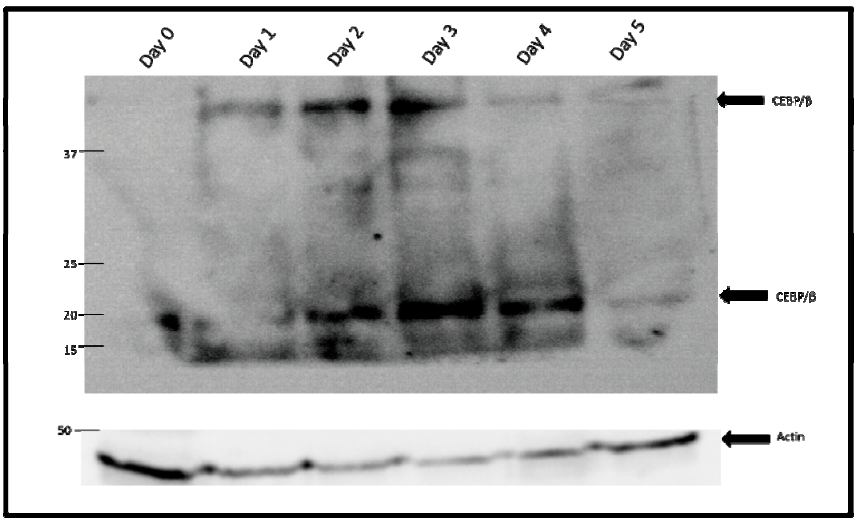

Figure 3.2. Expression levels of C/EBPβ during adipogenesis. Western blot analysis of the expression of C/EBPβ during the (A) first 6 days of 3T3-L1 and (B) first 5 days HMSC-ad of adipocyte differentiation. Equal number of cells per lane were loaded. Arrows highlight the detection of the two major forms of C/EBPβ (expected relative masses of 38kDa and 18 kDa) Actin was used as a loading control.

C/EBPβ localisation in 3T3-L1 cells

Six images were captured from random regions based on nuclear Hoechst staining on each slide for localisation analysis.

As expected, prior to the induction of differentiation the localisation of C/EBPβ in 3T3-L1 cells was cytoplasmic, with minimal nuclear staining as shown in the Day 0 panel of Figure 3.3. There was a distinct lack of nuclear localized C/EBPβ in 72% of observed cells (n = 21) pre-induction. Interestingly, there was strong perinuclear staining observed in 38% of uninduced cells, as illustrated by the blue arrow in the Day 0 panel of Figure 3.3. This staining could indicate a golgi or endoplasmic reticulum localisation. The intensity of fluorescence signal in uninduced cells was particularly low. This low signal was expected as the levels of C/EBPβ in preadipocytes was expected to be minimal, as confirmed by Western blot analysis (Day 0, Figure 3.1).

Localisation of C/EBPβ was found to be nuclear in 80% of observed cells (n = 40) upon the induction of differentiation as shown by red arrows, Day 1, Figure 3.3. This strong nuclear localisation persisted with 92% of observed cells found to have nuclear localized C/EBPβ (n = 51) 48 hours post-induction, as shown by red arrows on the Day 2 panel, Figure 3.3. Nuclear localisation was reduced 72 hours post-induction and punctate cytoplasmic structures were observed, indicated by the white arrow on the Day 3 panel of Figure 3.3. It was found that 71% of cells (n = 37) had lost the nuclear C/EBPβ localisation phenotype 3 days post-induction. Through Days 4 to 6 post-induction the nuclear localisation of C/EBPβ became less distinct with 14% of cells having nuclear localized C/EBPβ observed on Day 4 (n = 35), 0% on Day 5 (n = 52) and 5% (n = 56) on Day 6.

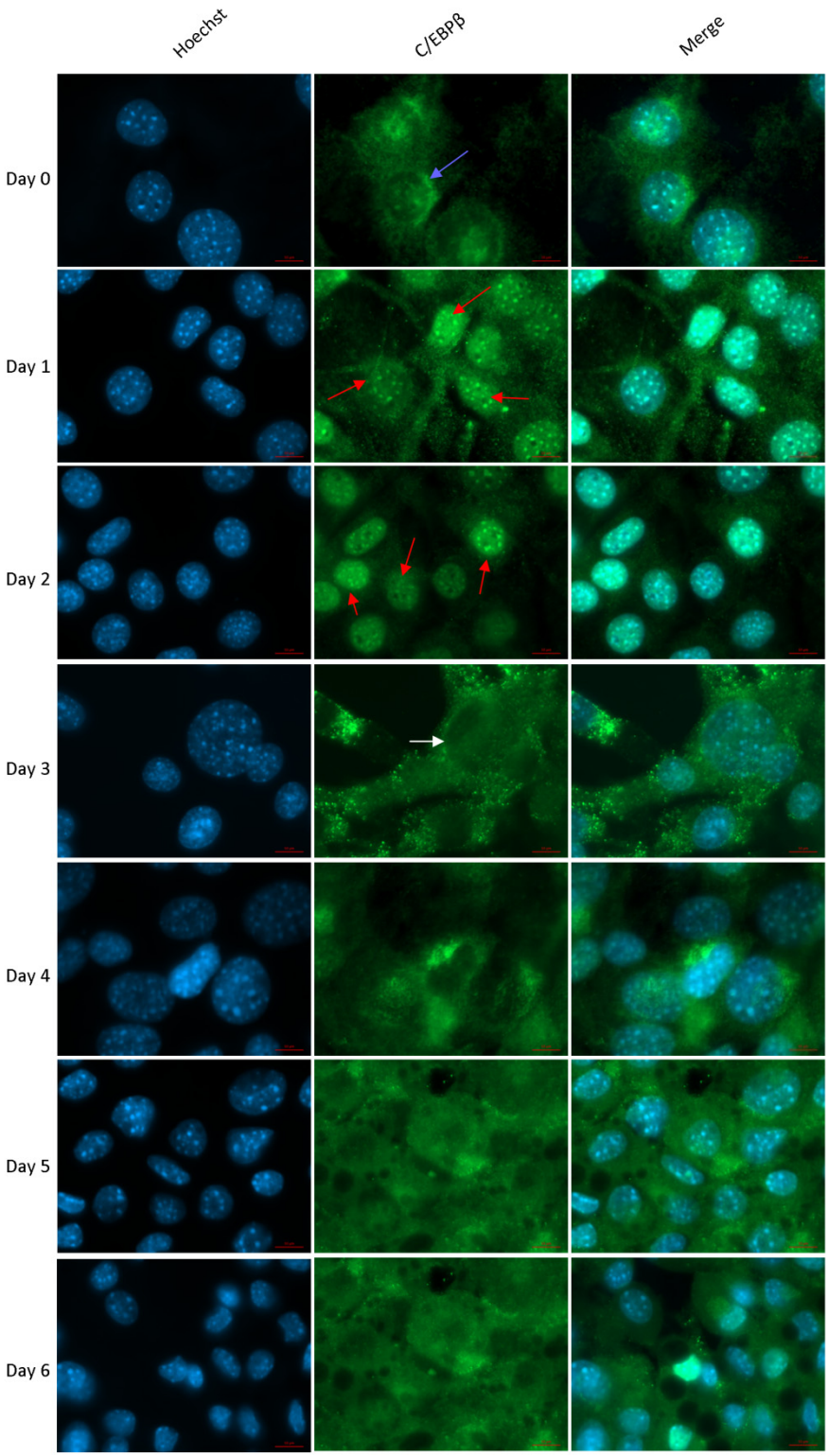

Figure 3.3: Localisation of C/EBPβ during 3T3-L1 adipocyte differentiation. Immunofluorescence analysis of the localisation of C/EBPβ through days 1 to 6 of 3T3-L1 adipocyte differentiation. Red arrows highlight the nuclear localisation of C/EBPβ during Days 1 and 2 post-induction, the white arrow is highlighting punctate structures observed on Day 3. Scale bars = 10 µm. Images were captured using a Zeiss AxioVert.A1 FL-LED

Fluorescence Microscope at 1000x magnification. Images representable of multiple images (n = 6).

C/EBPβ localisation in HMSC-ad cells

The localisation of C/EBPβ during adipogenesis was investigated in the first 3 days post induction in HMSC-ad cells as well. In pre-induced cells, localisation was distinctly cytoplasmic, with no nuclear localisation observed (n = 18). Interestingly, the localisation pattern was noticeably different to that of the C/EBPβ localisation in 3T3-L1 differentiation. As opposed to a nuclear localisation observed within the first 24 hours post-induction as seen in 3T3-L1 cells, C/EBPβ remained in the cytoplasm (n = 16) and was only observed to adopt a nuclear localisation 2 days post induction (30% of cells, n = 7) as highlighted in Figure 3.4. This nuclear localisation became more distinct 3 days post induction with 100% of observed cells (n = 11) having nuclear localized C/EBPβ and is in line with the high expression levels of C/EBPβ detected in the Day 3 lysates of Western blots (Figure 3.2B). This phenomenon was unexpected as lipid accumulation was observed much earlier in HSMC-ad cells, despite the delay in the nuclear localisation of C/EBPβ. In the 3T3-L1 preadipocyte model C/EBPβ is known to be one of the primary transcription factors activated upon induction, as illustrated in Figure 1.5. As lipid accumulation is distinctly evident (Figure 3.1B) prior to the nuclear localisation of C/EBPβ, this could indicate that another isoform of C/EBP could be expressed before C/EBPβ, which is evidently activated later in mesenchymal adipogenesis. Despite this result, the role of C/EBPβ in mesenchymal adipocyte differentiation has been reported to be essential (Qian *et al*., 2010; H. N. Yang *et al*., 2011) and its detection, and nuclear localisation are an indication of adipogenic events occurring in induced HMSC-ad cells.

Concentrated regions of C/EBPβ staining adjacent to nuclei were routinely observed in cells of all stages of differentiation. This could the localisation of C/EBPβ in the golgi or endoplasmic reticulum, as was observed in 3T3-L1 cells.

These results indicate that differentiation of the 3T3-L1 preadipocytes and of HSCM-ad mesenchymal stem cells into adipocytes was occurring in the same manner as reported in literature.

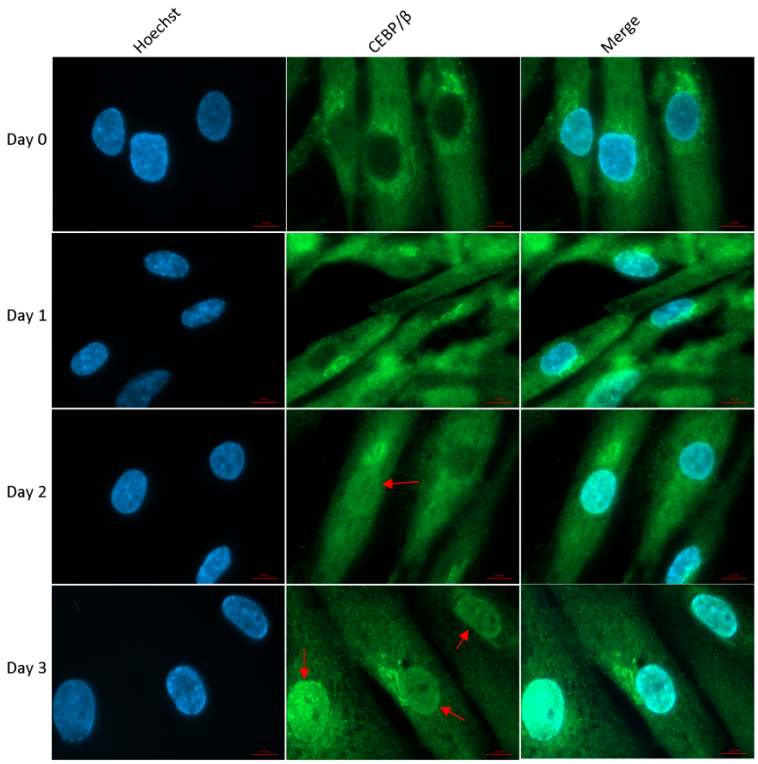

Figure 3.4: Localisation of C/EBPβ during HMSC-ad adipocyte differentiation. Immunofluorescence analysis of the localisation of C/EBPβ through days 1 to 3 of HMSC-ad adipocyte differentiation. Red arrows highlight the nuclear localisation of C/EBPβ during Days 2 and 3 post-induction. Scale bars = 10 µm. Images were captured using a Zeiss AxioVert.A1 FL-LED Fluorescence Microscope at 1000x magnification. Images representable of multiple images (n = 6).

3.2.2 Real time monitoring of differentiation using the ACEA xCELLigence RTCA system

Real time monitoring of differentiation of 3T3-L1 preadipocytes

Both 3T3-L1 cells and HMSC-ad cells were seeded at 5000, 10 000 and 15 000 cells per well to establish what density of cells gave the best results. It was found that 10 000 3T3-L1 cells and 5000 HMSC-ad cells per well resulted in the most accurate *CI* curves.

The ability of the xCELLigence system to measure the adipogenic events following induction of differentiation was investigated. The requirement of cytostaticity (G_0) prior to induction of differentiation of 3T3-L1 preadipocytes is well documented (Ntambi & Kim, 2000; Patel & Lane, 2000; Cao *et al.*, 2012), and is achieved by growing cells to post-confluence. Despite the requirement of post-confluent cells for efficient differentiation it was hypothesized that the xCELLignece system would be able to measure the morphological changes that accompany the induction of differentiation regardless of the general cell cycle state of the cells.

A cell cycle flow cytometry assay confirmed that pre-confluent cells were actively dividing with a distinct population of 39.56% of cells in the S phase while post-confluent cells had reached cytostaticity with over 90% of cells in the $G_{0/1}$ phase as shown in the cell cycle analysis (Figure 3.5A and B). Despite the reported requirement for cells to be cytostatic prior to induction of differentiation, the xCELLigence system was able to detect similar CI profiles for cells induced to differentiate regardless of their position in the cell cycle as seen in Figure 3.6.

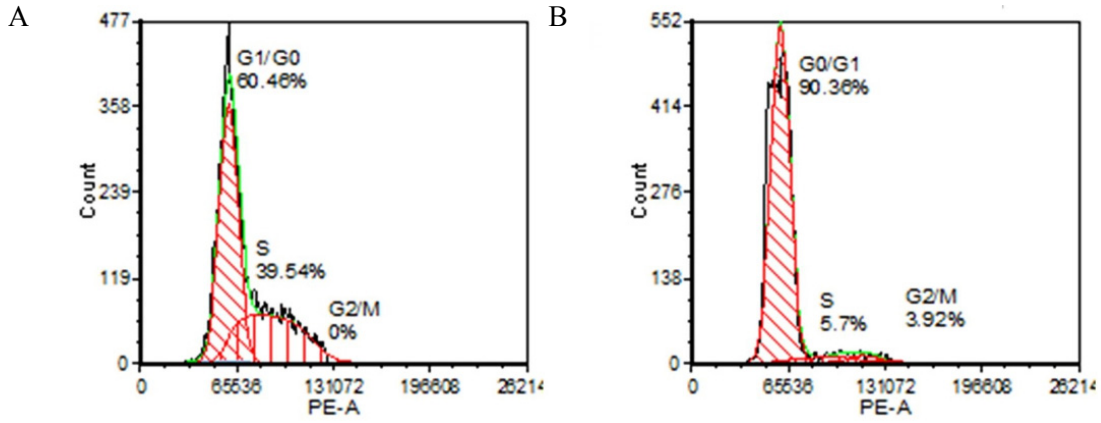

Figure 3.5. Cell cycle analysis of pre-confluent and post-confluent 3T3-L1 cells. Cells were judged to be (A) pre-confluent or (B) post-confluent by light microscopy and their

DNA content measured by flow cytometry to determine the cell cycle state cells were in. Data was analysed using FCSExpress 4 (De Novo Software) using built in cell cycle models.

Cells were seeded at the same density in three separate experiments and induced to differentiate before reaching confluence (Figure 3.6A), upon confluence (Figure 3.6B) and once post-confluent (Figure 3.6C) as judged by doubling times calculated 20 hours prior to the induction of differentiation using ACEA's xCELLigence RTCA software. In all three experiments, 3T3-L1 cells produced distinct *CI* profiles. Cells attached quickly to gold surface producing a *CI* versus time profile with a characteristic peak within 3 hours after plating. The *CI* values of the 3T3-L1 cells steadily increased in the same manner in all three experiments, and if allowed to grow to post-confluence, as seen in Figure 3.6C reached a maximum *CI* value of about 5.

Mitotic clonal expansion, as it involves active cell growth, should be able to be monitored using the xCELLigence system. However, as shown in Figure 3.6, the *CI* curves of cells induced to differentiate rapidly drop as opposed to the expected increase in *CI* values as a result of dividing cells. This dramatic drop was found to be reproducible and is thought to be a characteristic primary event in the *CI* curves of 3T3-L1 cells induced to differentiate. The drop in the *CI* values upon induction of differentiation was speculated to be caused by a dramatic change in morphology. Cell death was ruled out as a cause for the drop in *CI* values as *CI* values did not drop to 0 and upon microscopic analysis, cells appeared healthy.

The *CI* values were found to reproducibly drop to a value of approximately 1, after which values were found to remain relatively stable. The changes in the *CI* profiles after induction and the initial change in morphology are most probably as a result of cells moving on the surface and not as a result of active cell proliferation as was the case during the initial increase of *CI* values directly after seeding cells.

To confirm that these *CI* profiles were not an artefact of a single component of the differentiation cocktail and in fact as a result of the induction of differentiation, cells were individually treated with each of the components making up the differentiation cocktail.

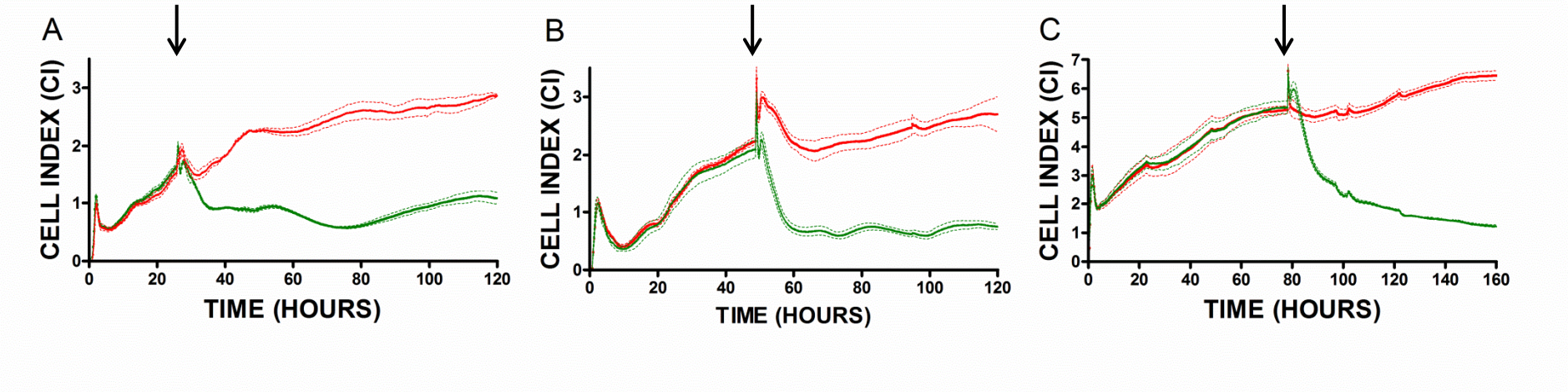

Figure 3.6. The effect of confluency on the ability of the xCELLigence system to detect differentiation events. (A–C): CI versus time curves of 3T3-L1 preadipocytes induced to differentiate at (A) pre-confluent (doubling time of 14.6 ± 0.58 h), (B) confluent (doubling time of 44.8 ± 0.6 h) and (C) post-confluent (doubling time of 283.6 ± 10.23 h) points as judged by the doubling times calculated 20 hours pre-induction. Red curves indicate uninduced samples while green curves indicate samples induced to differentiate. Dotted lines represent standard deviations. All curves were plotted as an average of quadruplicate treatments. Cells were plated at 0 hours, and induced to differentiate at points indicated by the black arrows. Data was plotted using GraphPad Prism v4.0

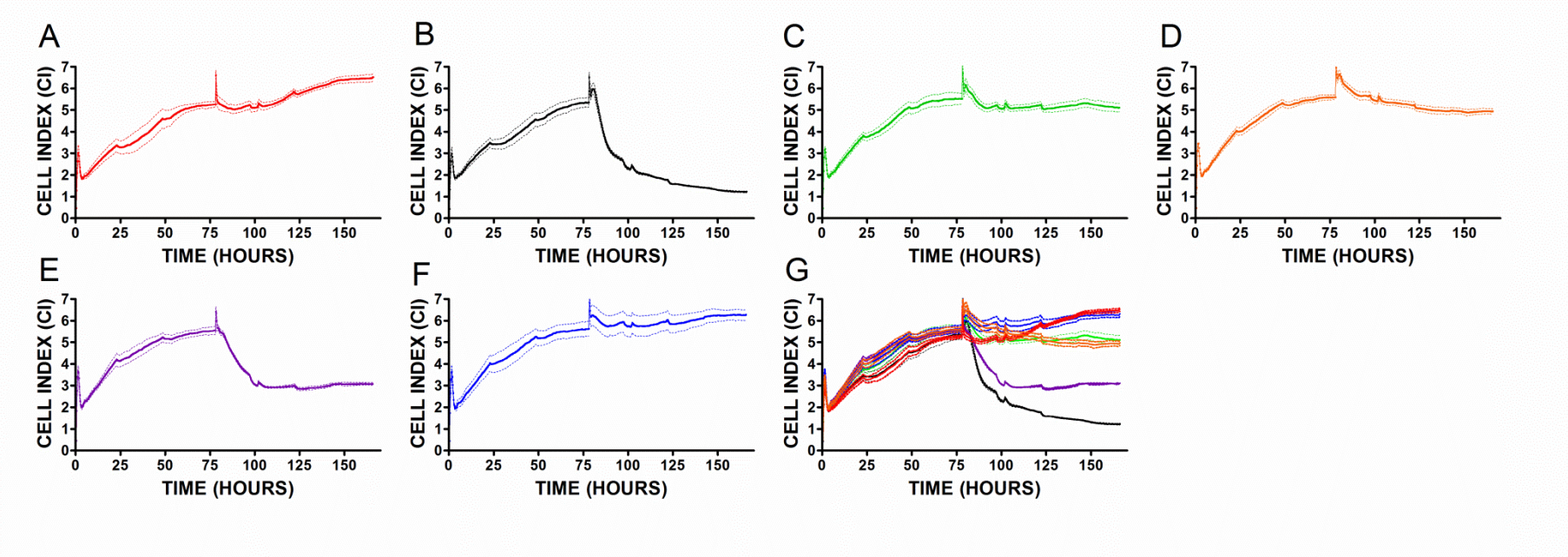

Figure 3.7: Effects of individual components of, and full differentiation cocktail on 3T3-L1 growth CI curves. Cells were treated at the same time with: A) DMSO and EtOH (control), B) Differentiation cocktail (INS/DEX/IBMX/ROSI), C) Insulin, D) Rosiglitazone, E) IBMX, and F) Dexamethasone. G) Comparison of all treatments. Dotted lines represent standard deviations. All curves were plotted as an average of quadruplicate treatments. Data was plotted using GraphPad Prism v4.0

Both insulin treatment and dexamethasone treatment resulted in significantly altered *CI* profiles however IBMX treatment was the only compound able to produce a *CI* profile similar to cells treated with the full differentiation cocktail. IBMX treated cells resulted in a reduction of *CI* values comparable but not identical to the full differentiation *CI* profile.

This characteristic drop in *CI* values was unexpected as upon induction of differentiation cells are reported to re-enter the cell cycle and undergo active growth. As the xCELLIgence system is an impedance based sensor the dramatic reduction in *CI* values were hypothesized to be as a result of a morphological change in the cells. It has been noted in our lab that upon the induction of differentiation, 3T3-L1 cells adopt a highly spindle-like morphology for the first 48 hours post induction. It is only after this period that cells become more rounded and start to accumulate lipid droplets.

Interestingly, dexamethasone, IBMX and insulin treatments all resulted in an increased nuclear localisation of C/EBPβ in the 3T3-L1 cells, as shown in Figure 3.8. As the morphological change was not observed (as determined by light microscopy and absence of a marked drop in *CI*) in cells treated with insulin or dexamethasone, IBMX must either activate the expression of separate proteins which result in this morphological change, in addition to C/EBPβ, or the resulting increase in cAMP as a result of IBMX treatment must lead to a change in morphology. Another possible explanation could be that the cAMP increase in IBMX treated cells is more dramatic than in insulin or dexamethasone treated cells, thus explaining the more pronounced morphological change. It has been reported that the inhibition of cAMP phosphodiesterases by N6-monobutyryl and dibutyryl cyclic AMP results in converting the morphology of Chinese Hamster Ovary (CHO) cells from a compact, epithelial like morphology to that of a spindle shaped fibroblast morphology (Hsie, Kawashima, O'Niell, & Shroder, 1975) and that treatment of sarcoma cells in tissue culture with cAMP phosphodiesterase inhibitors restores the morphological characteristics of normal fibroblasts (Johnson, Friedimant, & Pastan, 1971) It was speculated by Hsie *et al.* (1975) that cAMP-dependant protein kinase in microtubule polymerization may be involved in the observed morphological changes. The role of increased levels of cAMP in changing the morphology of cells has been further reported (Dong, 1998; Fujioka, Fujioka, & Duman, 2004; L. Zhang, Seitz, Abramczyk, Liu, & Chan, 2011). The increase in cAMP and the observed morphological change observed in 3T3-L1 cells may be a crucial event in adipocyte differentiation.

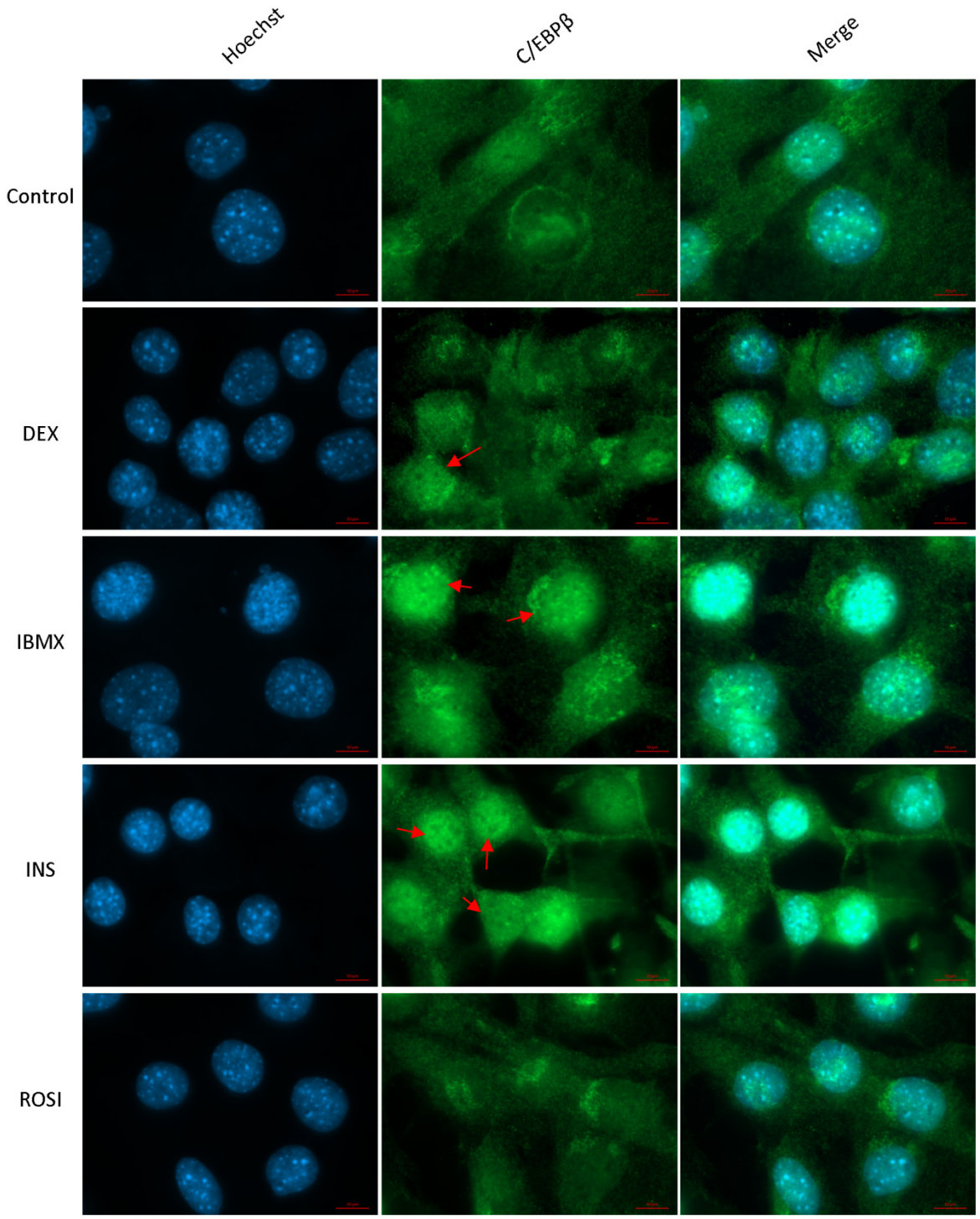

Figure 3.8: Effect of individual compound treatment (dexamethasone, IBMX, insulin or rosiglitazone) on the localisation of C/EBPβ. Cells were treated with individual compounds at the same concentration found in the differentiation media, for 2 day prior to immunofluorescence staining. Red arrows indicate nuclear localisation. Images representable of multiple images (n = 6).

Microscopic analysis confirmed that cells had adopted a spindle like morphology upon treatment with either IBMX or full differentiation cocktail as illustrated in Figure 3.9. This morphological change seems to be a characteristic primary event in 3T3-L1 differentiation and may be a useful measurement for the screening of pro- or anti-adipogenic compounds. Oil Red O staining showed that individual treatment with rosiglitazone, IBMX or dexamethasone resulted in an increase in the accumulation of lipids. It is important to note that differentiation was only monitored for 3.5 days post-induction and that Oil Red O staining was carried out at this point. As cells were not allowed to fully differentiate, Oil Red O staining was expected to be low. The accumulation of lipids was not detected by the xCELLigence system. This was expected as the system measures impedance and is therefore only able to measure changes as a result of cell size, morphology and membrane potential and not changes as a result of composition of cells.

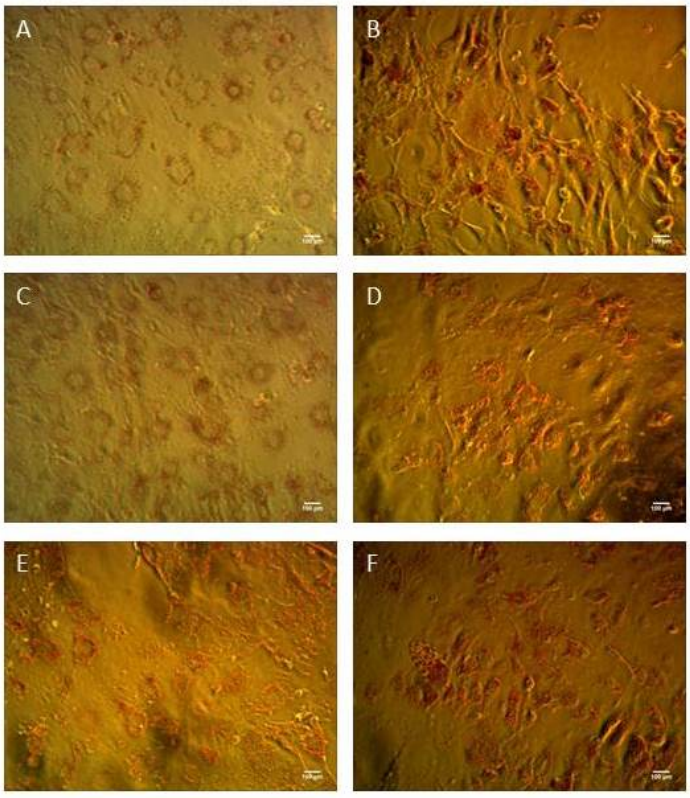

Figure 3.9: Oil Red O staining of xCELLigence samples 3.5 days post induction A) Maintenance media, B) Differentiation Media, C) Insulin Media, D) Rosiglitazone Media, E) IBMX Media, F) Dexamethasone Media. Scale bars = 100 μm

To illustrate that preadipocytes and differentiated adipocytes are completely different cell phenotypes, in terms of cell type, cell size, cell shape and cell property, both preadipocytes and 14 days old differentiated adipocytes were plated at the same density onto the xCELLigence system and growth monitored and compared. As expected, the 2 cell types had different *CI* profiles as shown in Figure 3.10. Interestingly, adipocytes had lost the distinctive *CI* peak directly after plating the cells. This peak was routinely observed when plating preadipocytes on the system. Differentiated adipocytes had much lower *CI* values, and, as analysed using the xCELLigence software, grow much more slowly. Doubling time was calculated between 5 and 22 hours post-seeding. Adipocytes were found to have a doubling time of 37 ± 1.06 h while that of the preadipocyte progenitors were found to have a doubling time of 21.6 ± 3.28 h. Lower *CI* values further indicate that adipocytes are not as adherent as their fibroblast-like progenitors.

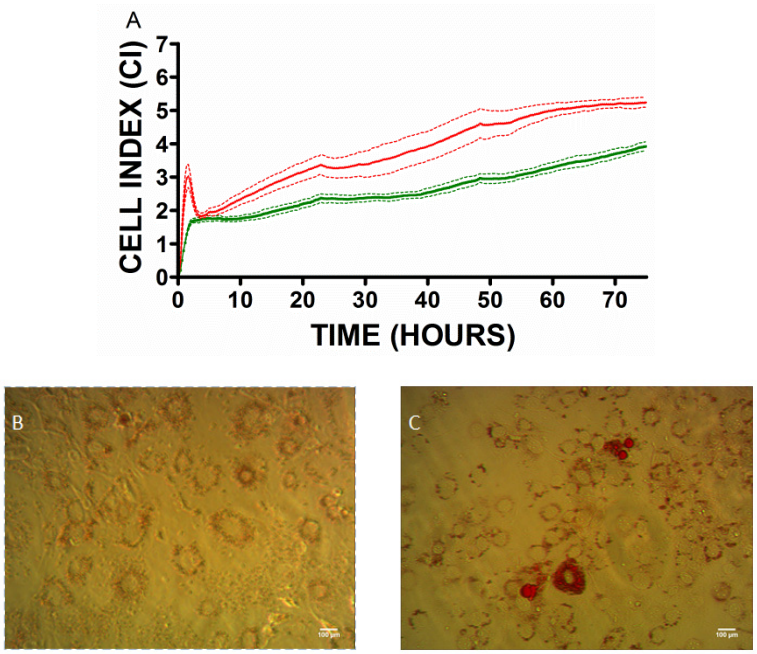

Figure 3.10: CI curves and Oil Red O staining of undifferentiated and differentiated adipocytes. (A) *CI* curves of 3T3-L1 preadipocytes (red) and differentiated adipocytes (green). Oil Red O staining of (B) preadipocytes and (C) adipocytes. All curves were plotted as an average of quadruplicate treatments. Data was plotted using GraphPad Prism v4.0

Real time monitoring of differentiation of HMSC-ad mesenchymal stem cells

xCELLigence RTCA experiments optimized using the 3T3-L1 line were repeated using the HMSC-ad cells to determine whether a similar results would be achieved and whether differentiation in these cells could be monitored effectively. Mesenchymal adipogenesis has been monitored previously using an impedance based system (Bagnaninchi & Drummond, 2011), however to date has not been monitored utilizing the xCELLigence RTCA system.

Mesenchymal stem cells remain in an undifferentiated state only in specific conditions and will spontaneously differentiate if these conditions are not met. For this reason, HMSC-ad cells must be grown in specific maintenance media which must be completely replaced upon the induction of differentiation with differentiation media. In xCELLigence experiments utilizing 3T3-L1 cells differentiation components were simply added to wells without the removal of basal media in which cells were seeded. As HMSC-ad maintenance media contains factors which maintain the undifferentiated state of HMSC-ad cells (Bone *et al*, 2009; Reed & Johnson, 2014), slight changes to the original xCELLigence protocol had to be made.

Cells were seeded onto the system in HMSC-ad maintenance media. Cells were then induced to differentiate, or treated with individual components of the differentiation cocktail 42 hours post-seeding, by completely removing HMSC-ad media, washing cells with PBS and finally adding basal media containing the relevant compounds at the required concentration.

HMSC-ad cells settled on the surface, with a distinctive peak, observed within the first 2 hours post-seeding. This peak was similar but not as pronounced as the peak observed with 3T3-L1 cells. *CI* values remained relatively low, possibly indicating that the cells did not adhere as strongly to surface as the 3T3-L1 preadipocytes. During the period prior to induction of differentiation, *CI* values remained relatively unchanged, as seen in Figure 3.11. Based on microscopic analysis, cells were found to be proliferating rapidly, and therefore *CI* values were expected to increase as well. The unchanged *CI* values could be an indication that the cells became confluent and then continued to grow in multilayers, meaning new cells did not come into contact with the electrode surface and a therefore no change in *CI* was measured. Uninduced mesenchymal stem cells proliferate symmetrically (discussed in Chapter 1, Section 1.1), and this may explain why when induced to differentiate, resulting in asymmetric division, a distinct change in *CI* values was observed. The untreated sample resulted in a *CI* curve which indicated the gradual increase in *CI* values potentially indicating

greater adherence to the sensor surface resulting from increased cells numbers, as shown in Figure 3.11A.

Interestingly, the induction of adipocyte differentiation (Figure 3. 10B) produced a distinctive *CI* curve. As opposed to a dramatic drop in *CI* values observed in 3T3-L1 differentiation, HMSC-ad cells induced to differentiate resulted in a dramatic increase in *CI* values. As undifferentiated HMSC-ad are much smaller and spindle-like than 3T3-L1, take up lipids more readily and increase in size upon induction of differentiation (Figure 3.1A and B) an increase in *CI* was expected. This increase can be further explained by 1) an increase in doubling time (i.e. growth); 2) increased adherence, and 3) a change in morphology. As previously mentioned, a switch from symmetric cell division to asymmetric division may explain further explain the dramatic change in *CI* values accompanied by the induction of differentiation.

It has been reported that Mitotic Clonal Expansion does not occur in bone marrow derived mesenchymal stem cell adipocyte differentiation and that these cells do not exhibit contact inhibition (Qian *et al.*, 2010). It has been noted in our lab that HMSC-ad cells too, do not exhibit contact inhibition. Despite the absence of contact inhibition and MCE, these results could indicate that HMSC-ad undergo a period of accelerated growth comparable to MCE in the 3T3-L1 model upon the induction of differentiation. This period of potential accelerated growth lasted for about 12 hours post-induction.

As these cells are normally cultured in specialized media containing a variety of factors to maintain their multipotent state, the effect of removing this specialised media and replacing it with basal media was investigated. Results indicated that upon the removal of HMSC media, *CI* values dramatically increased for about 24 hours, more so than that of cells induced to a directed differentiation. This increase in *CI* could indicate the initiation of uncontrolled growth and the spontaneous differentiation of the mesenchymal stem cells.

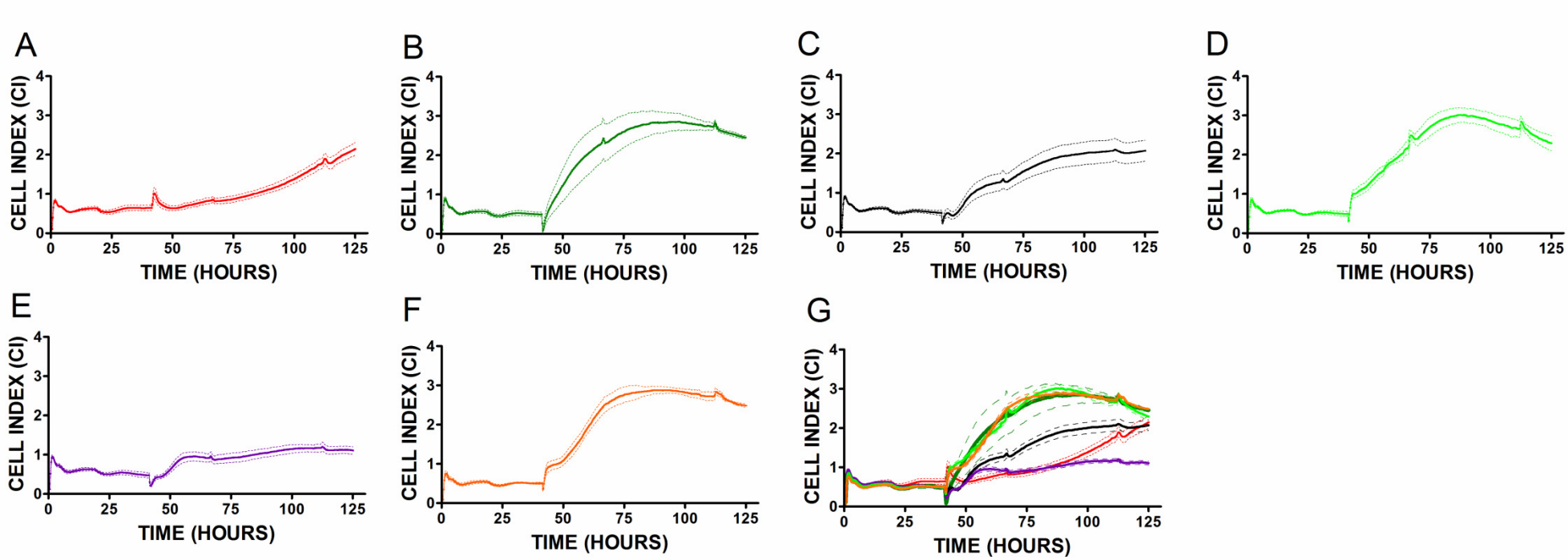

Figure 3.11: Effects of individual components of, and full differentiation cocktail on HMSC-ad growth CI curves. Cells were treated at the same time with: A) HMSC-ad maintenance media B) DMSO and EtOH (control), C) Differentiation cocktail (INS/DEX/IBMX/ROSI), D) Insulin, E) IBMX, and F) Dexamethasone. G) Comparison of all treatments. Dotted lines represent standard deviations. All curves were plotted as an average of quadruplicate treatments. Data was plotted using GraphPad Prism v4.0

The effect of the individual components of the differentiation media on the HMSC-ad cells was investigated as well. The removal of the HMSC media was expected to result in an increase in *CI* values as discussed previously. The addition of either insulin, dexamethasone or IBMX to the replacement basal media however, were found to alter the *CI* curves of the HMSC-ad cells. As was the case with 3T3-L1 cells, both insulin treatment (Figure 3.11D) and dexamethasone treatment (Figure 3.11F) resulted in significantly altered *CI* profiles when compared to cells in basal media, however IBMX treatment (Figure 3.11E) was the only compound able to produce a *CI* profile similar to that of cells treated with the full differentiation cocktail. IBMX treated cells resulted in an increase of *CI* values in a manner comparable but not identical to the full differentiation *CI* profile.

Oil Red O Staining was performed on all samples after the xCELLigence experiment was over, 3.5 days post-induction. It was found that lipid accumulation had occurred in cells treated with the full differentiation cocktail as shown in Figure 3.12B. Interestingly, small inclusions of lipids were detected in undifferentiated cells as well (Figure 3. 12A).

In all samples where the HSMC media had been removed, the morphology of the cells had changed significantly. Cells had become larger and more rounded, suggesting that the increase in *CI* values could have been a result of morphology changes occurring with the spontaneous differentiation of the cells. Cells treated with dexamethasone (Figure 3. 12F) or IBMX (Figure 3. 12E) had increased lipid accumulation, a result similarly observed in 3T3-L1 cells. Interestingly cells treated with dexamethasone had the most altered morphology.

It can be speculated, based on the *CI* curves resulting from the treatment of 3T3-L1 and HMSC-ad cells with individual components making up the differentiation cocktail that IBMX is the most important component. These results indicate that the action of IBMX, that is repressing Sp1, thereby leading to an increase in the expression of C/EBPβ, and allowing for intracellular cAMP levels to increase, are the main events leading to the induction of differentiation and associated primary morphological changes.

Again, to illustrate that mesenchymal derived adipocytes are completely different to undifferentiated mesenchymal stem cells, in terms of cell type, size, shape and property, both undifferentiated HMSC-ad cells and 7 day old differentiated adipocytes were plated at the same density onto the xCELLigence system and their growth monitored and compared. As expected, the 2 cell types had different *CI* profiles as shown in Figure 3.13A.

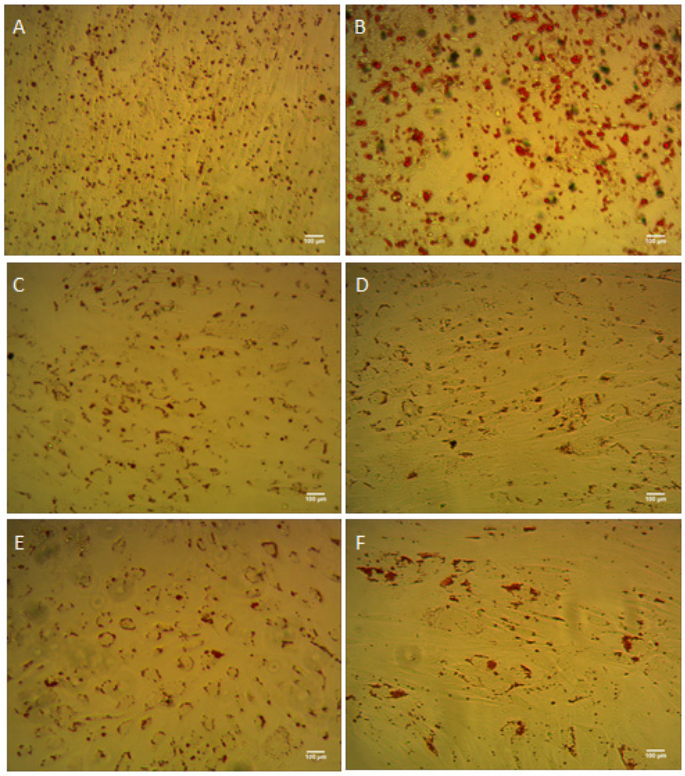

Figure 3.12. Oil Red O staining of HMSC-ad xCELLigence samples 3.5 days post-induction A) HMSC Maintenance media, B) Differentiation Media, C) Basal Media, D) Insulin Media, E) IBMX Media, F) Dexamethasone Media. Scale bars = 100 µm.

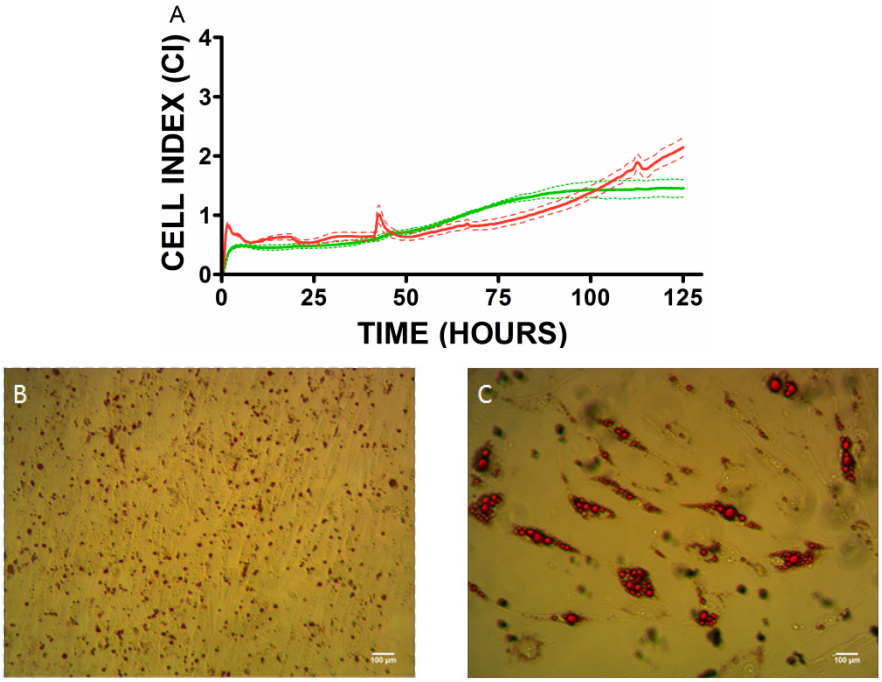

Figure 3.13. *CI* curves and Oil Red O staining of undifferentiated and differentiated HMSC-ad cells. (A) *CI* curves of uninduced HMSC-ad cells (red) and differentiated HMSC-ad derived adipocytes (green). Oil Red O staining of (B) uninduced HMSC-ad cell and (C) HMSC-ad derived adipocytes after plating. All curves were plotted as an average of quadruplicate treatments.

Similarly, as observed in the 3T3-L1 experiments, adipocytes lost the distinctive *CI* peak normally observed in undifferentiated cells directly after seeding. This peak was routinely observed when plating HMSC-ad cells on the system. Both cell types were found to have similar *CI* values, however curves of the two cell types were significantly different and eventually undifferentiated cell *CI* values increased while adipocyte *CI* values remained relatively constant

3.3 Conclusion

The development of an assay utilizing a commercially available impedance based real time cell analyser is reported here. The results reflected that the ACEAf xCELLigence RTCA SP system can effectively monitor the primary morphological changes that occur upon induction of differentiation of 3T3-L1 preadipocytes. Further to this, the ability of the system to monitor the changes in a 96-well plate format illustrates the possibility that it can be used to screen for pro-adipogenic compounds, and, therefore the system may be beneficial in the search for anti-adipogenic compounds.

Due to a limited supply, the individual effect of rosiglitazone on the *CI* profile of HMSC-ad cells was not investigated, and the experiment will have to be performed in the near future to complete the data set. Further experiments and controls would be beneficial to make the monitoring of adipogenic differentiation using the ACEA xCELLigence RTCA more robust. Western blot and immunofluorescence analysis to detect for further adipogenic factors such as C/EBPα and δ, as well as PPARγ would allow for a more in depth understanding of when in the differentiation process and perhaps why these primary morphological changes occur.

These experiments illustrate the potential use of the system in the development of optimal differentiation protocols. Further experiments could include treating cells with a range of concentrations of each differentiation component to allow for an optimal differentiation procedures to be developed. Although only the primary morphological changes associated with differentiation were investigated in this study, it would be interesting to monitor differentiation over an extended time, monitoring the entire differentiation process in an attempt to identify further morphological changes which may occur during differentiation. We have shown that the complete replacement of media has minimal effect on the ability of the xCELLigence system to make accurate *CI* measurements and therefore experiments can be run for extended periods of time.

This technology, combined with already established end point assays such as Oil Red O staining, as well as molecular techniques such as immunofluorescence microscopy and Western blot analysis can help immensely in the search for compounds which may induce, or inhibit cellular differentiation. By defining differentiation *CI* profiles for cells with the potential to differentiate, impedance based real time cell analysis can be used as an initial screen for compounds which may have pro- or anti- differentiation actions and allow for optimum differentiation protocols to be developed.

Chapter 4

An investigation of STAT3 expression, localisation, post-translational modifications and effects of inhibition during adipogenesis.

Specific objectives:

1. **Investigate levels and localisation of STAT3 during adipogenesis of both 3T3-L1 and HMSC-ad cells**
2. **Investigate the localisation of unphosphorylated and phosphorylated forms of STAT3 upon individual differentiation compound treatment and STAT3 and MEK inhibition within 3T3-L1 preadipocytes.**
3. **Utilize the xCELLigence real-time differentiation assay described in Chapter 2 to monitor differentiation of 3T3-L1 preadipocytes in the presence of a STAT3 and MEK inhibitor**

4. An investigation of STAT3 expression, localisation, post-translational modifications and effects of inhibition during adipogenesis.

As the regulation of transcription factor access to the nucleus is a means to control the transcription of certain genes, the nuclear trafficking of STAT3 is essential to its function as a transcription factor. It has been shown that STAT3 possesses a constitutive nuclear localisation signal and that import of STAT3 is independent of tyrosine phosphorylation but is dependent on the action of RanGTP and importin β1 (Cimica *et al.,* 2011). Liu *et al*., (2005) showed that although tyrosine phosphorylation of STAT3 is required for STAT3 to bind DNA, nuclear import occurs independently of tyrosine phosphorylation. STAT3 was shown to shuttle between cytoplasmic compartments while maintaining a prominent nuclear localisation.

This nuclear localisation of unphosphorylated STAT3 has been observed in multiple reports (Pranada *et al.*, 2004; Liu *et al.*, 2005). Further to this it has been reported that the shorter β isoform has a longer nuclear retention time that than the longer α isoform of STAT3. As previously described the isoforms of the STAT3 molecule result from alternative splicing of the same gene and differ only in the C terminus. STAT3β is shorter than STAT3α, where 55 amino acid residues of STAT3α are replaced by 7 residues in STAT3β on the C terminus (Schaefer *et al.,* 1997). The relative sizes of STAT3α and β are approximately 92 and 84 kDa respectively (Ng *et al.,* 2012). Properties of the two isoforms have been shown to differ with respect to DNA binding activities both *in vitro* (Park *et al.,* 1996) and *in vivo* (Schaefer *et al.,* 1997). STAT3α and STAT3β show no difference in terms of DNA binding strength but it has been shown that STAT3β dimers are more stable and this plays a critical role in determining the DNA binding activity of the STAT3 isoforms (Park *et al.,* 2000).

It has been shown that the kinetics of phosphorylation of the 2 isoforms differs and that there is sustained nuclear translocation and phosphorylation of STAT3β, the shorter of the two major isoforms. Interestingly the same research showed that STAT3β enhanced and prolonged the phosphorylation of STAT3α (Ng *et al.*, 2012). Huang *et al.* (2007) showed that STAT3β has a significantly prolonged nuclear retention time than STAT3α and concluded that the two isoforms have distinct intracellular dynamics.

The phosphorylation of the 727 serine residue most probably occurs on the STAT3α isoform of STAT3, which has the terminal 55 amino acid residues that STAT3α lacks. As the β isoform is only 722 amino acids in length, it lacks the serine 727 residue and this may play a role in the nuclear retention of STAT3β. The fact that pSTAT3S727 must be the α isoform of STAT3, that the phosphorylation of this residue has been implicated in the mitochondrial localisation of STAT3 and that STAT3α has a shorter nuclear retention time than its β counterpart are all good indications that the serine phosphorylated form of STAT3α may play a non-canonical role independently of its nuclear role.

STAT3 levels and localisation were investigated for the first 6 days of differentiation in 3T3-L1 cells and the first 3 days of differentiation in HMSC-ad cells based on the assumption that differentiation in the HMSC-ad cells was occurring more rapidly as lipid uptake was significantly higher as shown in Chapter 1, Section 2.2.1, Figure 2.1A and B.

4.1 Localisation of total STAT3, pSTAT3Y705 and pSTAT3S727 in 3T3-L1 cells during adipogenesis

Firstly, the localisation of total STAT3 (tSTAT3) was investigated. As expected, in uninduced cells (Figure 4.1, Day 0) tSTAT3 had a predominantly nuclear localisation (100% of cells, n = 32) with low signal being observed in the cytoplasm. This nuclear localisation persisted for 2 days (Day 1, 96% of cells, n = 47; Day 2, 79% of cells, n = 57) post-induction although cytoplasmic signals did increase. On Day 3 post-induction, a significant decrease in the nuclear localisation of total STAT3 was observed with a loss of nuclear localized tSTAT3 observed in 100% of cells analysed (n = 43) as indicated by the red arrows in the Day 3 panel of Figure 4.1. This loss of nuclear STAT3 did not persist and 4 days post-induction nuclear localisation was again observed in 71% of cells (n = 42). Finally, through days 5 and 6 of differentiation, the staining became diffuse throughout the cells. The changes in the localisation of tSTAT3 indicates that STAT3 is playing a potential role during differentiation. The punctate structures formed could be STAT3 localizing to specific organelles such as the mitochondria where STAT3 has been shown to localise (Wegrzyn *et al.*, 2009) or potentially to cytoplasmic endosomes (Xu *et al.*, 2007; Mukhopadhyay *et al.*, 2008).

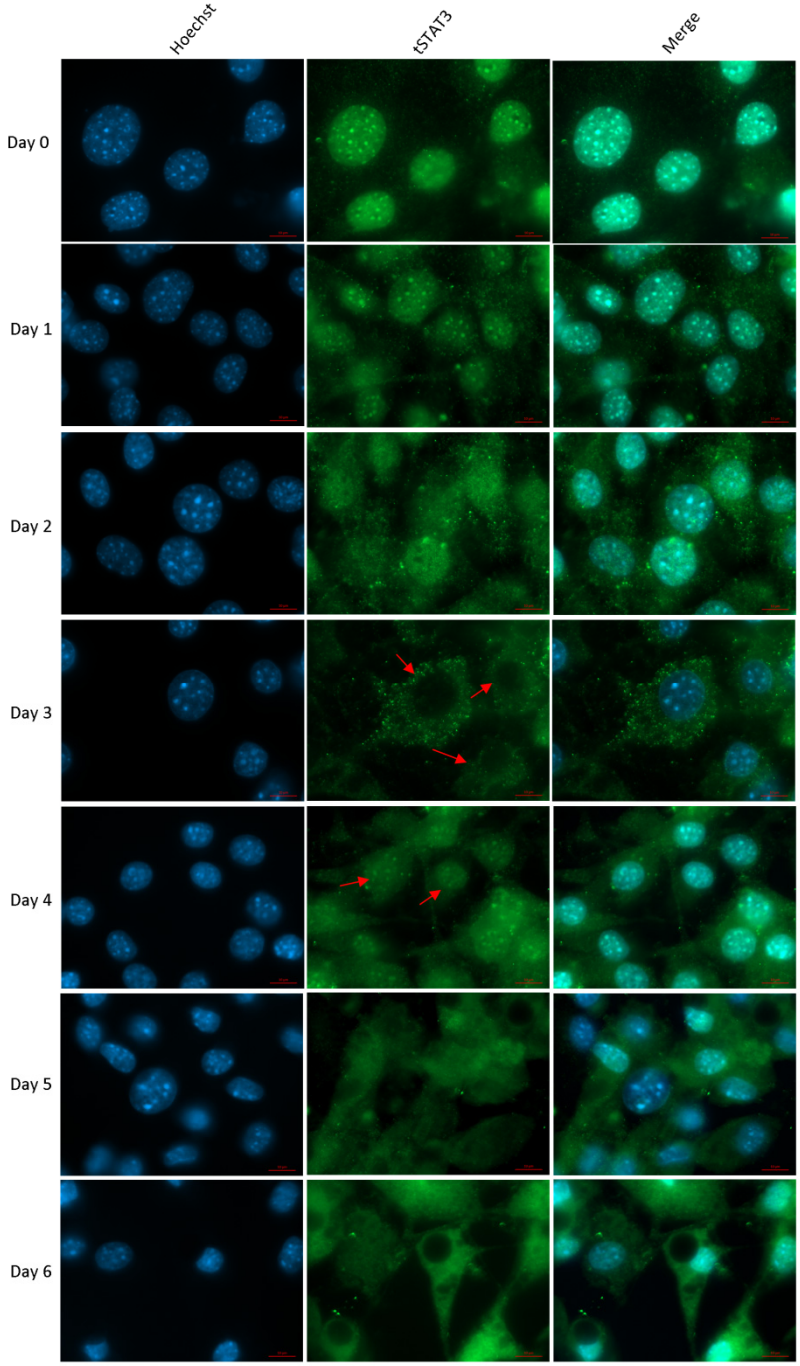

Figure 4.1: Localisation of whole STAT3 (tSTAT3) during 3T3-L1 adipocyte differentiation. Immunofluorescence analysis of the localisation tSTAT3 through days 1 to 6 of 3T3-L1 adipocyte differentiation. Red arrows highlight the loss of nuclear localisation on Day 3 and the return of nuclear localisation 4 days post induction. Scale bars = 10 µm. Images were captured using a Zeiss AxioVert.A1 FL-LED Fluorescence Microscope at 1000x magnification. Images representable of multiple images (n = 6).

Next, the localisation of tyrosine phosphorylated, the canonically activated form of STAT3 (pSTAT3Y705), was investigated. In uninduced cells (Figure 4.2, Day 0), as expected, pSTAT3Y705 had a distinctly nuclear localisation (100% of cells, n = 48) which became much less prominent upon the induction of differentiation. For Days 1 and 2 of differentiation (Figure 4.2) pSTAT3Y705 staining was diffuse throughout all cells observed, with higher staining in the cytoplasm than in uninduced cells being observed. On Day 3 of the differentiation procedure, a distinct lack of nuclear pSTAT3Y705, consistent with tSTAT3 staining was observed in 77% of observed cells (n = 35) as highlighted by the red arrow in Figure 4.2, Day 3. Distinct nuclear staining returned 4 days post-induction (86% of observed cells, n = 30), which persisted to Day 5 (52% of observed cells, n = 54). Staining then became diffuse throughout all observed cells 6 days post-induction (n = 52).

Attempts to investigate levels of pSTAT3Y705 were also made, with moderate success. Although the antibody performed well in immunofluorescence experiments, the antibody did not perform optimally during western blot experiments. This could have been the result of a number of reasons, for instance the epitope the antibody recognized may have been a secondary, tertiary or quaternary structure and may have been denatured during the preparation of Western blot samples. However, preliminary results indicate that levels of pSTAT3Y705 decrease during differentiation as shown in Figure 4.2B. Interestingly both the α and β isoform of STAT3 were detected when probing for the tyrosine 705 phophorylated STAT3 as seen if Figure 4.2B. This preliminary result shows that upon the induction of differentiation pSTAT3Y705 levels remain relatively unchanged for 3 days post induction and then start to decrease gradually through days 4 to 5 of differentiation.

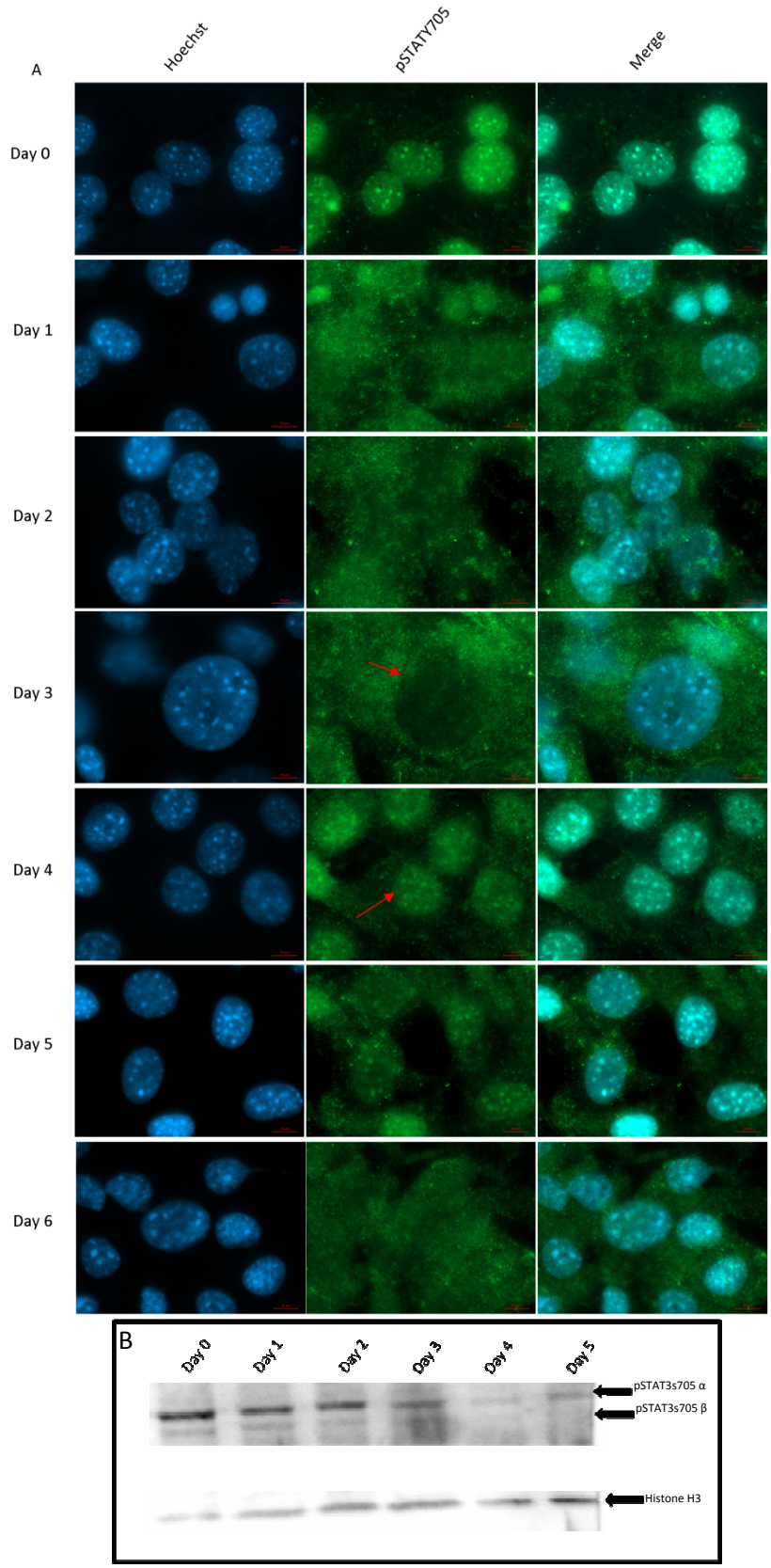

Figure 4.2: Localisation and levels of pSTAT3Y705 during 3T3-L1 adipocyte differentiation. (A) Immunofluorescence analysis of the localisation pSTAT3Y705 through days 1 to 6 of 3T3-L1 adipocyte differentiation. . Red arrows highlight the loss of nuclear localisation on Day 3 Scale bars = 10 µm. Images were captured using a Zeiss AxioVert.A1 FL-LED Fluorescence Microscope at 1000x magnification. Images representable of multiple images (n = 6). (B) Levels of pSTAT3Y705 during 3T3-L1 preadipocyte dipogenesis. (A) Western blot of pSTAT3Y705 through days 0 to 5 of differentiation. Equal amounts of protein were run and pSTAT3Y705. Histone H3 was used a loading control.

Finally, the localisation of the serine phosphorylated, the non-canonically activated form of STAT3 (pSTAT3S727) was investigated. Pre-induced preadipocytes were found to have nuclear localized pSTAT3S727 (80% of cells observed, n = 24) although this nuclear staining with was noticeably different to that of pSTAT3705 staining and did not appear to be as defined as shown in Figure 4.3A, Day 0. High signals were also observed in the cytoplasm of the cells as compared to the tyrosine phosphorylated form of STAT3. Staining for pSTATS727 in preadipocytes also revealed slight punctate and reticulate staining not observed in either tSTAT3 staining, probably masked due to additional signal as a result of unphosphorylated STAT3 and pSTATY705 staining; or in pSTAT3Y705 staining. Upon differentiation, Figure 4.3 Day 1, nuclear staining persisted (87%, n = 53) while there was a definite increase of pSTAT3S727 signal detected in the cytoplasm of cells as shown in Figure 4.3A, Day 1.

On Day 2, nuclear staining became less distinct while cytoplasmic staining became more prominent with only 51% of observed cells (n = 64) having nuclear staining, and by Day 3 nuclear staining was not observed at all (n = 50), consistent with both tSTAT3 and pSTAT3Y705 staining. Cytoplasmic staining on Day 3 revealed distinct punctate structures as highlighted by red arrows in Figure 4.3, Day 3. This staining pattern persisted to Day 4 (74%, n = 43), with the nuclear localisation of pSTATS727 starting to return 5 days post-induction (42%, n = 70) and becoming more distinct on Day 6 (53%, n = 34) (Figure 4.3A, Day 6).

The levels of pSTAT3S727 were investigated through Western blotting and densitometric analysis utilizing ImageJ (NCBI). Results indicated that levels of pSTAT3S727 increased during differentiation as shown in Figure 4.3B with levels at Day 6 found to be highest. One distinct band at approximately 90 kDa was routinely detected when probing for pSTAT3S727, and was most probably the larger STAT3α isoform being detected. This is in line with the speculations about the isoform of pSTAT3S727 previously discussed.

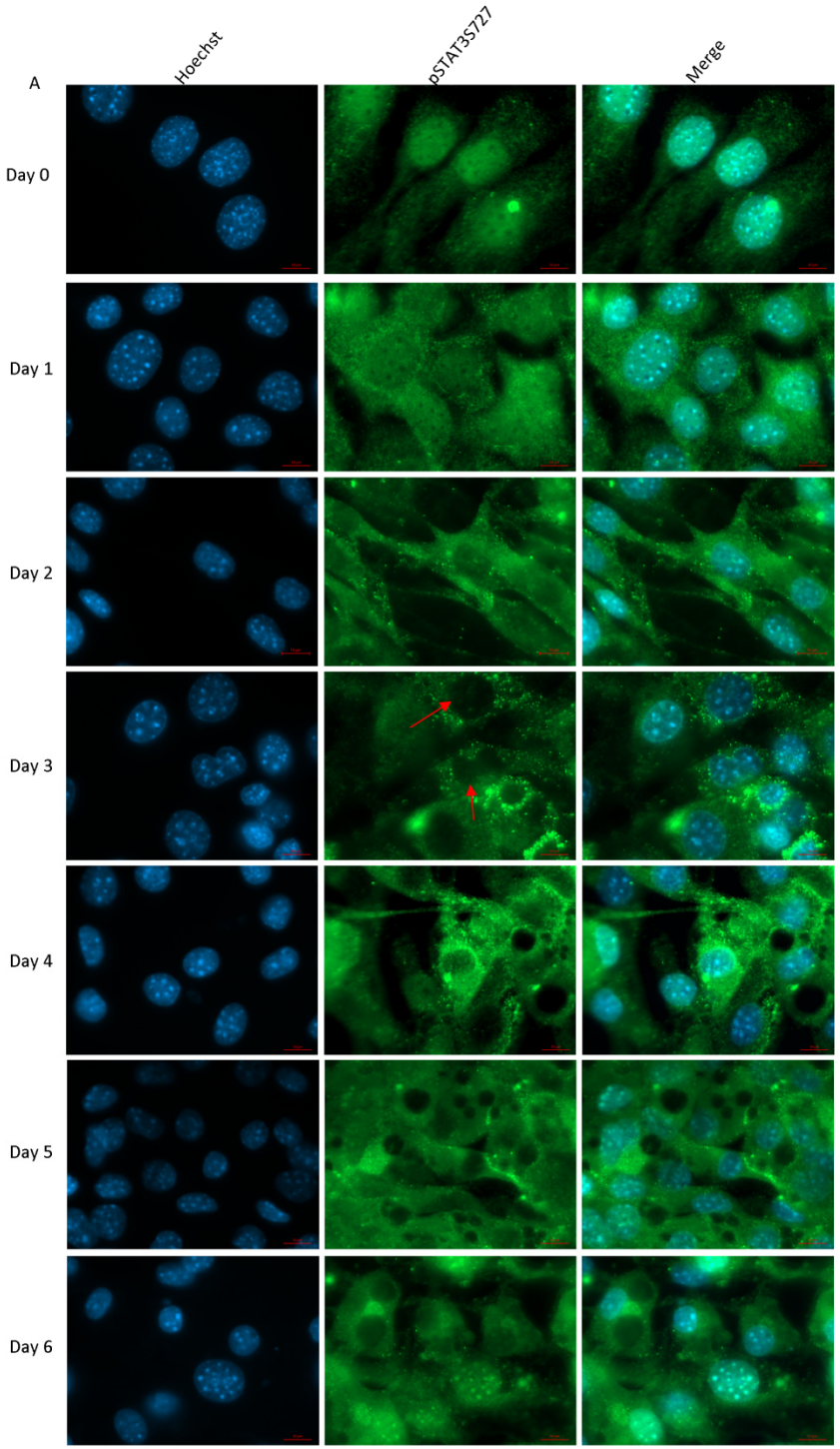

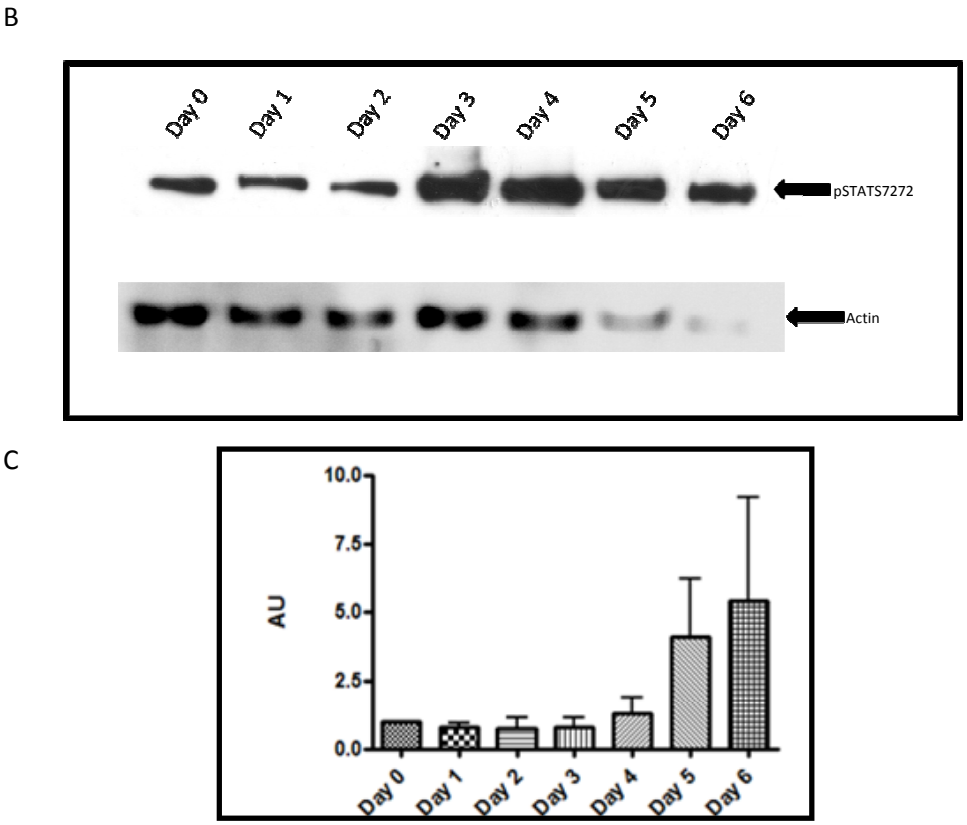

Figure 4.3: Localization and levels of pSTAT3S727 during 3T3-L1 adipocyte differentiation. (A) Immunofluorescence analysis of the localization pSTAT3S727 through days 1 to 6 of 3T3-L1 adipocyte differentiation. Red arrows highlight the loss of nuclear localization on Day 3. . Scale bars = 10 µm. Images were captured using a Zeiss AxioVert.A1 FL-LED Fluorescence Microscope. Analysis was performed at 1000x magnification. Images representable of multiple images (n = 6). (B) Western blot of pSTAT3S727 through days 0 to 6 of differentiation. Equal amounts of protein were run and pSTAT3S727 signal normalised against actin as a loading control. (n = 3). (C) Densitometry analysis of levels of pSTAT3S727 during differentiation (n = 3). Data was plotted using GraphPad Prism V4.0

.

These results indicate that pSTAT3Y705 is more active, as indicated by the dominant nuclear localisation, in preadipocytes than in differentiating cells. When cells are induced to differentiate, there is a distinct loss of nuclear localized pSTAT3Y705 24 hours post induction, indicating a loss of tyrosine phosphorylated STAT3. Similar conclusions were drawn by Deng *et al.,* (2000) who showed that STAT3 was highly tyrosine phosphorylated in preadipocytes, but not in adipocytes. The group also showed that inducing preadipocytes to differentiate led to a delayed but prolonged increase in pSTAT3Y705 lasting 3 days. The fact that pSTAT3Y705 levels are higher in proliferating preadipocytes and that levels only start to decrease after mitotic clonal expansion could indicate that canonically activated STAT3 is important during proliferation and not necessarily in later adipogenic events. It has been shown that pSTAT3Y705 is activated upon the induction of adipogenesis in 3T3-L1 cells and results of the same study indicate that pSTAT3Y705 is potentially involved in regulating the expression of C/EBPβ (Zhang *et al.,* 2011).

The action of pSTAT3Y705 reported by Zhang and colleagues occurs within the first 2 hours of adipogenic induction, during the early stages of adipogenesis. As analysis of the localisation and expression levels of pSTAT3Y705 was run on samples collected at 24 hour intervals in this investigation and is most likely the reason the increased levels of pSTAT3Y705 reported by Zhang *et al.,* (2011) were not detected here.

Notably, nuclear localisation of pSTAT3Y705 was observed in later stages of adipogenesis as shown by the red arrow, Figure 4.2, Day 5. This result may be explained by the expression of PPARγ, which is known to only be activated a few days post induction (see Figure 1.5 Chapter 1, Section 3.2). The expression of PPARγ has been reported to mediated by canonically active STAT3 (Wang *et al*., 2010), which may explain the reoccurrence of the nuclear localisation of pSTAT3Y705 observed later during differentiation (Figure 4.2, Day 4 and 5).

The overall reduction in the levels of pSTAT3Y705 may be further explained by the role insulin plays during differentiation and the fact that cells were fed with media supplemented with insulin for a further 2 days after exposure to the full differentiation cocktail. It has been shown in 3T3-L1 adipocytes that insulin has an inhibitory effect on IL-6 signalling by reducing tyrosine phosphorylation of STAT3 by activating protein tyrosine phosphatase, required for the dephosphorylation of pSTAT3Y705. The same research showed that insulin increases serine phosphorylation of STAT3 (Campos *et al.,* 1996).

Little is known about the role pSTAT3S727 plays during differentiation events. Results indicating that levels increase during differentiation suggest that the non-canonical form of STAT3 is playing a crucial role in adipogenesis. As mentioned previously, it has been reported that insulin reduces tyrosine phosphorylation and increases serine phosphorylation of STAT3 (Campos *et al.*, 1996). Reports have shown that serine phosphorylation of STAT3 happens independently of tyrosine phosphorylation and that insulin stimulated serine phosphorylation of STAT3 occurs via a mitogen activated protein kinase (MEK) dependant pathway (Ceresa *et al.*, 1997).

Serine phosphorylated STAT3 had been implicated as playing a role in the mitochondria (Demaria & Poli, 2011; Gough *et al*., 2009; Wegrzyn *et al*., 2009). It may be that the increase in levels of pSTAT3S727 during differentiation may be a result of increased mitochondrial biogenesis, which is known to occur during adipocyte differentiation (Wilson-fritch *et al.*, 2003). This explanation would also account for the punctate staining observed during the differentiation of 3T3-L1 cells, however further experiments are required to confirm these hypotheses.

4.2 Localisation of tSTAT3, pSTAT3Y705 and pSTAT3S727 in 3T3-L1 cells treated with individual components of the differentiation cocktail

As insulin is known to result in the serine phosphorylation of STAT3, it was investigated whether the increase in levels of pSTAT3S727 observed during differentiation was as a result of differentiation and not an artefact of a single component of the differentiation cocktail, such as insulin. Cells were treated with each component for 0-6 days and levels investigated by Western blot analysis. Further to this, to investigate whether the changes in the localisation of all forms of STAT3 was a result of differentiation or, a response to a single component in the differentiation cocktail, cells were treated with either ethanol (EtOH) and DMSO (solvent controls), dexamethasone, IBMX, insulin or rosiglitazone for 3 days (the point at which the most dramatic change in localisation was observed during differentiation) and subjected to immunofluorescence analysis.

Immunofluorescence analysis revealed that the localisation of tSTAT3 did not change and remained primarily nuclear with all treatments (Figure 4.4). All cells treated with the solvent control (n = 32) had distinctly nuclear localized tSTAT3, as did cells treated with dexamethasone (n = 36), IBMX (n = 28), insulin (n = 8) and rosiglitazone (n = 26).

The localisation of pSTAT3Y705 did not change upon treatment with DMSO and EtOH (n = 34) dexamethasone (n = 46), IBMX (n = 31), or rosiglitazone (n = 43) with all cells found to have strong nuclear localisations of pSTAT3Y705. However, there was a clear loss of the nuclear localisation of pSTATY705 when cells were treated with insulin as seen in Figure 4.5, with only 13% of observed cells having nuclear localized pSTAT3Y705 (n = 37).

The localisation of pSTAT3S727 remained relatively unchanged in cells treated with EtOH and DMSO, dexamethasone and IBMX with 78% (n =27), 93% (n = 27) and 91% (n = 32) of cells having nuclear localized pSTATS727. When treated with insulin, the nuclear localisation of pSTAT3S727, in contrast to pSTAT3Y705 localisation, seemed to increase with 95% of observed cells (n = 45) having more prominently nuclear localized pSTAT3S727. Treatment with rosiglitazone seemed to decrease the nuclear localisation pSTAT3S727 and result in cytoplasmic punctate structures being formed as shown in Figure 4.6. This phenotype was observed in 89% of observed cells (n = 27)

Despite the effects both insulin and rosiglitazone had on the localisation of pSTAT3Y705 and pSTAT3S727, the dramatic changes of the localisation observed in cells induced to differentiate was not observed. The fact that rosiglitazone resulted in an increase in cytoplasmic staining is of particular interest as rosiglitazone has been shown to increase mitochondrial biogenesis (Pardo *et al.*, 2011; Wilson-fritch *et al.*, 2003), and this result warrants further investigation.

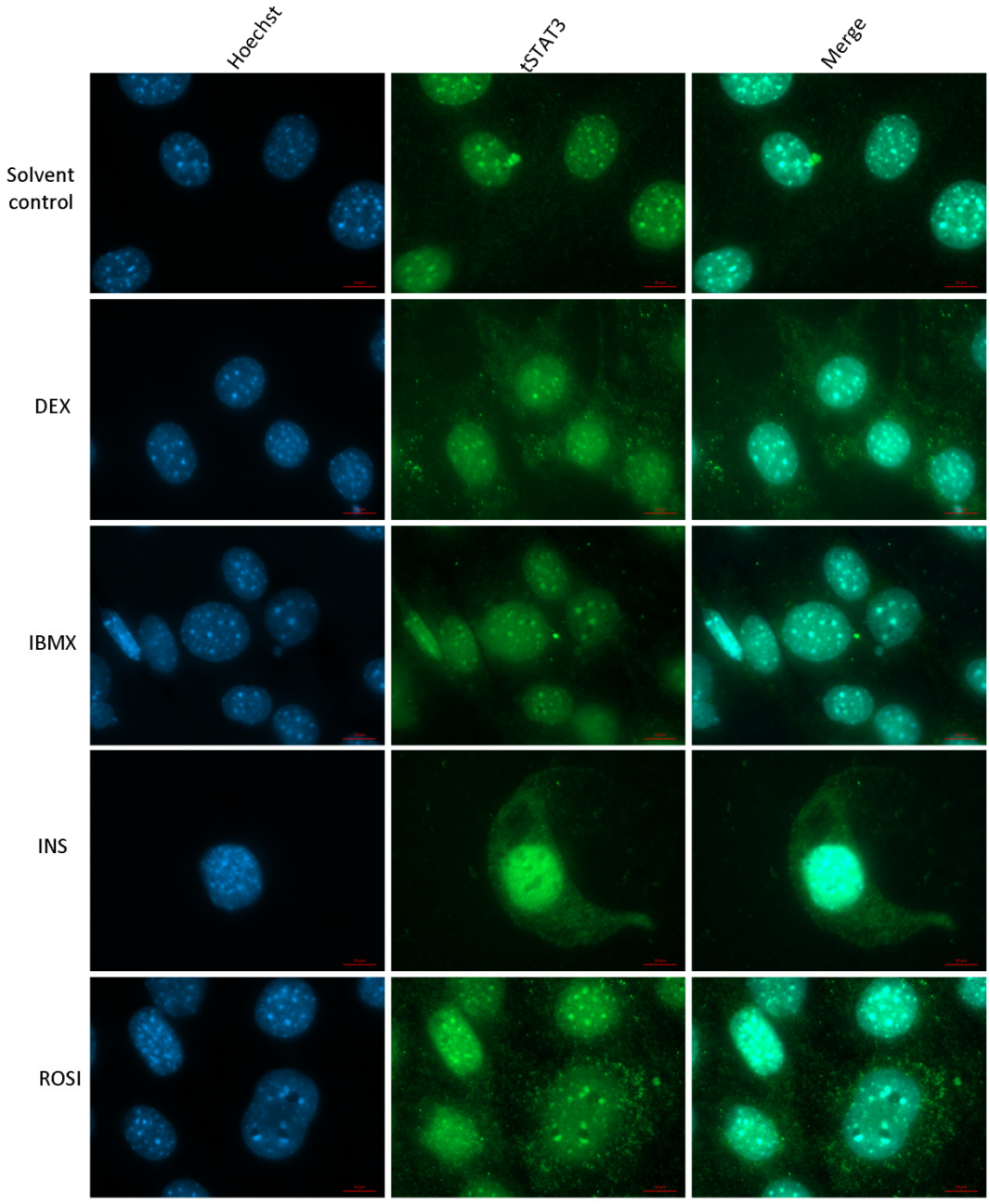

Figure 4.4: Localisation of tSTAT3 in 3T3-L1 preadipocytes treated with individual components making up the differentiation cocktail. Immunofluorescence analysis of the localisation tSTAT3 in 3T3-L1 preadipocytes after 3 days of treatment with dexamethasone, IBMX, insulin or rosiglitazone. Scale bars = 10 µm. Images were captured using a Zeiss AxioVert.A1 FL-LED Fluorescence Microscope at 1000x magnification. Images representable of multiple images (n = 6).

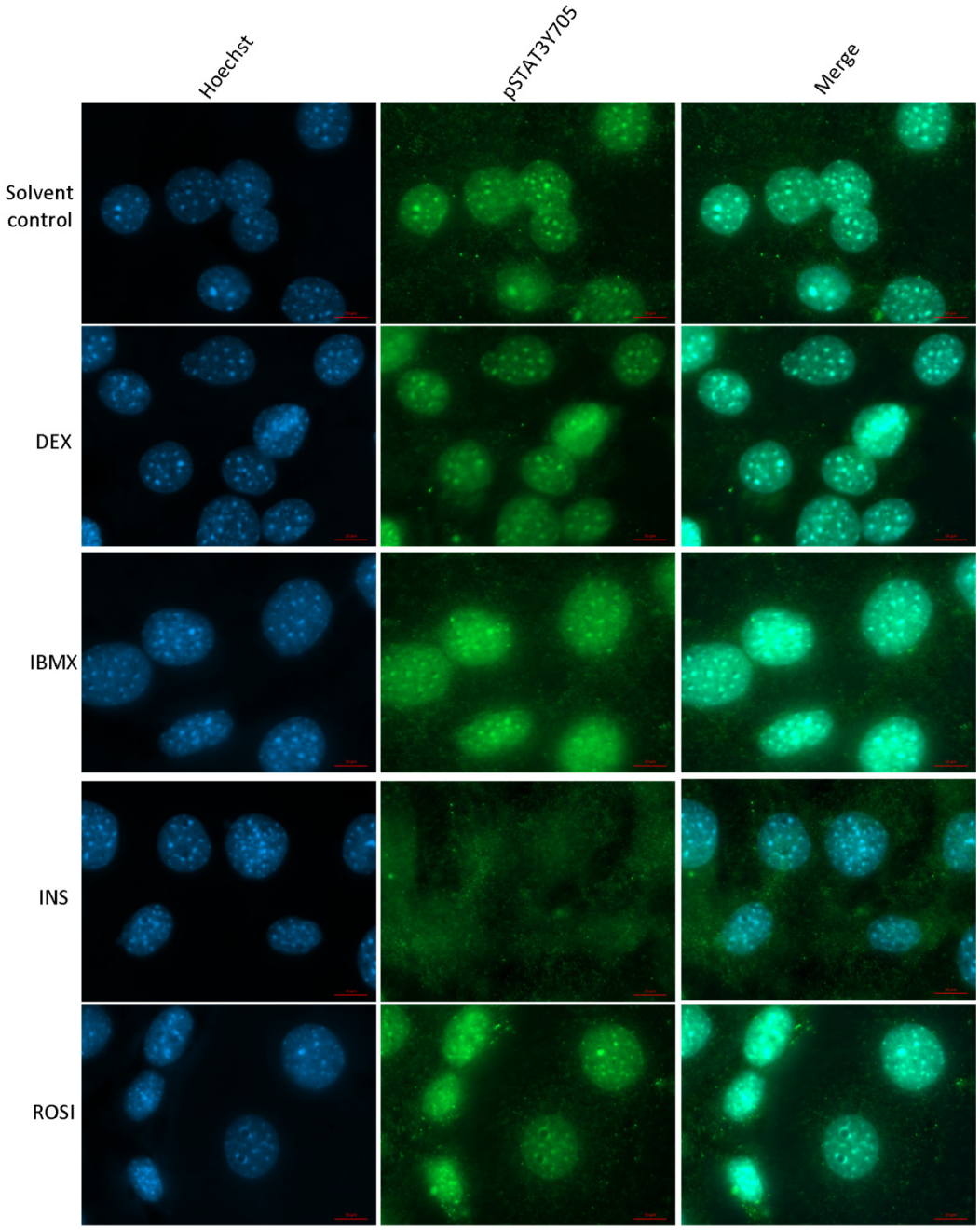

Figure 4.5: Localisation of pSTAT3Y705 in 3T3-L1 preadipocytes treated with individual components making up the differentiation cocktail. Immunofluorescence analysis of the localisation pSTAT3Y705 in 3T3-L1 preadipocytes after 3 days of treatment with dexamethasone, IBMX, insulin or rosiglitazone. Scale bars = 10 µm. Images were captured using a Zeiss AxioVert.A1 FL-LED Fluorescence Microscope at 1000x magnification. Images representable of multiple images (n = 6).

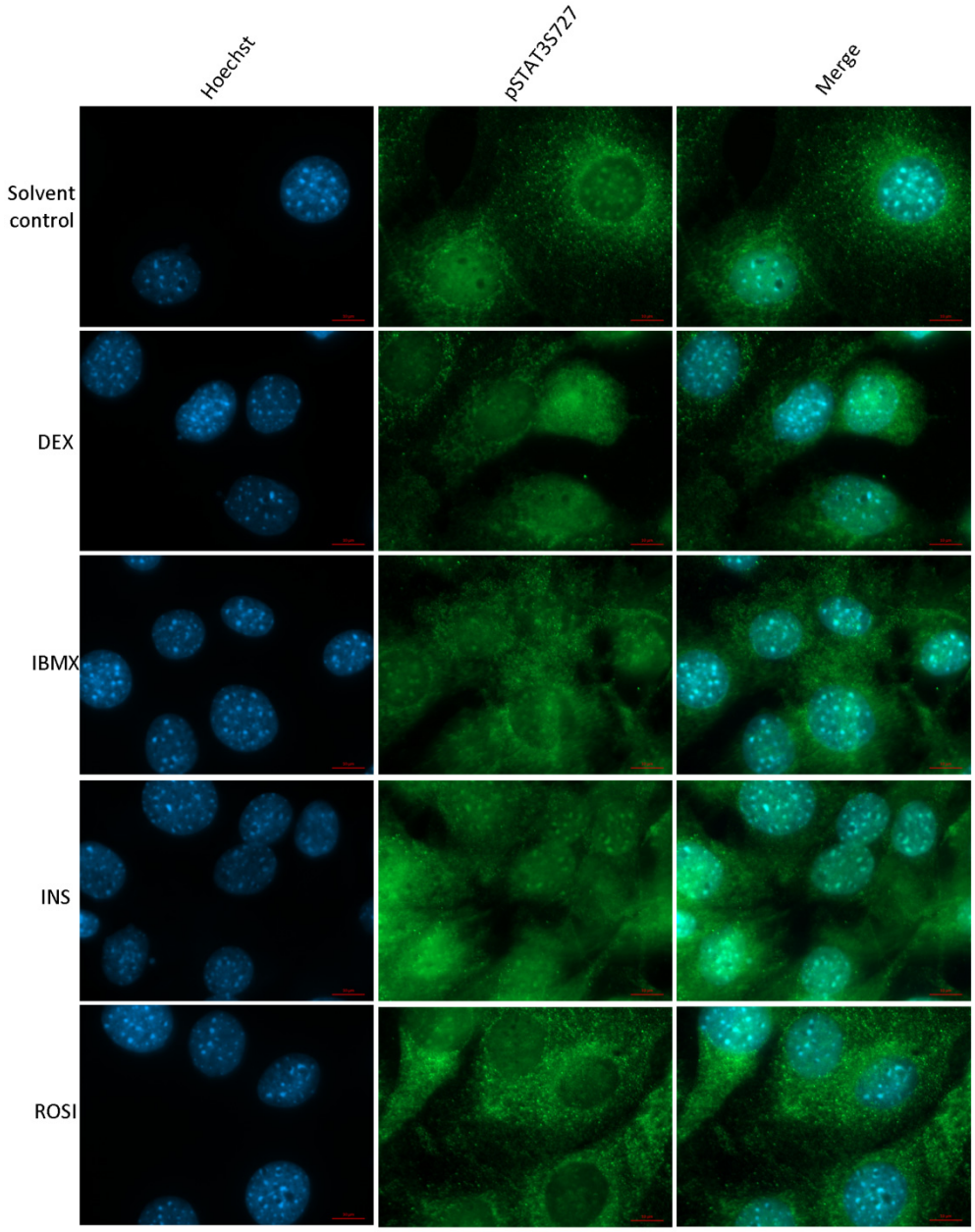

Figure 4.6: Localisation of pSTAT3S727 in 3T3-L1 preadipocytes treated with individual components making up the differentiation cocktail. Immunofluorescence analysis of the localisation pSTAT3S727 in 3T3-L1 preadipocytes after 3 days of treatment with dexamethasone, IBMX, insulin or rosiglitazone. Scale bars = 10 µm. Images were captured using a Zeiss AxioVert.A1 FL-LED Fluorescence Microscope at 1000x magnification. Images representable of multiple images (n = 6).

Western blot analysis was used to determine the effect each component had on the levels of pSTAT3S727 in 3T3-L1 preadipocytes. In cells treated with dexamethasone (Figure 4.7A) pSTAT3S727 levels were slightly decreased but no distinct trend in an increase of levels was observed. In insulin treated cells (Figure 4.7B), levels did increase but again, no distinct observable trend was found. Similar results were observed in cells treated with IBMX and in cells treated with rosiglitazone, pSTAT3S727 levels remained constant. These results indicate that although insulin, dexamethasone and IBMX treatment do result in elevated levels of pSTAT3S727, the distinct trend of an increase of pSTAT3S727 during differentiation is an event which occurs as a result of the induction of differentiation by activation of pathways by the full differentiation cocktail.

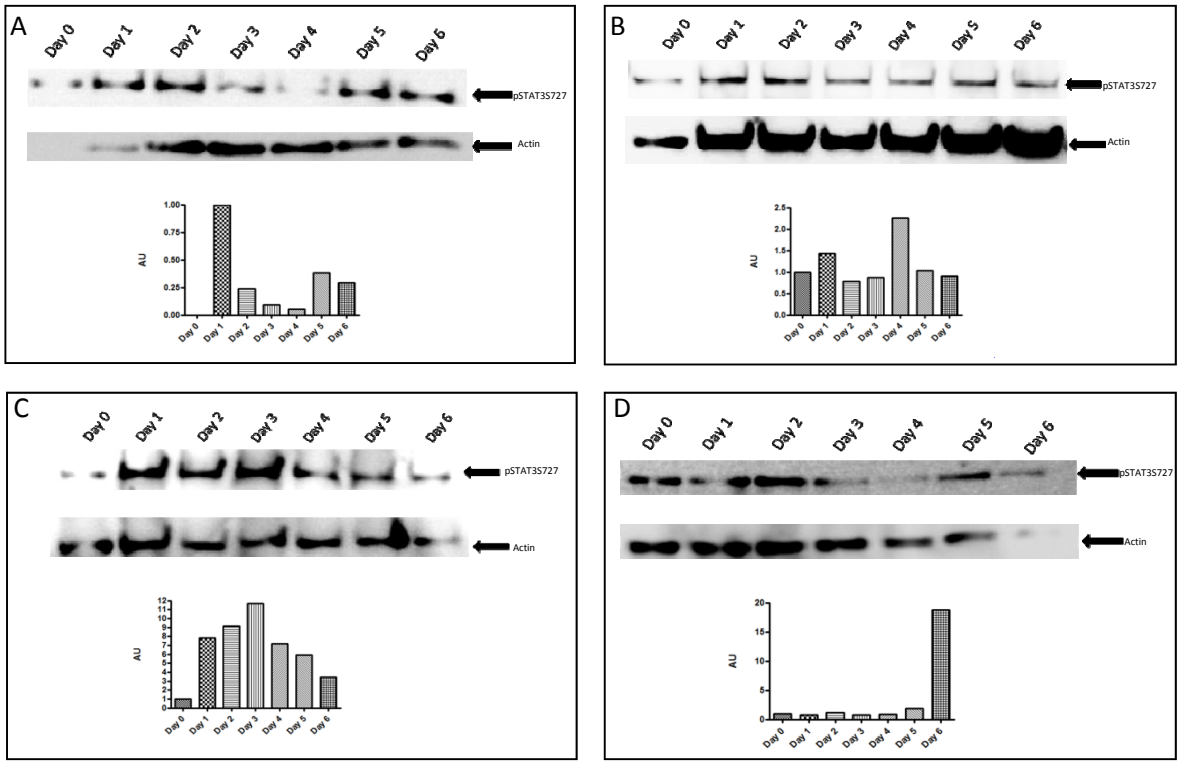

Figure 4.7: Levels of pSTAT3S727 during treatment of 3T3-L1 preadipocytes with components of the differentiation cocktail. Cells were treated for 0 to 6 days with: (A) Dexamethasone, (B) Insulin, (C) IBMX, or (D) Rosiglitazone. Equal amounts of protein were run and pSTAT3S727 signal normalised against actin as a loading control. Data was plotted using GraphPad Prism V4.0

4.3 Localisation of tSTAT3, pSTAT3Y705 and pSTAT3S727 in HMSC-ad cells during adipogenesis

Select experiments were repeated on adipose derived human mesenchymal stem cell (HMSC-ad) to investigate whether similar results in terms of the localisation and levels of STAT3 would be observed in a different model of adipogenesis.

Firstly the localisation of tSTAT3 during mesenchymal adipogenesis was investigated. Staining revealed tSTAT3 had a predominantly nuclear localisation which did not change through days 0 to 3 of differentiation as shown in Figure 4.8. Nuclear localisation was observed in 80% of cells on day 1, n = 30; 100% of cells on day 2, n = 12 and 84% on day 3, n = 16.

Although pSTAT3Y705 staining did reveal nuclear staining (as illustrated by red arrows in Figure 4.9) in uninduced and differentiating cells, nuclear staining was not as distinct as it was in 3T3-L1 cells. Staining revealed no distinct localisation of pSTAT3Y705 within the uninduced or differentiating HMSC-ad cells and this staining pattern remained relatively unchanged throughout duration of monitoring the differentiation. .

Finally, the localisation of pSTAT3S727 was investigated during differentiation. In uninduced cells, pSTAT3S727 staining was disperse throughout the cells, with slightly higher concentration being observed the nucleus in 36% of cells observed (n = 11). Upon the induction of differentiation a distinct change in the localisation was observed. Nuclear staining became much more prominent and distinct reticular like structures of pSTAT3S727 was observed throughout the cytoplasm of all cells observed, this staining pattern is highly similar to mitochondrial staining of mesenchymal stem cells as seen in Zhang *et al*, (2013). This staining pattern persisted through day 2 with 100% of observed cells displaying the phenotype. On day 3 the majority of cells continued to display the same staining pattern, however 33% of cells (n = 12) had lost the nuclear localisation of pSTAT3S727.

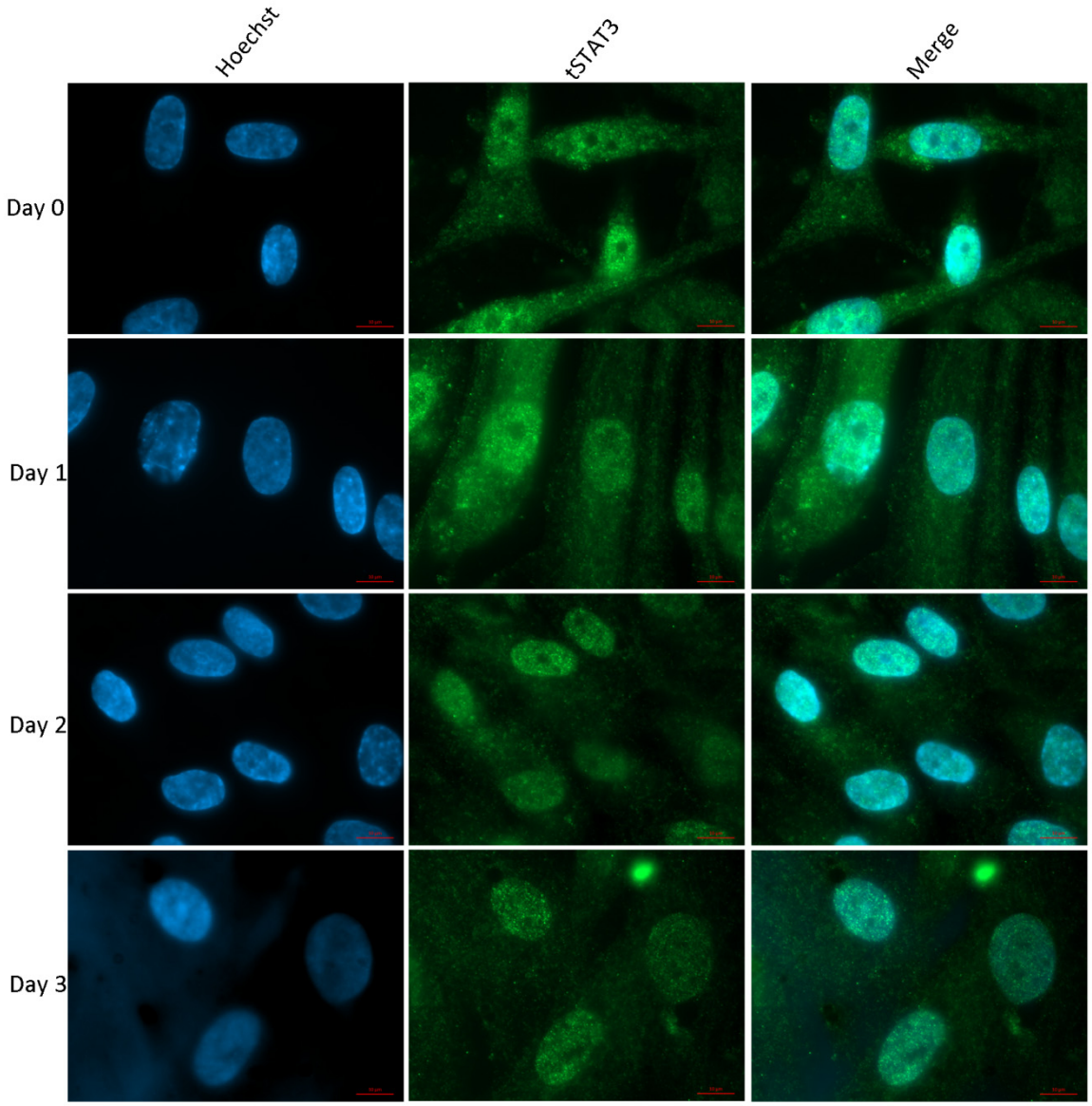

Figure 4.8: Localisation of tSTAT3 in HMSC-ad mesenchymal stem cells during adipogenic differentiation. Immunofluorescence analysis of the localisation tSTAT3 in 3T3-L1 preadipocytes during the first 3 days of differentiation. Scale bars = 10 µm. Images were captured using a Zeiss AxioVert.A1 FL-LED Fluorescence Microscope at 1000x magnification. Images representable of multiple images (n = 6).

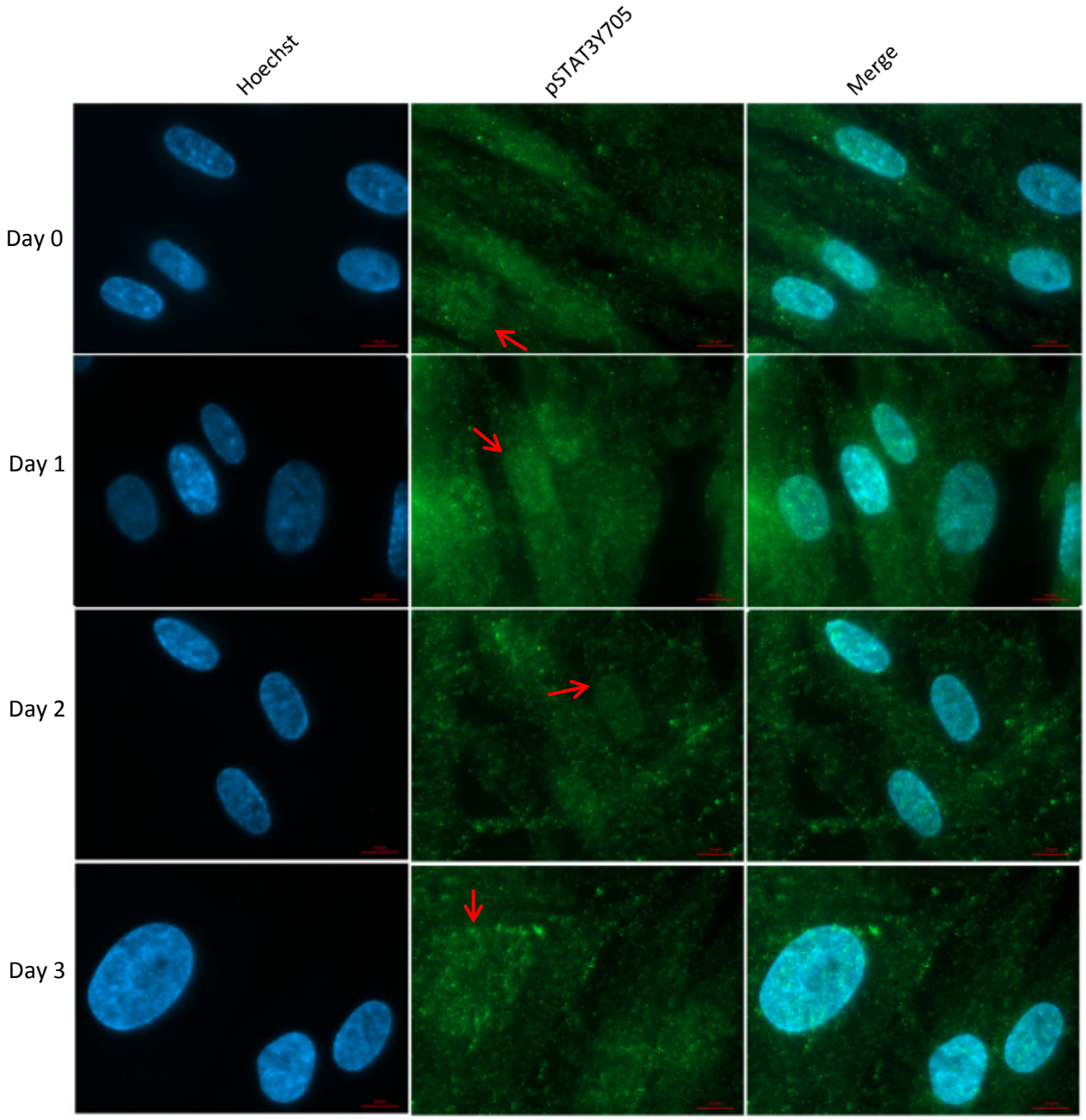

Figure 4.9: Localisation of pSTAT3Y705 in HMSC-ad mesenchymal stem cells during adipogenic differentiation. Immunofluorescence analysis of the localisation pSTAT3Y705 in 3T3-L1 preadipocytes during the first 3 days of differentiation. Scale bars = 10 µm. Images were captured using a Zeiss AxioVert.A1 FL-LED Fluorescence Microscope at 1000x magnification. Images representable of multiple images (n = 6).

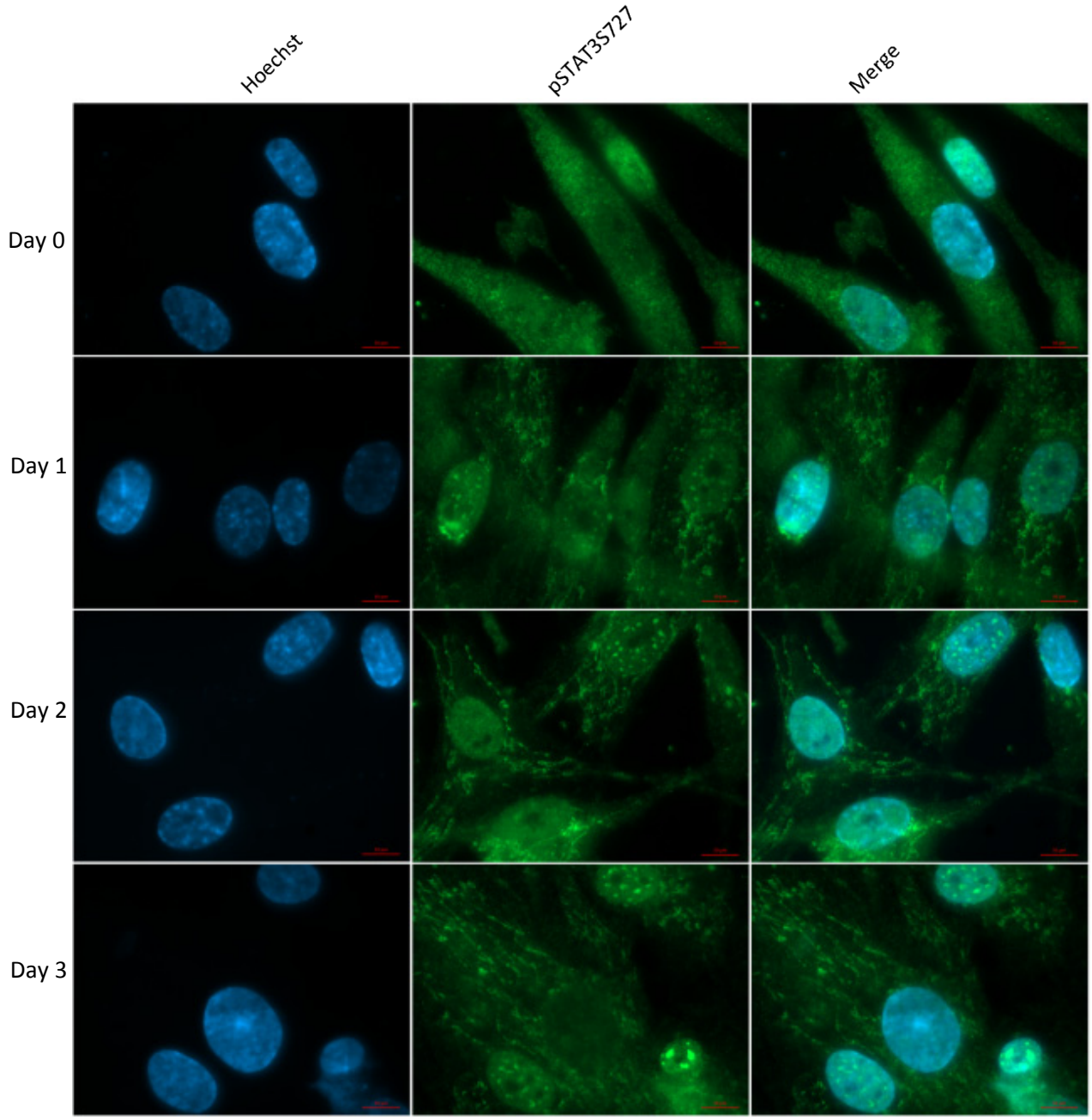

Figure 4.10: Localisation of pSTAT3S727 in HMSC-ad mesenchymal stem cells during adipogenic differentiation. Immunofluorescence analysis of the localisation pSTAT3S727 in 3T3-L1 preadipocytes during the first 3 days of differentiation.

Expression levels of pSTAT3S727 during adipogenesis was investigated in HMSC-ad cells. Similarly to 3T3-L1 preadipocytes, levels of pSTATS727 was found to increase during differentiation as shown in Figure 4.11. The trend of an increase of pSTAT3S727 during adipogenesis in both human mesenchymal stem cells and in the murine 3T3-L1 cells strongly suggest that the serine phosphorylated form of STAT3 is playing an important role during differentiation events.

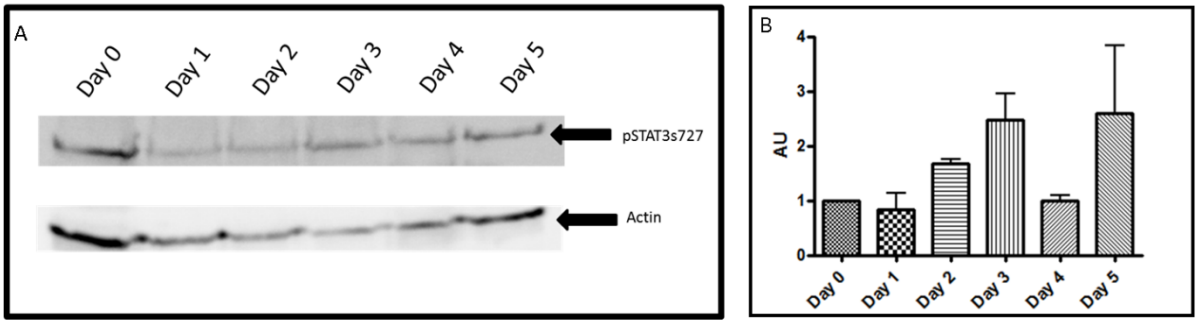

Figure 4.11: Levels of pSTAT3S727 during HMSC-ad adipogenesis. (A) Western blot of pSTAT3S727 through days 0 to 5 of differentiation. Equal amounts of protein were run and pSTAT3S727 signal normalised against actin as a loading control. (n = 3). (B) Densitometry analysis of levels of pSTAT3S727 during differentiation (n = 3). Data was plotted using GraphPad Prism V4.0

The increased levels of pSTAT3S727 levels and distinct changes in the localisation of pSTAT3S727 observed indicate that pSTAT3S727 is playing a role during adipogenesis in both 3T3-L1 and HMSC-ad cells. The punctate staining observed during 3T3-L1 differentiation and reticulate staining during adipogenesis in HMSC-ad cells is suggestive of mitochondrial staining. The presence of STAT3 within the mitochondria has been reported multiple times (Wegrzyn *et al.*, 2009; Gough *et al.*, 2009b; Demaria & Poli, 2011; Tammineni *et al*., 2013) and may play a crucial role during the differentiation of cells.

Individual treatment of 3T3-L1 cells with components the differentiation cocktail revealed that rosiglitazone induced similar punctate pSTAT3S727 staining observed during adipogenesis. Interestingly rosiglitazone is known to promote mitochondrial biogenesis (Wilson-fritch *et al*., 2003; Pardo *et al*., 2011). This cytoplasmic punctate staining may represent pSTAT3S727 within the newly formed mitochondria as a result of rosiglitazone treatment.

An investigation on the levels of ROS, the levels of mitochondrial STAT3 and a co-localisation analysis of pSTATS727 with mitochondrial proteins during adipogenesis of both 3T3-L1 and HMSC-ad cells will be presented in Chapter 4 of this manuscript.

4.4 The effect of MEK inhibition and pSTAT3Y705 inhibition on 3T3-L1 differentiation.

In order to study the importance of the different phosphorylated forms of STAT3 during 3T3-L1 adipogenesis, a real time monitoring assay of adipogenesis was utilized as described in Chapter 3 and Kramer *et al.* (2014) (see Appendix A3). Two inhibitors were specifically chosen, S31-201 a selective pSTAT3Y705 inhibitor and PD0325901, a selective mitogen-activated protein kinase kinase (MAPK/ERK kinase or MEK) inhibitor which inhibits the dual specific protein kinases MEK1 and MEK2. No specific pSTAT3S727 inhibitor currently exists, and a general serine kinase inhibitor would have been too broad of an inhibitor to use in such an experiment.

The role of MEK in 3T3-L1 adipogenesis has been investigated before. Tang *et al,* (2003), investigated the role of MEK during adipogenesis by treating 3T3-L1 cells with a different MEK inhibitor, PD98059 which selectively inhibits MEK1. It was found that MEK inhibition resulted in a delay in the initiation of mitotic clonal expansion and therefore differentiation. Mitogen activated protein kinase (MAPK) is constitutively expressed by growth arrested preadipocytes and rapidly and transiently phosphorylated by MEK1. . The study argued that by inhibiting the phosphorylation of MAPK, resulted in lowering the expression levels cell cycle regulatory proteins such cyclin A and cdk2 and, which resulted in less efficient differentiation.

The same research found that the addition of a more potent MEK inhibitor U0126, which inhibits both MEK1 and MEK2, to cells which had completed MCE had no effect on the differentiation of 3T3-L1 cells. This research illustrates the importance of MEK during the initial phases of adipogenesis. The successful measurement of a variation in the differentiation *CI* profile of 3T3-L1 cells treated with a MEK inhibitor using the xCELLigence system would provide proof of concept of the assay in terms of finding chemical morphogens with pro- or anti- adipogenic effects.

Further to this, MEK inhibition may provide insights into the role pSTAT3S727 may have during adipogenesis. The STAT3 serine phosphorylation site is embedded in a conserved PMSP sequence, which contains a mitogen activated protein kinase (MAPK) consensus target sequence (PXS/TP) (Decker & Kovarik, 2000). It has been shown that treatment of cells with the MEK inhibitor PD98059 blocks serine phosphorylation of STAT3 in response to IL-2 (Chung *et al.*, 1997) and that the insulin triggered serine phosphorylation of STAT3 is

mediated by a Ras/Raf/MEK dependant pathway (Ceresa *et al.*, 1997). MEK kinase 1 (MEKK1) has been reported to be involved in the regulation of STAT3 activation by growth factors as well. It was found that kinase inactive MEKK1 inhibits phosphorylation of STAT3 on both serine and tyrosine residues while active MEKK1 was found to induce serine and tyrosine phosphorylation of STAT3. Serine 727 phosphorylation was found to be phosphorylated by MEKK1 *in vitro* while tyrosine 705 phosphorylation was induced by MEKK1 involving Src and Janus kinases *in vivo* (Lim & Cao, 2001). Recently the involvement of the MEK pathway in the serine phosphorylation of STAT3 has further been noted (Gough *et al.*, 2013)

Therefore MEK inhibition may block the serine phosphorylation of STAT3 during adipogenesis. The use of PD0325901 was chosen for this set of experiments to provide a basic insight of what pSTAT3S727 inhibition could potentially have during adipogenesis as well as validate the real time monitoring of differentiation assay using the xCELLigence system. The inhibitor has been shown to be affective against both MEK1 and MEK2 (Sebolt-Leopold & Herrera, 2004)

Cells were seeded on the xCELLigence system as previously described and allowed to reach confluence as judged by the doubling time calculated using ACEA's xCELLigence software. Differentiation was then induced by the addition of the differentiation cocktail, in the presence of 10 nM of PD0325901 or 30 μM of S31-201; the determined IC50 values of each compound (see Appendix A2). Differentiation was then monitored using the ACEA xCELLigence RTCA SP system and Oil Red O staining was performed 3 days post induction to measure lipid uptake and extent of differentiation, as previously described.

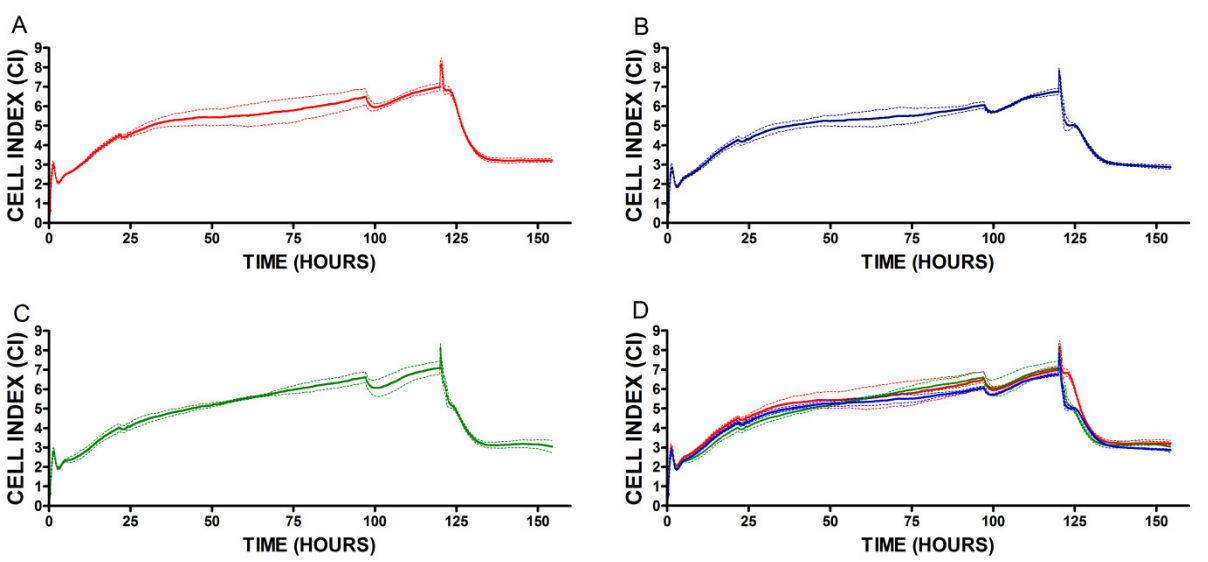

Figure 4.12. Real time monitoring of differentiation of 3T3-L1 preadipocytes in the presence of the MEK inhibitor (PD0325901) and pSTAT3Y705 inhibitor (S31-201). 3T3-L1 cells were seeded onto the xCELLigence system and induced to differentiate as previously. Differentiation was induced in the presence of A) DMSO/EtOH (solvent controls), B) 10 nM of the MEK inhibitor PD0325901 or C) 30 µM of the pSTATY705 inhibitor S31-201. C) An overlay of all 3 *CI* differentiation profiles. Dotted lines represent standard deviations. All curves were plotted as an average of quadruplicate treatments. Data was plotted using GraphPad Prism v4.0

The resulting *CI* plots resemble plots discussed in Chapter 3. Deviations at 25 and 100 hours are a result of a drop in CO_2 levels as a consequence of the incubator being opened. The *CI* profile of cells induced to differentiate displayed the typical drop in *CI* values observed and discussed in Chapter 2, as expected. This drop in the *CI* profile represents the dramatic change in morphology that occurs upon the induction of differentiation. However, cells that were induced to differentiate in the presence of either the MEK inhibitor PD0325901 or the pSTATY705 inhibitor S31-201 produced slightly altered *CI* profiles as seen in Figure 4.12. The *CI* profile of cells induced to differentiate in the presence of the MEK inhibitor initially drops as expected, however the drop in *CI* values is much more extreme than that of cells induced to differentiate in the absence of any inhibitors. Further to this, *CI* values were found to plateau an hour post induction for a period of about 5 hours before the drop in *CI* values

continued. A similar differentiation *CI* curve was produced when cells were induced to differentiate in the presence of the pSTAT3Y705 inhibitor S31-201. The *CI* curve shows a pause in the drop of *CI* values, similar but not as distinct as that of cells treated with the MEK inhibitor.

The dramatic change in morphology of 3T3-L1 cells induced to differentiate measured by the xCELLigence system has been determined to be a characteristic event during the initial phases of differentiation (Kramer *et al.,* 2014). The deviation of the differentiation profile as a result of chemical morphogens such as inhibitors as PD0325901 and S31-201 indicates that there is some effect on the initial change of the morphology of the cells and it can be speculated that these compounds must therefore have some effect on the differentiation events occurring upon induction of differentiation. Oil Red O staining was next performed to investigate the effect these inhibitors had on lipogenesis during differentiation. Figure 4.13 shows the resulting lipogenensis of cells induced to differentiate in the presence of the inhibitors.

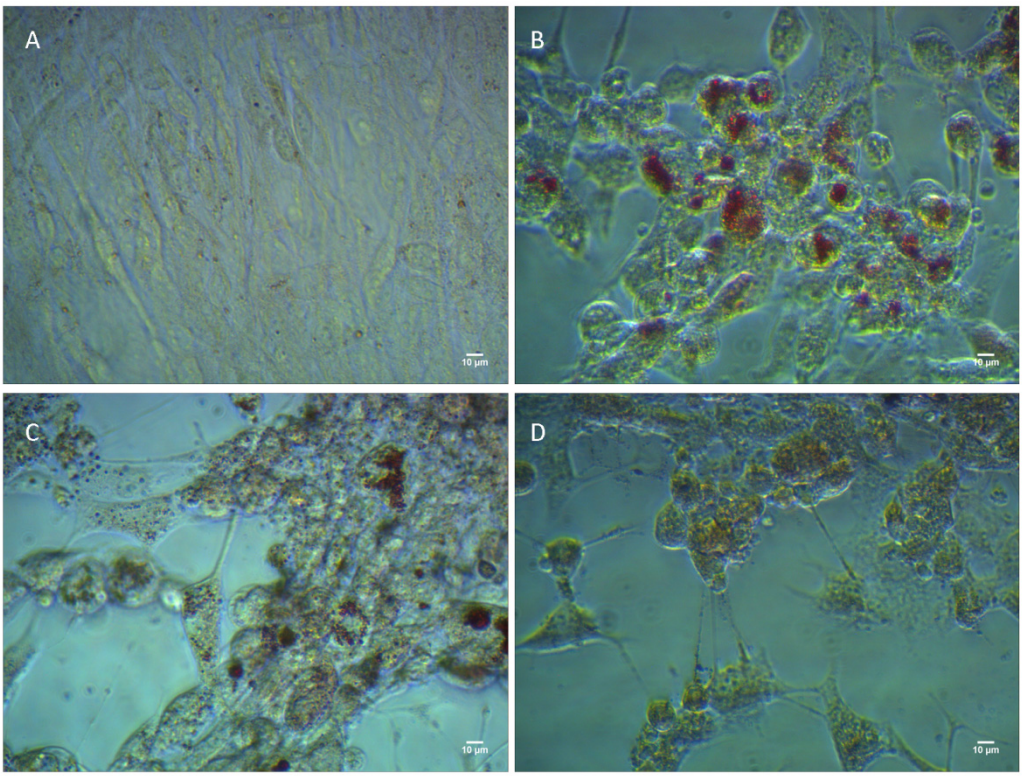

Figure 4.13. Oil Red O staining of xCELLigence samples 3 days post induction. A) Uninduced 3T3-L1 preadipocytes, B) differentiation media, C) differentiation media with 30 µM S31-201, D) differentiation media with 10 nM PD0325901. Scale bars = 10 µM.

As expected, uninduced 3T3-L1 cells had very low levels of Oil Red O staining while a distinct amount of the stain indicating lipid uptake was observed in cells treated with the differentiation media as shown in Figure 4.13 A and B respectively. Oil Red O staining revealed that cells treated with S31-201 had markedly reduced levels of accumulated lipid droplets (Figure 4.13C) when compared to cells induced to differentiate in the absence of any inhibitors. Cells treated with the MEK inhibitor did not accumulate any of the stain (Figure 4.13C).

Although inhibition with the two inhibitors blocked the accumulation of lipids, the distinctive change in morphology was observed when cells were induced to differentiate despite the presence of the inhibitors. This could suggest that STAT3 plays a role during lipogenesis. Buettner *et al.,* (2006) showed that STAT3 signalling plays a crucial role in leptin signalling. Leptin is an adipokine that regulates energy uptake and expenditure. Despite the 2006 research showing that STAT3 activation is required for the effects of leptin on food intake and hepatic glucose metabolism, later research conducted by Buettner *et al.*, (2008) showed that leptin controls adipose tissue lipogenesis via central, STAT3 independent mechanisms. However, it has been shown that the hepatic overexpression of STAT3 results in an overabundance of mRNAs for fatty acid synthase and acetyl CoA corboxykinase which synthesize the fatty acids. This result may indicate that STAT3 plays a role in lipogenesis in the liver. (Kinoshita *et al.*, 2008)

Despite the Buettner *et al.*, (2008) finding, STAT3 may play a direct role in lipogenesis as well as in adipogenesis which may explain the lack of lipid accumulation, while a change in morphology consistent with differentiation still observed.

These results indicate the importance of both MEK and both activated forms of STAT3 during adipogenesis. Although conclusions about the roles these proteins play during differentiation events cannot be made, it can be inferred that they are crucial during 3T3-L1 adipocyte differentiation. To further investigate what effect these inhibitors have on STAT3, 3T3-L1 preadipocytes were treated for 3 days with each of the inhibitors and the localisation of tSTAT3, pSTAT3Y705 and pSTAT3S727 were investigated via immunofluorescence analysis.

As previously described, the localisation of tSTAT3 in cells treated with the solvent control was distinctly nuclear with 100% of cells displaying this phenotype (n = 32). There was a distinct change in the staining pattern in cells treated with the MEK inhibitor PD0325901.

Nuclear localized tSTAT3 was observed in all cells analysed (n = 47), however in 79% of cells staining was distinctly diffuse and the nuclear staining not as defined as in untreated cells as seen in Figure 4.10. Similar results were recorded for cells treated with the pSTAT3Y705 inhibitor S31-201, with 74% of observed cells displaying diffuse staining and less defined nuclear staining (Figure 4.14), although all observed cells were found to have nuclear localized tSTAT3 (n = 42).

The localisation of pSTAT3Y705 was also investigated upon treatment of cells with the inhibitors. Untreated cells were found to have a distinctly nuclear localisation of pSTAT3Y705 (n = 34). Similarly, as found in tSTAT3 staining, upon treatment with the MEK inhibitor pSTAT3Y705 staining became diffuse throughout the cells with less prominent, however present, nuclear staining found in 75% of observed cells (n = 36). Treatment with the pSTAT3Y705 inhibitor S31-201 produced similar results with 76% of cells observed (n = 51) displaying diffuse staining with less prominent nuclear staining as shown in Figure 4.15.

Finally the localisation of pSTAT3S727 was investigated in 3T3-L1 cells treated with the inhibitors. Unexpectedly, MEK inhibition did not have the dramatic effect on the localisation of pSTAT3S727 as hypothesized. Cytoplasmic staining did increase, however 90% of observed cells (n = 30) were found to have distinct nuclear staining comparable to the control. Interestingly, pSTAT3S727 staining in cells treated with the so called pSTATY705 specific inhibitor, S31-201, was found to be distinctly different from the staining of the controls. In 3T3-L1 cells treated with S31-201, nuclear staining of pSTAT3S727 was lost with 92% of cells observed (n = 30) lacking nuclear localized pSTAT3S727 as seen in Figure 4.16.

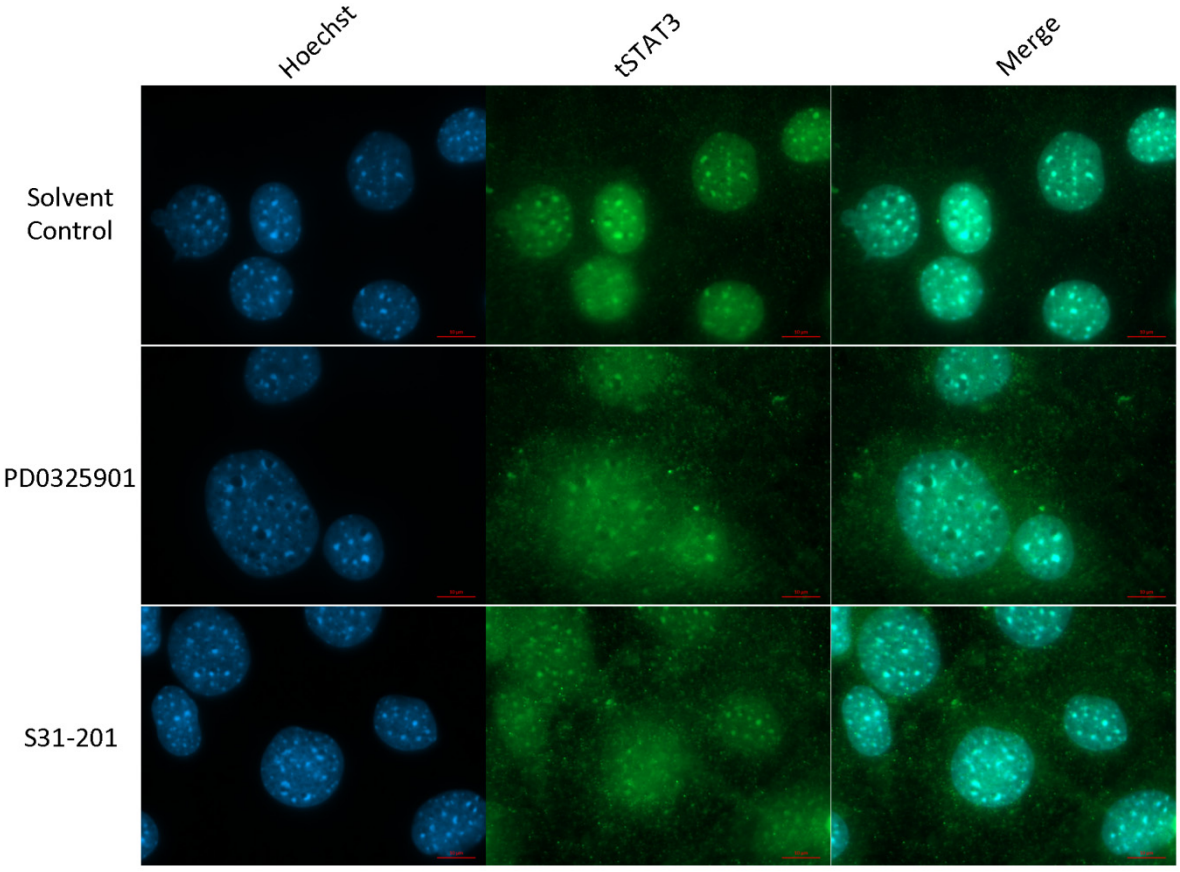

Figure 4.14. Localisation of tSTAT3 in 3T3-L1 preadipocyte treated with MEK or pSTAT3Y705 inhibition. 3T3-L1 preadipocytes were treated with PD0325901 or S31-201 inhibitors before being treated for immunofluorescence analysis. Scale bars = 10 µm. Images were captured using a Zeiss AxioVert.A1 FL-LED Fluorescence Microscope at 1000x magnification. Images representable of multiple images (n = 6).

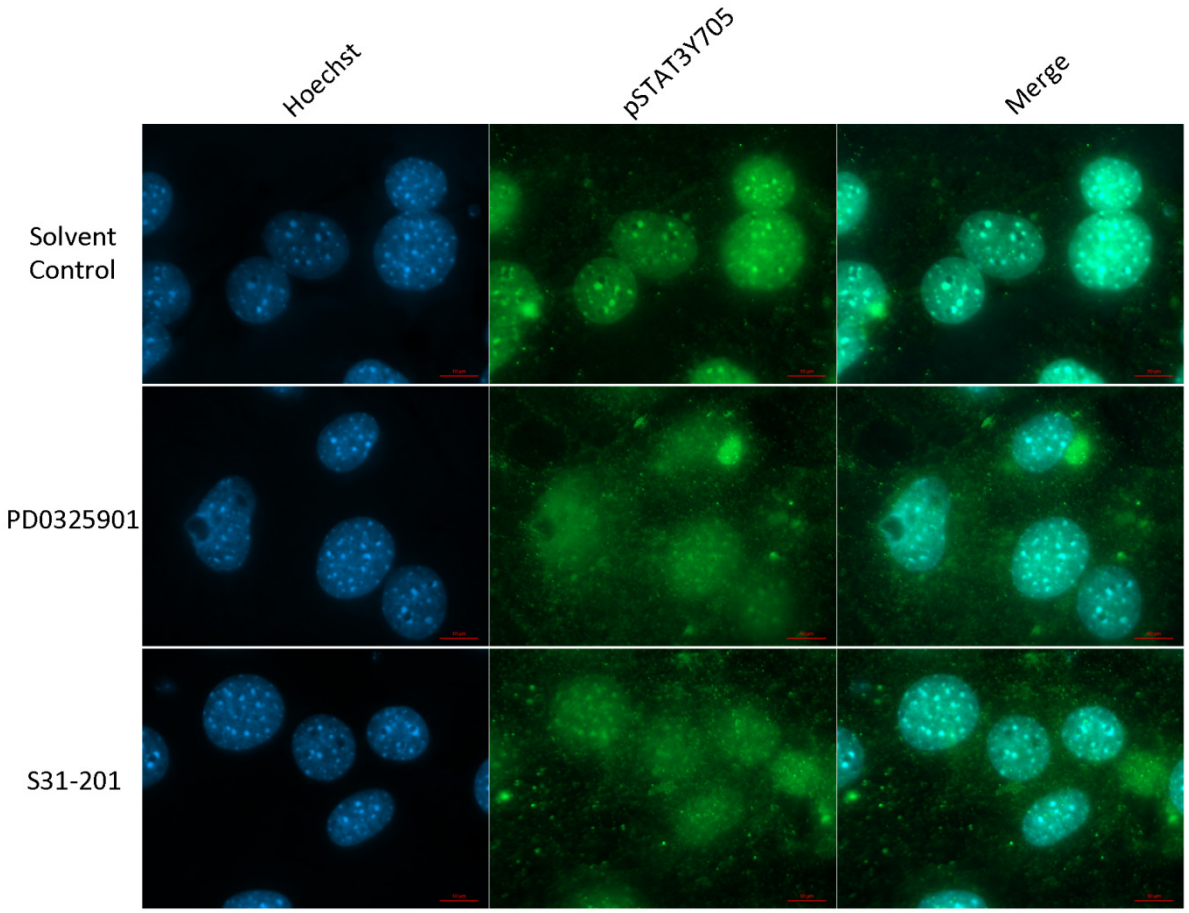

Figure 4.15. Localisation of pSTAT3Y705 in 3T3-L1 preadipocyte treated with MEK or pSTAT3Y705 inhibition. 3T3-L1 preadipocytes were treated with PD0325901 or S31-201 inhibitors before being treated for immunofluorescence analysis. Scale bars = 10 µm. Images were captured using a Zeiss AxioVert.A1 FL-LED Fluorescence Microscope at 1000x magnification. Images representable of multiple images (n = 6).

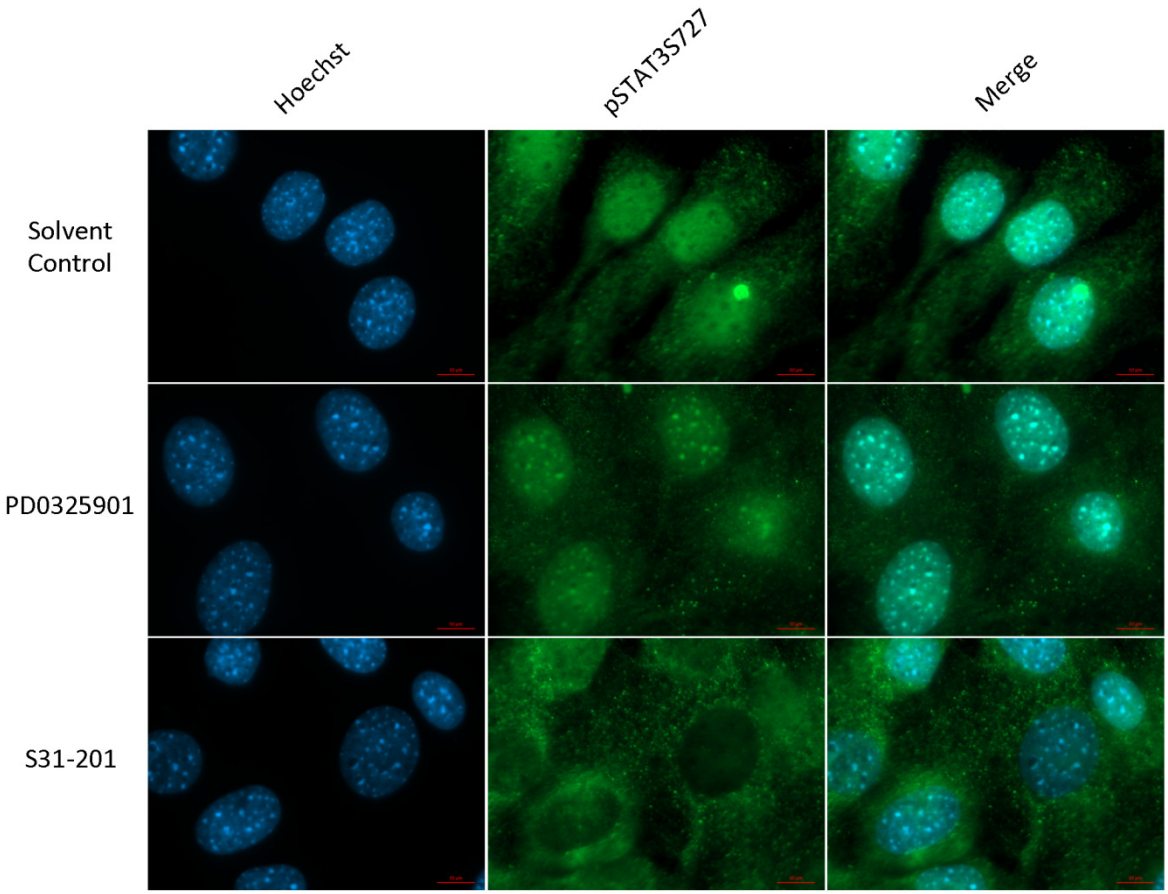

Figure 4.16. Localisation of pSTAT3S727 in 3T3-L1 preadipocyte treated with MEK or pSTAT3Y705 inhibition. 3T3-L1 preadipocytes were treated with PD0325901 or S31-201 inhibitors before being treated for immunofluorescence analysis. Scale bars = 10 µm. Images were captured using a Zeiss AxioVert.A1 FL-LED Fluorescence Microscope at 1000x magnification. Images representable of multiple images (n = 6).

Both pSTAT3Y705 and indirect pSTAT3S727 inhibition via inhibition of MEK by PD0325901 had an effect on the differentiation events of 3T3-L1 cells. Preadipocytes treated the inhibitors in question revealed changes in the localisation of the different isoforms of STAT3, with the majority of cells revealing more diffuse cytoplasmic staining and less defined nuclear staining. These staining patterns indicate that the inhibitors did have an effect on the localisation and therefore most probably had an effect on the function of STAT3. By inhibiting the phosphorylation of STAT3, the molecule would be actively translocated to either the nucleus, in the case of tyrosine phosphorylation or to the mitochondria in the case of serine phosphorylation. Interestingly, as seen in Figure 4.12, the treatment of cells with the pSTAT3Y705 inhibitor resulted in a distinct loss of nuclear localized pSTATS727. This could indicate that in order for S727 to enter or remain the nucleus, the Y705 residue must too be phosphorylated. The small molecule S31-201 prevents STAT3 from being phosphorylated, dimerising and translocating to the nucleus. STAT3 molecules which had already been phosphorylated prior to the exposure of S31-201 may very well have remained phosphorylated and therefore remained in the nucleus; this may explain why nuclear localized tSTAT3 and pSTAT3Y705 was observed despite exposure to S31-201. As it has been shown that STAT3 is imported into the nucleus independently of phosphorylation events, the observation of nuclear localised STAT3 despite being treated with S31-201 is expected.

Serine phosphorylated STAT3 is most likely the α isoform of STAT3 which has been shown to have a shorter nuclear retention (Huang *et al*., 2007; Ng *et al*., 2012) as previously discussed. It may be necessary for the tyrosine residue of serine phosphorylated STAT3α to be phosphorylated as well in order for pSTAT3S727 to remain in the nucleus for extended periods. This could explain the distinct loss of nuclear localized pSTAT3S727 upon treatment with S31-201. STAT3 phosphorylated only on the serine residue, and lacking tyrosine phosphorylation would have left the nucleus, resulting in the staining pattern observed.

The results presented here show that serine phosphorylated STAT3α may have function within the cytoplasm independent of the nuclear localisation. Punctate structures observed during differentiation and inhibition studies show changes in localisation suggesting that pSTAT3S727 may play a role in the cytoplasm. Based on the punctate structures observed and reports of mitochondrial STAT (Wegrzyn *et al.,* 2009; Szczepanek *et al.,* 2012) it can be

speculated that STAT3 may play a role in mitochondria during adipogenesis. It has been shown that STAT3 could play a role in regulating the activity of the electron transport chain and therefore in regulating Reactive Oxygen Species (ROS) production (Szczepanek *et al.*, 2012)

The accumulation of ROS during adipogenesis is well known (Tormos *et al.,* 2011) and mitochondrial STAT3 has been shown to have dramatic effects on the activity of complex I of the electron transport chain and the accumulation of ROS (Zhang *et al.*, 2013). As previously stated, in site directed mutagenesis experiments conducted by Tammineni *et al.,* (2013) it was shown that a S727A mutation reduced the import and assembly into complex I of STAT3 by GRIM-19. Given that STAT3 has been implicated in activating the Warburg effect as well as its potential role in the mitochondrial ETC and, combined with the localisation changes observed during differentiation, it can be speculated that pSTAT3S727 may play a role in mediating ROS signalling during adipogenesis.

Chapter 5

An investigation on the levels of Reactive Oxygen Species (ROS), and levels of mitochondrial pSTAT3S727 during adipogenesis.

Specific objectives

1. **Utilize confocal microscopy to investigate co-localisation between pSTAT3S727 and the mitochondrial Voltage Dependent Anion Channel (VDAC) within differentiating 3T3-L1 and HMSC-ad cells**
2. **Investigate levels of mitochondria in differentiation 3T3-L1 and HMSC-ad cells.**
3. **Isolate mitochondria of differentiating 3T3-L1 and HMSC-ad cells.**
4. **Investigate the levels of pSTAT3S727 within isolated mitochondria.**
5. **Investigate the levels of Reactive Oxygen Species (ROS) within differentiating 3T3-L1 and HMSC-ad cells**

5: An investigation on the levels of Reactive Oxygen Species (ROS), and levels of mitochondrial pSTAT3S727 during adipogenesis.

5.1 Co-localisation analysis between pSTAT3S727 and mitochondrial Voltage Dependant Anion Channel

A co-localisation analysis between the mitochondrial marker, Voltage Dependant Anion Channel (VDAC) and pSTAT3S727, the mitochondrial isoform of STAT3 was carried out on differentiating 3T3-L1 preadipocytes and HMSC-ad cells to determine whether there was a change in the mitochondrial localisation of pSTAT3S727 during adipogenic events.

Images were captured using the Zeiss Meta confocal LSM microscope and analysed using the ImageJ Intensity Correlation Analysis plugin (Li *et al.*, 2004) which calculates, amongst other values, Mander's Overlap coefficient (R), *Intensity Correlation Quotient* (ICQ) and *Product of the Differences from the Mean* or PDM values. The results of this analysis are summarized in Figure 5.1 and 5.2 along with representative images of each analysis (n = 3).

Co-localisation coefficients such Mander's Overlap coefficient (R) and the *Intensity Correlation Quotient* (ICQ) values were calculated. Mander's Overlap coefficient ranges between 0 and 1; with 1 being high overlap and 0 being low. The Intensity Correlation Quotient (ICQ) relates to the synchrony in variation of intensities between images. If images are dependant (co-localize) they will vary around the respective mean image intensities together. ICQ values range between -0.5 and 0.5. Random staining has values close to 0; segregated staining has values between -0.5 and 0 while dependant staining has values between 0 and 0.5. Related to ICQ, is the *Product of the Differences from the Mean* or PDM value. The PDM value is based on the assumption that for pixels of random intensities (no co-localisation) the sum of their product with be zero. If two intensities are dependant, the product will be positive and if they are segregated, negative. The ICA plugin in ImageJ creates PDM images highlighting co-localized pixels in yellow and segregated pixels in blue, as seen in Figure 5.1 and 5.2. Finally, fluorescence scattergrams show the pixel-pixel overlap of the signals between the two channels and give a general overview of the extent of co-localisation.

The mitochondrial Voltage Dependant Anion Channel (VDAC) was chosen for co-localisation analysis. This protein is one of the major constituents of the in the outer membrane of mitochondria and has a primary function to mediate transport of nucleotides,

ions and metabolites into mitochondria (Hoogenboom *et al.*, 2007). This mitochondrial protein was chosen for co-localisation studies due to its abundance in mitochondria, after attempts using underperforming antibodies to mitochondrial markers such as Complex IV (COXIV) failed.

As seen in Figure 5.1, in the imaged Day 0 sample pSTAT3S727 was found in the nucleus while VDAC was distinctly cytoplasmic. The generated PDM image revealed punctate structures in a few of the cells and the resulting scattergram indicates some level of overlap. In the Day 1 panel nuclear localised pSTAT3S727 is no longer observed, while and VDAC staining remains cytoplasmic. The resulting scatter gram reveals slight more independent pSTAT3S727 staining (red channel). There are distinct co-localised punctate areas in certain cells indicated by the PDM image. The Day 2 panel reveals cytoplasmic staining for both proteins with PDM images revealing very little co-localisation in any cells in the image. The resulting scattergram indicates little overlap between the two channels. Next, the Day 3 image showing cytoplasmic staining of both VDAC and pSTAT3S727, and the PDM images shows that some cells have punctate co-localised area in the cytoplasm and the resulting scatter gram shows some level of overlap with more independent pSTAT3S727 staining again observed. Similar observations were made on Day 4, with a few cells having positive PDM values as was the case on Day 5. Day 6 revealed a few cells with positive PDM values and the scattergram indicates more overlap in the sample than was observed on days 4 or 5.

Co-localisation analysis of differentiating 3T3-L1 cells revealed that there was distinct overlap between VDAC and pSTAT3S727 signals with Mander's coefficients of above 0.6. The ICQ values, although not particularly high, do indicate some level of co-localisation, with values above 0.15. Quantitative analysis revealed that there was no distinct change in the levels of co-localisation during adipogenesis with Mander's coefficient having a range of 0.1 and ICQ values remaining relatively constant with a value of about 0.1. These analyses are based on co-localisation analysis on the average of 3 whole fields of view and therefore give a very general idea of the extent co-localisation. As STAT3 is found in both the cytoplasm as well as the nucleus, whole cell analysis may not give an accurate representation of mitochondrial localised STAT3. What may be more relevant to the changes in co-localisation, are PDM images generated by the ICA plugin. These images highlight regions of co-localisation based on the product of the differences of the mean for each pixel, as previously described. As seen in Figure 5.1, two PDM images are generated. The first shows

both positive PDM values in yellow and negative values in blue, and the second highlights only pixels with positive values.

PDM based co-localisation analysis was performed by counting cells displaying distinctly positive PDM values and displaying typical mitochondrial like structures as seen in PDM generated images in Figures 5.1 and 5.2. During 3T3-L1 differentiation, analysis revealed that more cells had positive PDM values during Days 0 (55%, n = 42) and 1 (48%, n = 33) of differentiation. Incidences of cells with positive PDM values decreased during Days 2 (33%, n = 60) and 3 (45% n = 54), and then started increasing during Days 5 (48%, n = 54) and 6 (53%, n = 43) of the differentiation procedure.

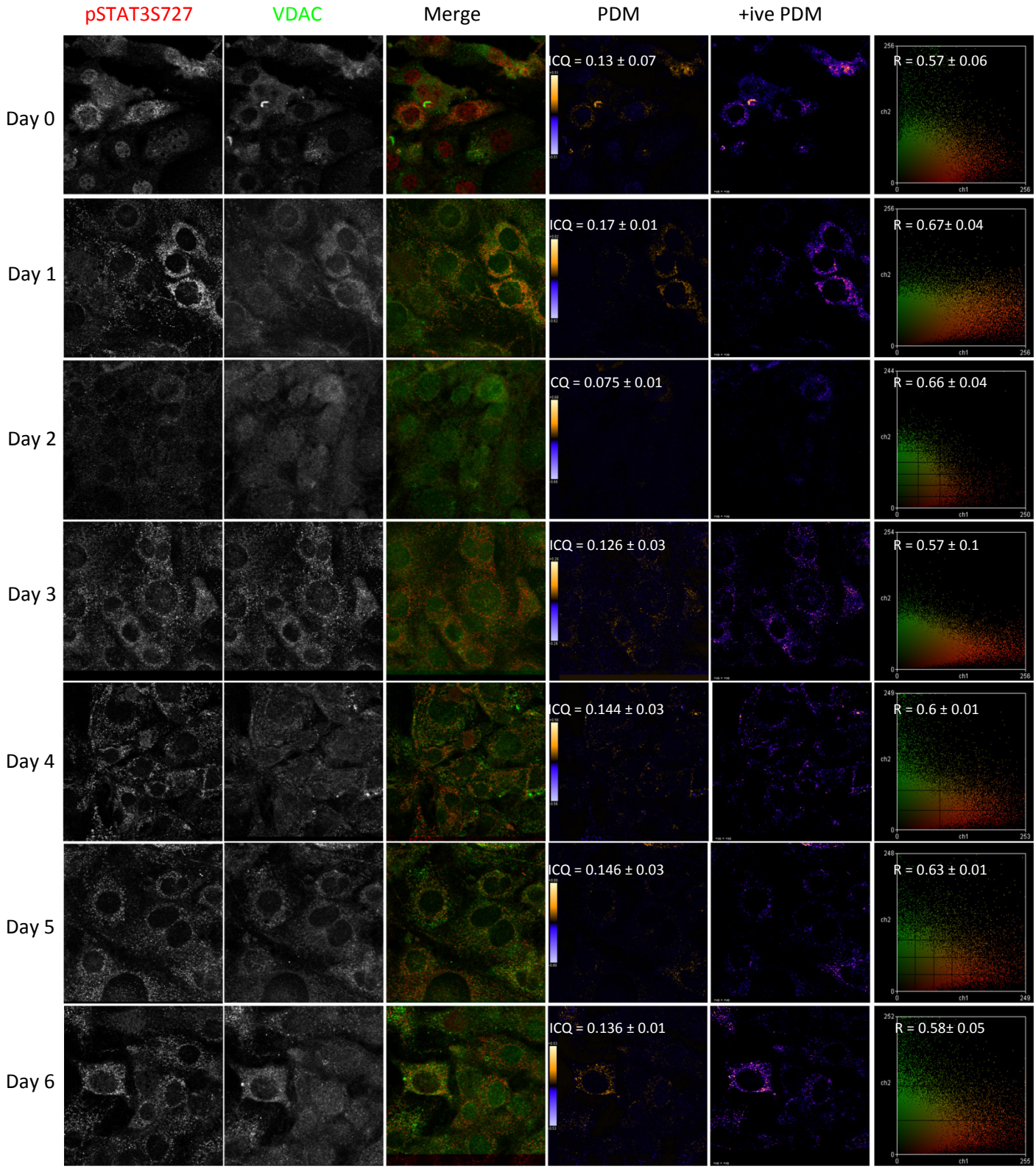

Figure 5.1: Co-localisation analysis of pSTAT3S727 and VDAC in differentiating 3T3-L1 preadipocytes. Preadipocytes were induced to differentiated and subjected to immunofluorescence staining as previously described. Images were captured using the Zeiss LSM 510 Meta confocal microscope and co-localisation analysis was performed using ImageJ software (NCBI). Panels represent: the red channel (pSTAT3S727), green channel (VDAC); PDM images highlighting co-localized pixels in yellow and segregated pixels in blue; fluorescence scattergrams showing the pixel-pixel overlap of the signals between the two channels.

As shown in Figure 5.2, imaged HMSC-ad cells displayed nuclear localised pSTAT3S727 during all days of the differentiation. As observed before pSTAT3S727 staining revealed reticulate staining on all day post induction of differentiation. VDAC staining remained unchanged and found to be punctate and cytoplasmic as expected. Generated PDM images indicated regions of co-localised pixels in all samples imaged with little change being observed. Scattergrams also remained relatively unchanged and indicated some level of overlap in all days imaged as seen in Figure 5.2

Similar quantitative results were observed in the co-localisation analysis of pSTAT3S727 and VDAC within HMSC-ad cells. Mander's coefficients were found to be between 0.61 and 0.66 for each day of differentiation analysed while ICQ values were between 0.16 and 0.2. Co-localisation values for the HMSC-ad cells were found to be much more uniform throughout the differentiation as compared with 3T3-L1 cells. Generated PDM images revealed the same trend, with certain cells in each field of view displaying overlapping pixels, with very little difference in overlap patterns through each day of differentiation. On day 0, 48% of cells (n = 26) displayed positive PDM values, and little change in incidences of cells with positive PDM values was observed with 48% (n = 26) on day 1, 51% (n = 31) on day 2 and 52% (n = 31) on day 3.

Although STAT3 has been reported to play a function within mitochondria, the exact mitochondrial proteins with which it interacts is not completely known, and there are no reports of STAT3 interacting directly with VDAC. As VDAC resides in the outer mitochondrial membrane and mitochondrial STAT3 is hypothesized to reside and be involved in the electron transport chain located in the inner membrane, VDAC may not be the best mitochondrial marker to study the localisation of STAT3 within mitochondria. This may be the reason for the low Manders and ICQ values observed in the co-localisation analysis. For these reasons, co-localisation analysis between these two proteins can only give a general idea of whether the two proteins in question are in the same compartment, and not to what extent STAT3 has localised to mitochondria.

Microscopic analysis has many limitations, and a more general overview of the levels of mitochondrial STAT3 within the entire population of cells was determined by Western blot analysis.

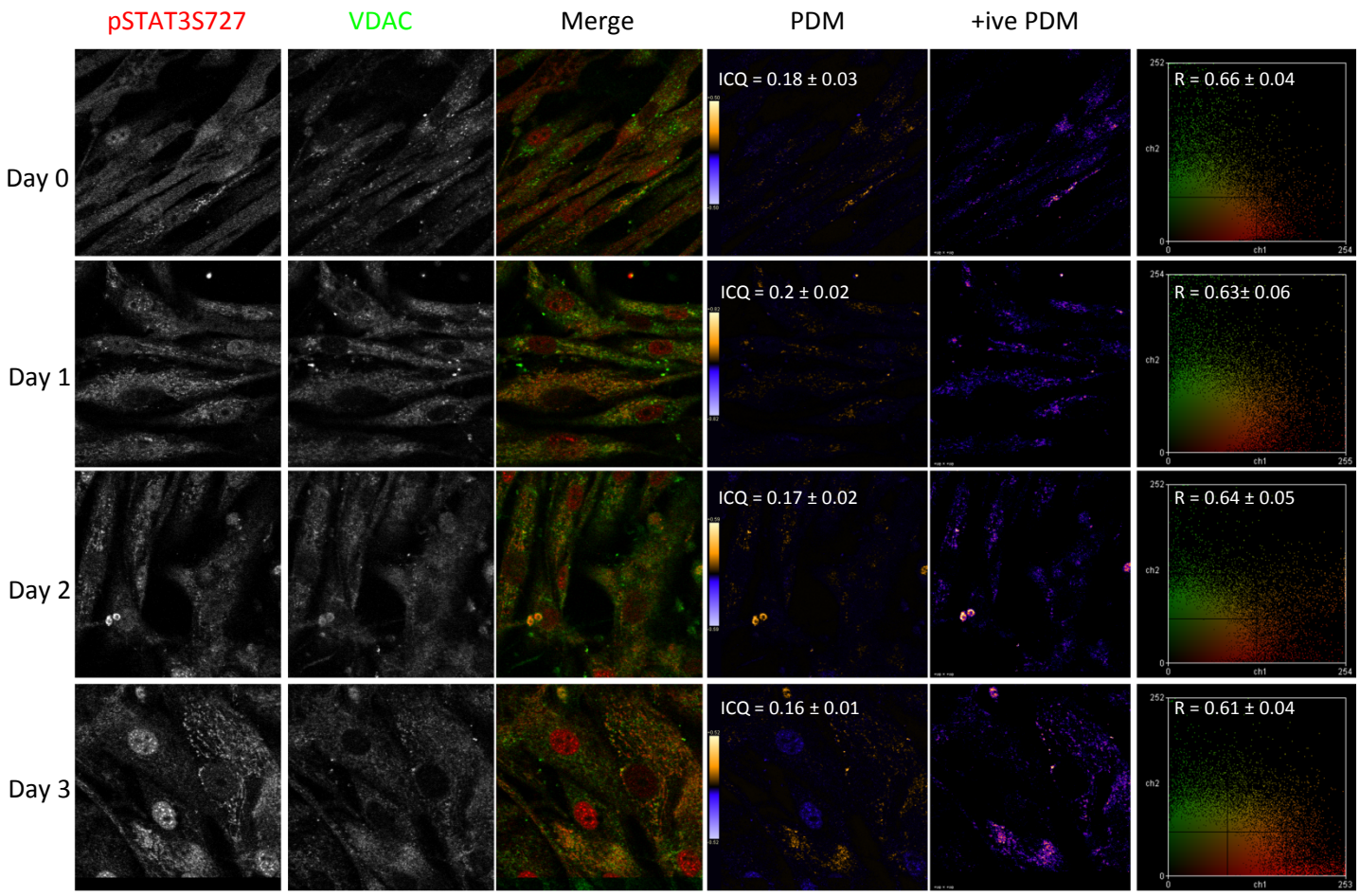

Figure 5.2: Co-localisation analysis of pSTAT3S727 and VDAC in differentiating HMSC-ad cells. Mesenchymal cells were induced to differentiated and subjected to immunofluorescence staining as previously described. Images were captured using the Zeiss LSM 510 Meta confocal microscope and co-localisation analysis was performed using ImageJ software (NCBI). Panels represent: the red channel (pSTAT3S727), green channel (VDAC); PDM images highlighting co-localized pixels in yellow and segregated pixels in blue; fluorescence scattergrams showing the pixel-pixel overlap of the signals between the two channels.

5.2 Levels of mitochondrial pSTAT3S727 during differentiation

Western blot analysis was used to determine whether there was an increased amount of mitochondria in differentiating cells. Prohibitin (PHB) is a mitochondrial protein localised in the inner mitochondrial membrane and has been reported to act a chaperone within the mitochondria (Zhou *et al*., 2012; Yang *et al*., 2014). Prohibitin was not used in co-localisation experiments as the species of pSTAT3S2727 and PHB antibodies available were identical and therefore different secondary antibodies could not be used.

Blots were probed for PHB and the relative levels of protein analysed via densitometry using ImageJ (NCBI). Actin was used as a loading control. Densitometric analysis revealed that there was a general trend of increasing levels of PHB in differentiating 3T3-L1 cells as shown in Figure 5.3. This result was particularly interesting as levels of pSTAT3S727 were shown to increase during adipogenesis as well as discussed in Chapter 3. Despite this result, it cannot be concluded that there was an increased number of mitochondria, only that there was an increased amount of the mitochondrial protein, PHB. It was assumed however that PHB levels are directly related to mitochondrial levels.

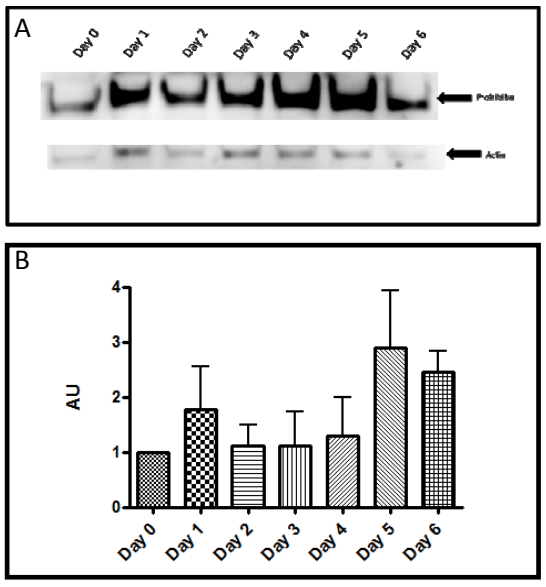

Figure 5.3. Levels of Prohibitin during 3T3-L1 adipocyte differentiation. (A) Western blot of Prohibitin through days 0 to 6 of differentiation. Equal amounts of protein were run and Prohibitin signal normalised against actin as a loading control. (n = 3). (B) Densitometric analysis of levels of Prohibitin during differentiation (n = 3).

Mitochondria were next isolated from differentiating 3T3-L1 preadipocytes and HMSC-ad cells and probed for pSTAT3S727 to determine firstly, whether pSTAT3727 would be detected, and secondly, if detected whether the levels of pSTAT3S727 changed within mitochondria during differentiation. Isolated mitochondrial samples were probed for Actin, Lysosomal-associated membrane protein 1 (LAMP1) and Histone H3 to determine levels of cytoplasmic, lysosome and nuclear contamination respectively. Actin and LAMP1 was not detected in any samples, yet Histone was detected in all samples as shown is Figure 5.4B. As STAT3 is known to localise to the nucleus, Histone contamination is concerning and had to be taken into account when analysing the data. However, it has been put forward that Histone H3 is targeted to the mitochondria (Zanin *et al.,* 2010) and that Histone H3 associates to the out mitochondrial membrane (Choi *et al*., 2011) suggesting that the detection of Histone H3 in mitochondrial isolations may not be nuclear contamination.

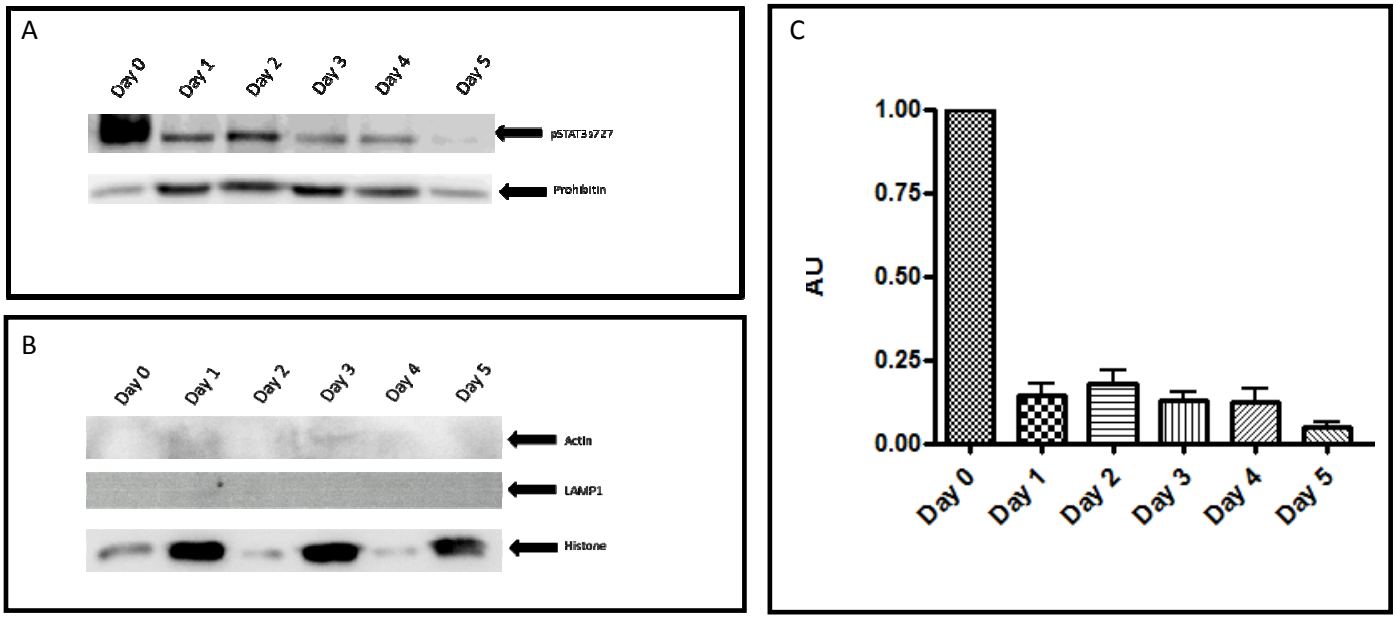

Figure 5.4. Levels of pSTAT3S727 within isolated mitochondria during 3T3-L1 adipocyte differentiation. (A) Mitochondria were isolated from differentiating cells on day 0 to 5 of differentiation and subjected to western blot analysis to determine levels of pSTAT2S7272. The mitochondrial marker Prohibitin was used as a loading control. (n = 3). (B) Blots were probed for Actin, LAMP1 and Histone H3 to determine levels of cytoplasmic, lysosome and nuclear contamination respectively (C) Densitometric analysis of mitochondrial levels of pSTAT3S727 during differentiation (relative to Prohibitin) (n = 3).

Serine 727 phosphorylated STAT3 was detected in all mitochondrial samples and analysis revealed surprisingly, that levels were highest in mitochondria isolated from uninduced

undifferentiated cells. Levels of Histone within Day 0 samples were minimal as compared to Days 1 to 5 and therefore the higher levels of mitochondrial pSTAT3S727 could not be as a result of nuclear contamination. Levels were found to significantly drop upon the induction of differentiation. This was unexpected as whole cell levels of pSTAT3S727 were found to increase as differentiation progressed, as discussed in Chapter 4. Mitochondrial isolations were performed on HMSC-ad cell and levels of mitochondrial pSTAT3S727 were again assessed by Western blot analysis. .

The same trend was not observed in HMSC-ad cells; however this is based on preliminary results. Nonetheless, pSTAT3S727 was detected in all samples as seen in Figure 5.5. It appears, based on the appearance and a basic densitometric analysis that levels of pSTAT3S727 remain relatively constant until Day 6 of differentiation where levels appear to be slightly elevated. However, this experiment requires replicates in order to obtain robust data. Nonetheless, pSTAT3S727 was found to be present within the mitochondria of both differentiating 3T3-L1 preadipocytes and HMSC-ad mesenchymal cells.

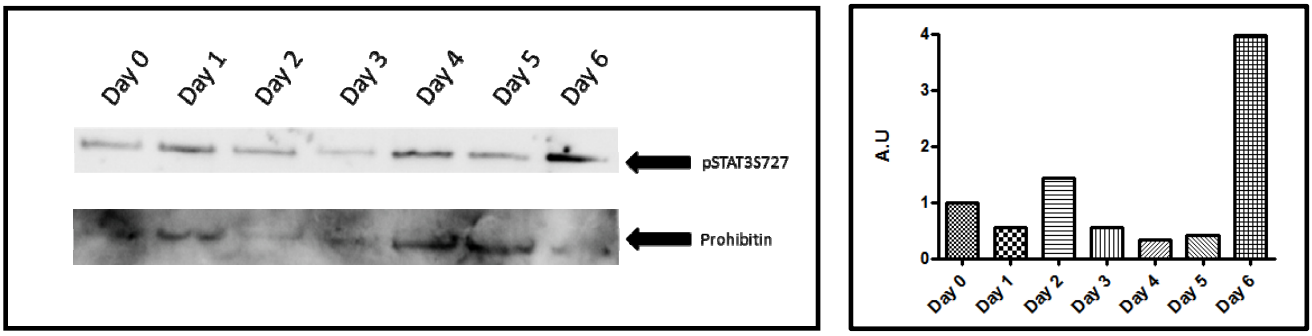

Figure 5.5. Levels of pSTAT3S727 within isolated mitochondria during HMSC-ad adipocyte differentiation. (A) Mitochondria were isolated from differentiating cells on day 0 to 5 of differentiation and subjected to western blot analysis to determine levels of pSTAT2S7272. The mitochondrial marker Prohibitin was used as a loading control

The results of the co-localisation analysis as well as the investigation on the levels of pSTAT3S727 within isolated mitochondria suggest that pSTAT3S727 is indeed present within mitochondria. Results indicate that mitochondrial pSTAT3S727 levels in 3T3-L1 preadipocytes decrease upon the induction of differentiation. Although conclusions about the changes in the levels of mitochondrial pSTAT3S727 within HMSC-ad cells cannot be made, preliminary data indicates that the levels of mitochondrial pSTAT3S727 does change during

adipogenesis. STAT3 may play a role in regulating mitochondrial respiration and ROS production within the mitochondria of differentiating cells

5.3 Levels of Reactive Oxygen species during differentiation of 3T3-L1 preadipocytes and HMSC-ad cells.

Levels of Reactive Oxygen Species (ROS) in differentiating 3T3-L1 preadipocytes and HMSC-ad cells was investigated by a 2', 7- dichloro-3', 5-dihydrofluorescein diacetate (DCF-DA) flow cytometry assay. The acetate groups of the non-fluorescent substrate are cleaved *in vivo* by endogenous esterases, and subsequent oxidation by intracellular peroxides produces fluorescent 2',7-dichlorofluorescin, which can be detected by flow cytometry in the FITC channel (Saretzki *et al.*, 2004). HMSC-ad cells were induced to differentiate for 0 to 5 days, and 3T3-L1 cells for 0 to 7 days, and intracellular ROS levels determined by incubating cells with DCF-DA prior to analysis on the Becton Dickson FACS Aria II flow cytometer.

Figures 5.6 shows the gating strategy used to analyse intracellular levels of ROS during differentiation of 3T3-L1 preadipocytes and Figure 5.8 in HMSC-ad cells. The live population was selected based on the forward scatter (FSC) fluorescence profile. Forward scatter is directly proportional to size of cells, the larger the cell, the larger the FSC signal recorded. Cellular debris and dead cells (with low FSC signals) were excluded from the analysis by gates including only a subpopulation of recorded events considered to be live for subsequent ROS analysis. The analysis of levels of ROS within each live population involved specifying gates based on the 3 major DCF-DA stained populations observed. Histograms of Counts (y-axis) versus FITC-H (DCF-DA) fluorescence revealed populations of low, medium and high staining as shown in Figures 5.6A,B,C and 5.7A,B,C. The proportion of cells with high staining in each sample was used as an indication of an increase in the levels of ROS within each live population and results are represented as bar graphs in Figures 5.6D and 5.8D.

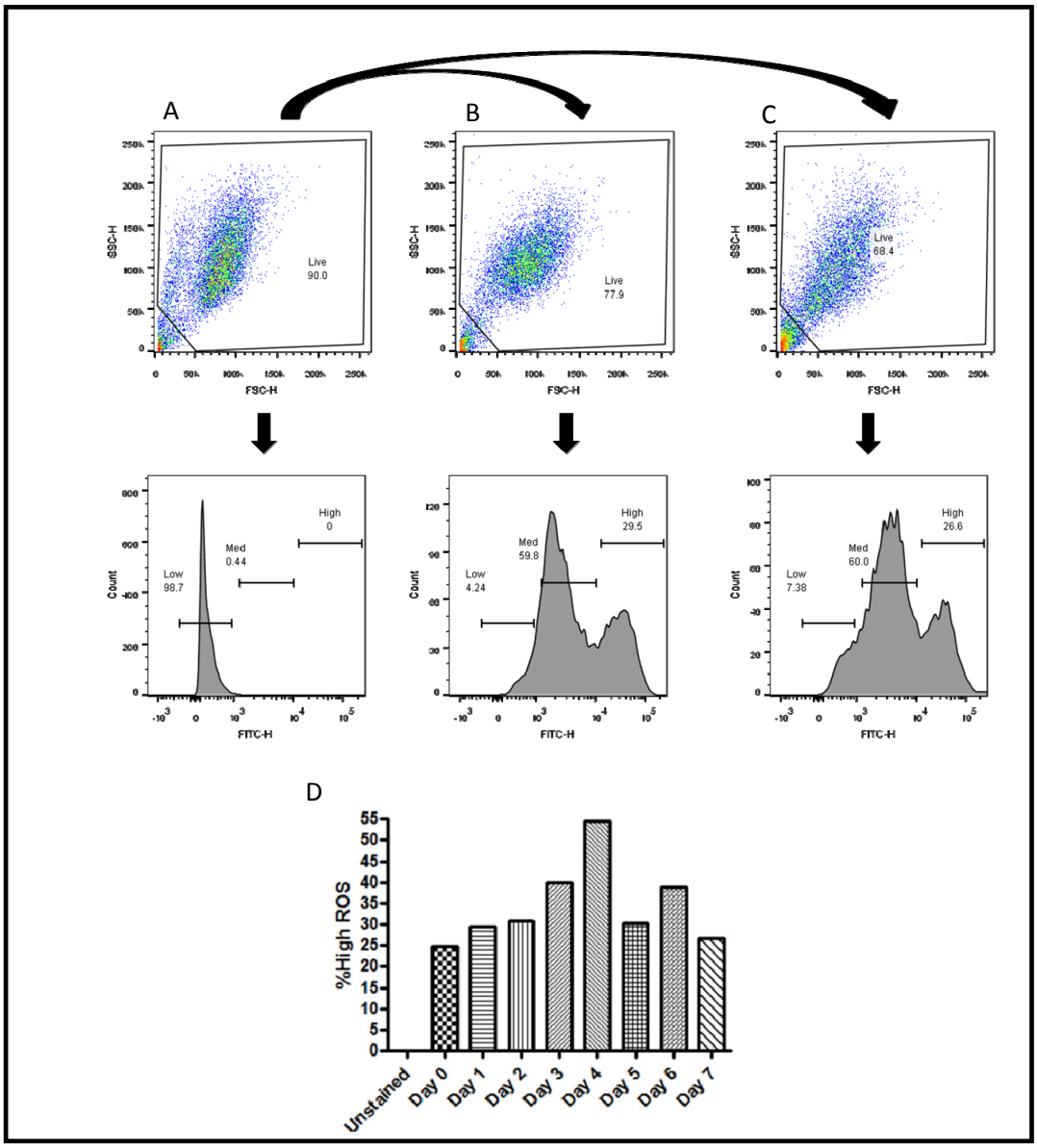

Figure 5.6. Gating strategy and analysis of ROS levels in differentiating 3T3-L1 preadipocytes through Days 0 to 7 of differentiation. The live population gate was defined forward scatter (x-axis) to exclude events that were small in size (low FSC), representing dead cells and debris. Gates were defined using the (A) unstained sample and duplicated on all remaining samples, as indicated by arrows from A to B and C. Live events were then represented as histograms as FITC-H intensity (DCF-DA fluorescence) plotted against Counts. Three populations were defined, namely ROS Low, ROS Medium and ROS High using the (B) Day 0 and (C) Day 7 samples, and gates copies to all remaining samples. (D) The proportion of ROS high events from Days 0 to 7. Results are representative of 2 independent experiments.

Intracellular levels of ROS within 3T3-L1 cells steadily increased upon the induction of differentiation for 4 days, after which levels were found to drop back to normal levels. Figure 5.7 shows Zebra plots (illustrating major populations) of FITC-H (DCF-DA fluorescence) on the x-axis versus SSC on the y-axis and show the shift of the live population with low DCF-DA signal to a population with high DCF-DA signal as differentiation progressed. Interestingly there is a population of cells with high levels of ROS in undifferentiated cells, as seen in Figure 5.7B, however this population does not contain particularly granular cells, which were observed once cells were induced to differentiate. Cells in this ROS high population become more granular, as seen in Figure 5.7C-I, showing that the increase in the levels of ROS is accompanied by an increase in cellular granularity (resulting in increased SSC signal). This increase in cellular granularity in differentiating 3T3-L1 preadipocytes was observed by Lee *et al.*, (2004) who utilized flow cytometry to monitor 3T3-L1 differentiation. The change in granularity represents a change in the morphology of the cells as well as increased lipid content that was observed and discussed in Chapter 3.

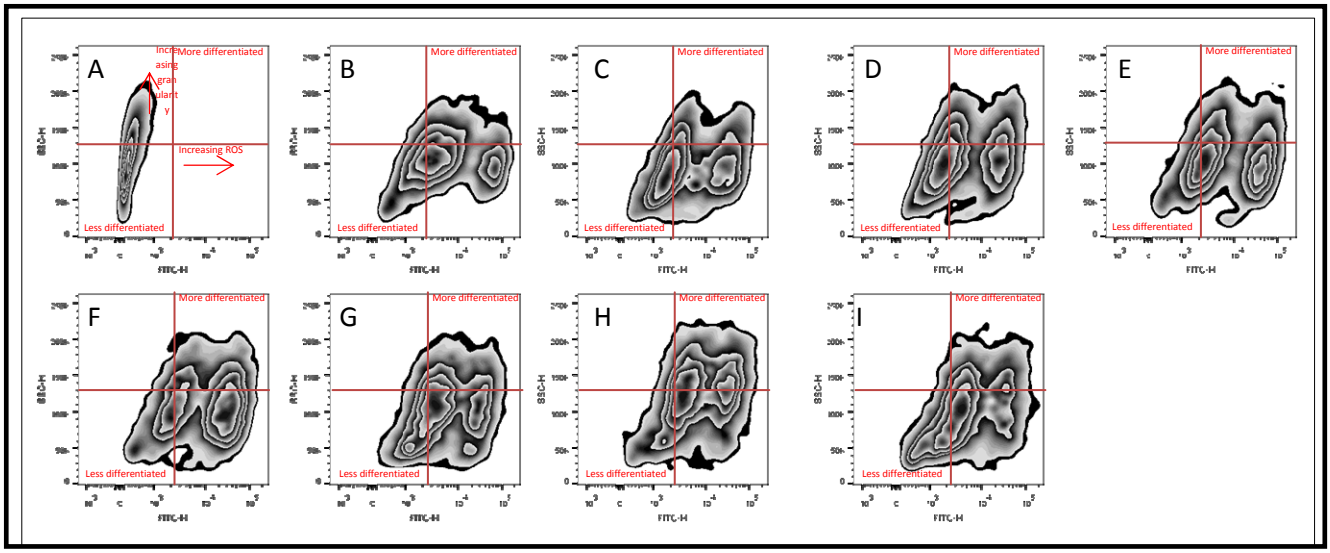

Figure 5.7. Zebra plots of FITC-H (DCF-DA fluorescence) against SSC (granularity) of differentiating 3T3-L1 preadipocytes stained with DCF-DA through days 0 to 7 of differentiation. Samples were either (A) unstained, or incubated in the presence of DCF-DA after (B) Day 0, (C) Day 1, (D) Day 2, (E) Day 3, (F) Day 4, (G) Day 5, (H) Day 6 and (I) Day 7 of differentiation. Defined regions indicate increased differentiation (Higher ROS levels and increased granularity). Plots generated using FlowJo v10.0

Intracellular ROS analysis of differentiating HMSC-ad cells was carried in same manner as described for 3T3-L1 preadipocyte ROS analysis. Levels of intracellular ROS within HMSC-

ad cells was found to steadily increase during differentiation as seen in Figure 5.8B. Zebra plots of DCF-DA signal against SSC clearly show the shifting of cells from a ROS low, SSC low population to a ROS high, SSC high population. In later stages of differentiation (days 4 and 5, Figure 5. 9 F and G), there is a high proportion of highly granular cells despite not having high DCF-DA signal. This again indicates the change in morphology and composition of cells that occurs during differentiation.

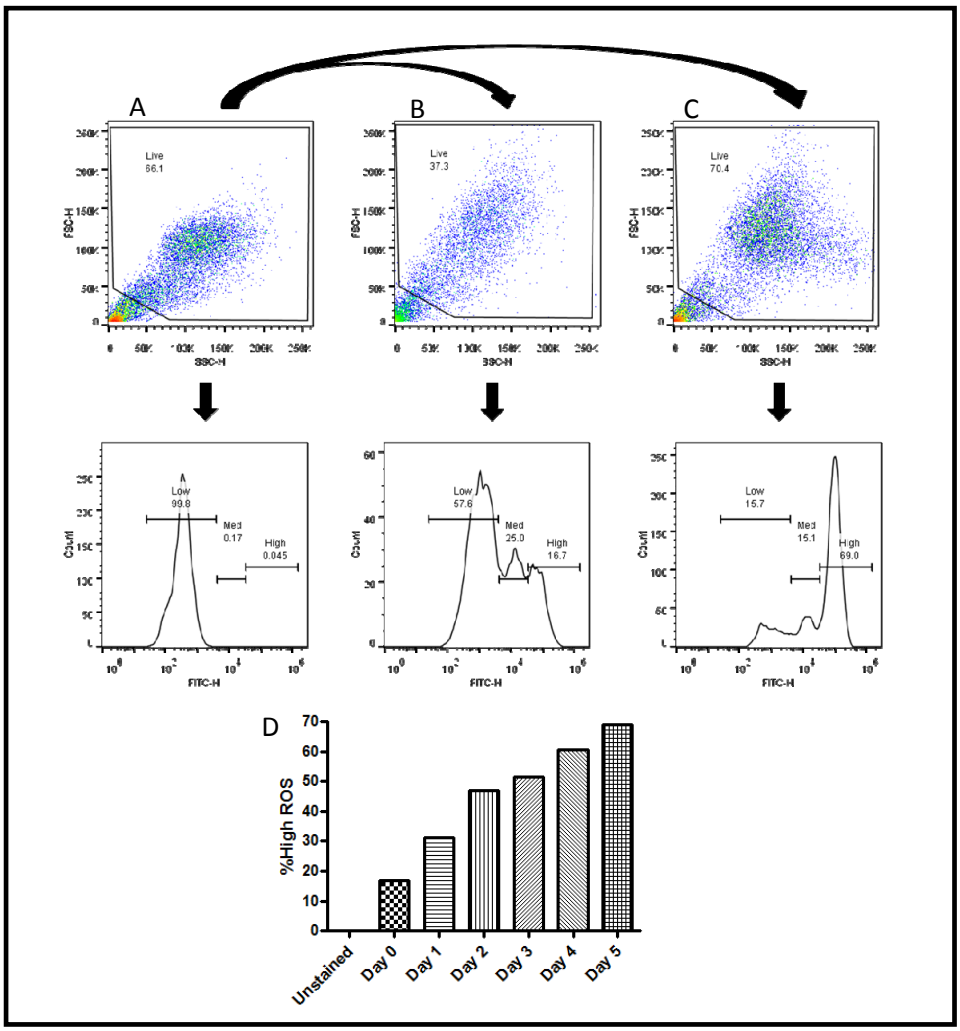

Figure 5.8. Gating strategy and analysis of ROS levels in differentiating HMSC-ad mesenchymal stem cells through Days 0 to 5 of differentiation. Gating on HMSC-ad cells was performed as previously described. (A) Unstained day 0 sample, (B) Stained Day 0 sample, (C) Stained Day 5 sample.

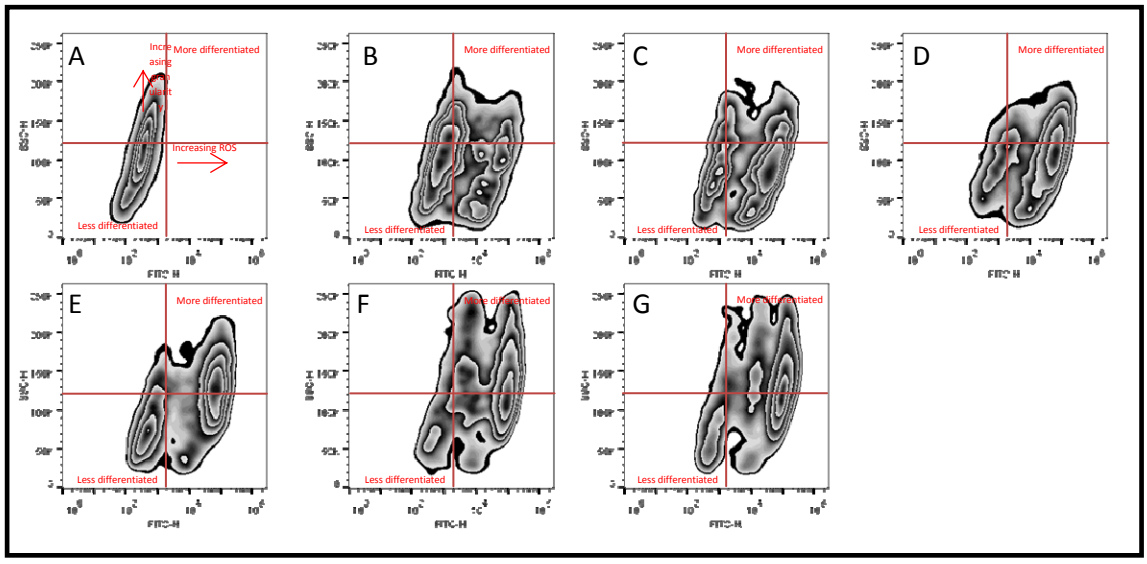

Figure 5.9. Zebra plots of FITC-H (DCF-DA fluorescence) against SSC (granularity) of differentiating HMSC-ad cells stained with DCF-DA through days 0 to 7 of differentiation. Samples were either (A) unstained, or incubated in the presence of DCF-DA after (B) Day 0, (C) Day 1, (D) Day 2, (E) Day 3, (F) Day 4, (G) Day 5, (H) Day 6 and (I) Day 7 of differentiation. Defined regions indicate increased differentiation (Higher ROS levels and increased granularity). Plots generated using FlowJo v10.0

Increased ROS levels have been reported during adipogenesis and it has been revealed that increased ROS levels play an important role during adipogenesis. In 3T3-L1 preadipocytes is has been shown that that ROS facilitates differentiation by accelerating mitotic clonal expansion (Lee *et al*, 2009). The research showed that increased levels of ROS result in C/EBPβ having greater DNA binding affinity which results in accelerated MCE and therefore greater differentiation efficiency. The same research demonstrated that that treatment of 3T3-L1 cells with H_2O_2 during differentiation resulted in accelerated cell cycle progression and that antioxidant treatment resulted in an arrest of MCE indicating that ROS must play a particularly important role during 3T3-L1 adipogenesis.

High levels of ROS have also been shown to play an important role during adipogenesis of mesenchymal stem cells. Tormos *et al.* (2011) showed that mesenchymal stem cells undergoing adipogenesis have increased mitochondrial metabolism and increased levels of ROS generation. As was found in the 3T3-L1 model, treatment of the mesenchymal stem cells with mitochondrial targeted antioxidants resulted in the inhibition of adipocyte

differentiation and this was reverted by the addition of exogenous H_2O_2 (Tormos *et al*., 2011). It was concluded that ROS production was not a consequence of differentiation, but that increased levels of ROS are required for differentiation. More recently, it has been shown that mitochondrial biogenesis and oxygen consumption increase during adipogenesis and reducing mitochondrial respiration by hypoxia or inhibition of the mitochondrial electron transport chain results in less efficient adipocyte differentiation of mesenchymal stem cell (Zhang *et al.,* 2013).

The results presented here show that 3T3-L1 cells have increases levels of ROS for the first four days of differentiation, and then drop back to normal levels. This result correlates with the expression levels of C/EBPβ during adipogenesis shown in Chapter 3, Section 2.3, Figure 3.2A where levels of C/EBPβ start to drop after day 4 of differentiation as well as the distinct loss of nuclear localised C/EBPβ four days post induction as seen in the Chapter 2, Section 2.3 Figure 2.3.

Interestingly, ROS levels in HMSC-ad cells are maintained past day 4 of differentiation with levels increasing to day 5. These maintained ROS levels may explain why HMSC-ad cells accumulate more lipids more rapidly and seemingly differentiate more quickly than 3T3-L1 preadipocytes. Although the levels and localisation of C/EBPβ in HMSC-ad cells were distinctly different to those in 3T3-L1 preadipocytes (discussed in Chapter 2, Section 2.3.1), it could be possible that increased levels of ROS play a role in activating other important adipogenic proteins such as the α and δ isoforms of C/EBP which may be expressed earlier in mesenchymal adipogenesis.

Chapter 6

Conclusions and Future Work.

6. Conclusions and Future Work

6.1 Conclusions

Data suggesting STAT3 localises to the mitochondria was originally presented by Wegrzyn *et al*., (2009) where it was shown to potentially play a role in respiration. Since then STAT3 has been reported to play a role in the mitochondria in multiple investigations. It was found to facilitate Ras dependant oncogenic transformation by augmenting the electron transport chain activity of complexes II and V in murine cells (Gough *et al.*, 2009) and that this mitochondrial STAT3 activity requires the MEK pathway to phosphorylate the STAT3 serine 727 residue (Gough *et al.,* 2013). Then Szczepanek *et al*., (2011) showed that mitochondrial-targeted STAT3 protects against ischemia-induced changes in the electron transport chain and the generation of ROS in transgenic mice. More recently it was then shown that mitochondrial STAT3 promotes breast cancer growth via phosphorylation of the serine 727 residue of STAT3 (Zhang *et al.*, 2013).

The data presented in this manuscript has shown that STAT3 plays a role in adipogenesis by cycling into and out of the nucleus as well as the mitochondria. It has been shown here that levels of pSTAT3S727 increase while levels of pSTAT3Y705 decrease during differentiation (Figure 4.2 and Figure 4.3). Surprisingly, despite levels of pSTAT3S727 being found to increase in the whole cell, data suggest that levels of pSTAT3S727 within the mitochondria decrease upon the induction of differentiation (Figure 5.4), however this result needs to be explored further.

Levels of mitochondria were shown to increase (Figure 5.3) as were the levels of ROS during adipogenesis in both 3T3-L1 (Figure 5.6) and HMSC-ad cells (Figure 5.8). Through the development of a real-time differentiation assay, it was shown that the blocking of the tyrosine 705 phosphorylation of STAT3 resulted in markedly altered differentiation *CI* profiles (Figure 4.8) and reduced lipogenesis as did blocking of MEK1/2 and serine 727 phosphorylation of STAT3 via a MEK inhibitor (Figure 4.9).

Based on this data it is hypothesized that STAT3 is involved in modulating levels of ROS during differentiation. STAT3 has been implicated in activating the Warburg effect (Demaria *et al.,* 2010) in a canonical manner by regulating the expression of certain genes and therefore affecting ROS levels. However, STAT3 may be regulating ROS in a more direct non-

canonical manner. Recently, it has been shown that STAT3 interacts directly with GRIM-19, a subunit of complex I of the mitochondrial electron transport chain (Tammineni *et al.*, 2013). Complex I is an area of known ROS production (Hirst *et al.*, 2008). Interestingly it has been shown that the nuclear localisation sequence, DNA-binding domain, the SH2 domain and tyrosine 705 of the STAT3 molecule are not required for the actions of mitochondrial pSTAT3S727 (Zhang *et al.*, 2013). This suggests that mitochondrial STAT3 must be the longer α isoform of the protein.

Data presented in this manuscript show that levels of mitochondrial STAT3 change during the differentiation process, suggesting that STAT3 is playing a role in mitochondrial respiration and ROS production. The question remains, if STAT3 is actively regulating ROS production in the mitochondria, how does this process work? Zhang *et al.,* (2013) showed that phosphorylation of serine 727 of the STAT3 molecule enhanced coupling of complex I and resulted in decreased production of ROS in 4T1 mouse mammary carcinoma cells. This result may explain why lower levels of mitochondrial pSTAT3S727 were found in differentiating cells. When cells are induced to differentiate, levels of ROS increase. If STAT3 functions in the mitochondria to reduce ROS levels, upon induction mitochondrial STAT3 levels may decrease allowing for higher levels of ROS to be produced. This model is illustrated in Figure 6.1.

Higher levels of ROS have been shown to play an important role during adipogenic differentiation. It has been reported that ROS production at complex III regulates adipogenesis of human mesenchymal stem cells (Tormos *et al.,* 2011). Further to this, it has been shown that higher levels of ROS within differentiating 3T3-L1 cells accelerate mitotic clonal expansion and increase the differentiation efficiency (Lee *et al.*, 2009). The primary action of ROS within differentiating 3T3-L1 cells may be on the DNA binding efficiency of CCAAT/enhancer binding protein β. As discussed previously, C/EBPβ is an early adipogenic protein expressed within the first few hours of adipocyte differentiation. Interestingly, C/EBPβ DNA binding has been shown to be enhanced by oxidation and that increased levels of ROS result in enhanced C/EBPβ DNA binding activity (H. Lee *et al*., 2009). It was found that levels of ROS correlated with the nuclear localisation of C/EBPβ in this study. It was too shown that levels of mitochondrial STAT3 were reduced upon induction of differentiation.

A

Pre-induction of differentiation

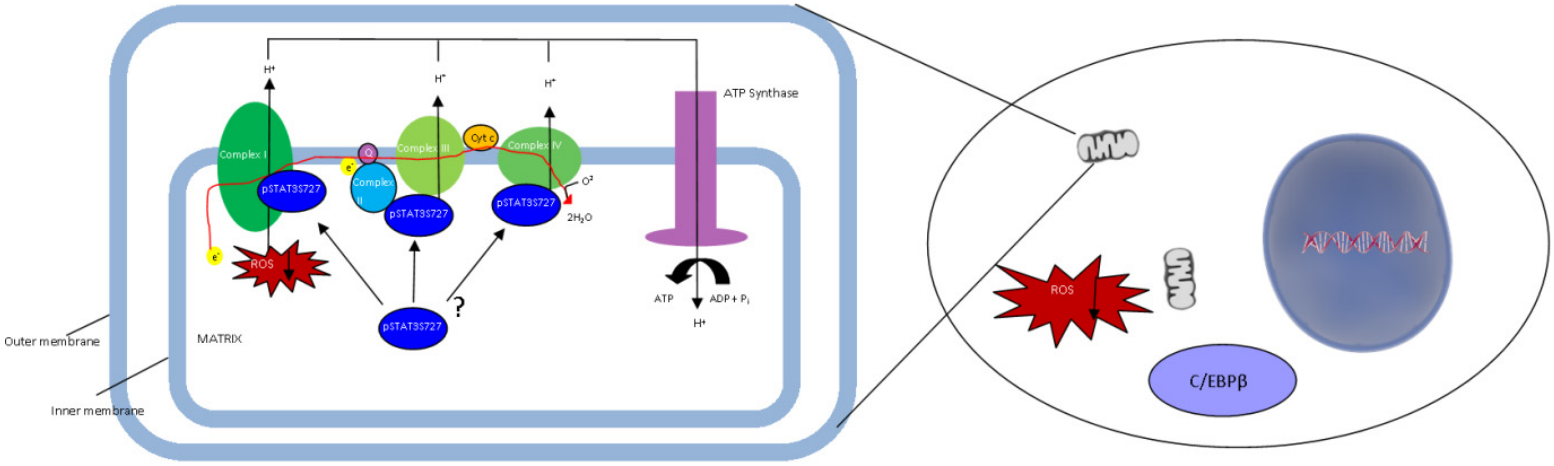

B

Post-induction of differentiation

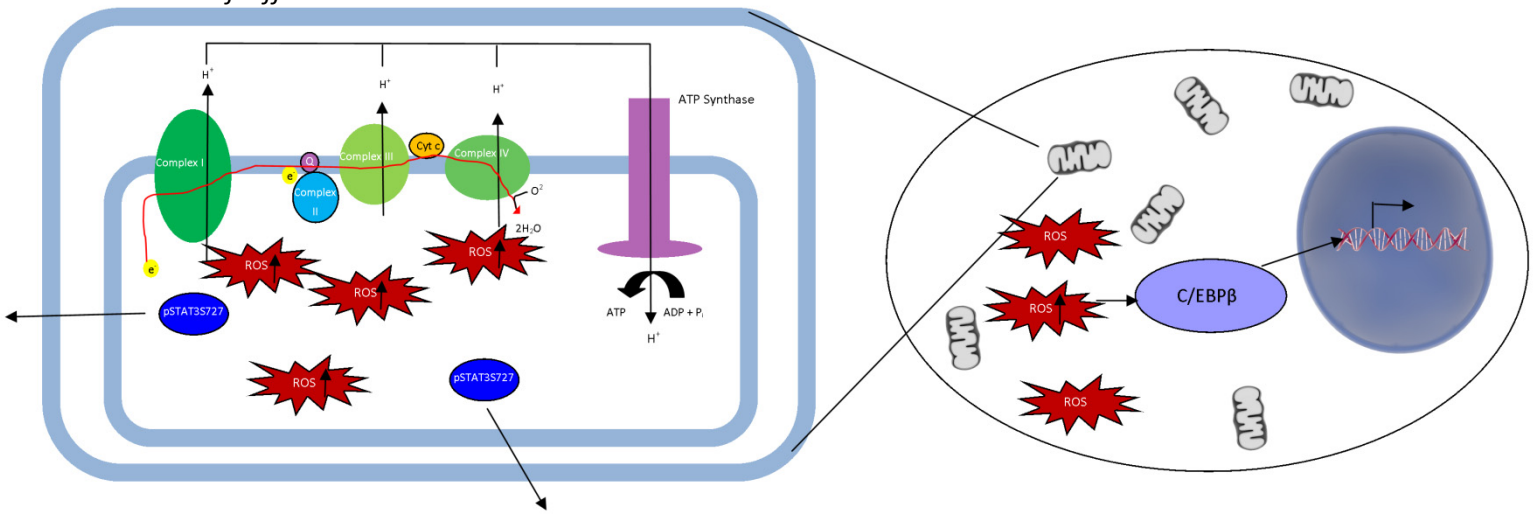

Figure 6.1. STAT3 potentially regulates ROS during differentiation by cycling into and out of mitochondria. (A) When cells maintain potency STAT3 is present in high levels in the mitochondria maintaining low levels of ROS by modulating activity of the complexes of the electron transport chain. STAT3 is most probably found at Complex I, II or III. (B) When cells are induced to differentiate levels of mitochondria increase and STAT3 leaves the mitochondria. This results in increased levels of ROS. Increased levels of cellular ROS lead to a conformational change in adipogenic transcription factors such as C/EBPβ, which, in turn increases the DNA binding activity of these factors. This results in the expression of adipogenic proteins.

This reduction of mitochondrial STAT3 may be the cause of increased levels of ROS, which in turn results in enhanced DNA binding of adipogenic transcription factors such as C/EBPβ, allowing for efficient adipocyte differentiation. Immunofluorescence analysis revealed cytoplasmic punctate structures of pSTAT3S727 during differentiation which could be

indicative of mitochondrial STAT3 actively cycling into and out of mitochondria, potentially regulating ROS production throughout the differentiation process, as shown in Figure 6.1.

Interestingly, in HMSC-ad cells higher ROS levels were sustained for a longer period and this may account for the more efficient adipogenesis of these cells. Through immunofluorescence analysis it was determined that the process in which human HMSC-ad mesenchymal cells differentiate into adipocytes is different from the process of adipocyte differentiation of murine 3T3-L1 preadipocytes. The localisation changes of C/EBPβ observed in HMSC-ad cells was distinctly different to those observed in the murine 3T3-L1 adipogenesis model. Further to this it has been reported that mesenchymal stem cells do not undergo contact inhibition and therefore do not display mitotic clonal expansion (Qian *et al*., 2010). However, immunofluorescence analysis of these cells display mitochondrial like structures when stained for pSTAT3S727 and Western blot analysis revealed the presence of pSTAT3S727 in mitochondrial isolations. This could indicate that although the adipocyte differentiation processes are different between organisms, the role of mitochondrial STAT3 and ROS regulation during differentiation could be conserved.

6.2 Future work

Future experiments should be carried out to gain a better understating of the role mitochondrial STAT3 plays during adipogenesis. An interesting and more robust experiment to quantify levels of pSTAT3S727 within the mitochondria through the use of flow cytometry as described in Mattiasson (2004) could be designed. In this experiment large quantities of intact functional mitochondria would be isolated from cells in different stages of differentiation and would be stained with anti-pSTAT3S727 antibodies to then be run through a flow cytometer to detect relative levels of the protein.

A very useful tool, quantitative real time polymerase chain reaction (RT-PCR) allows the monitoring of the production of mRNA molecules, however this does not necessarily mean that proteins of interest are being expressed, only that mRNA required for the production of the proteins has been produced. Further experiments utilizing RT-PCR would allow for further confirmation of the induction of adipogenesis by measuring mRNA levels of adipogenic factors such as C/EBPβ and PPARγ. It could also provide data concerning the mRNA levels of STAT3, however the phosphorylation events of interest in this study would not be detected utilizing this method. Although RT-PCR would be useful in measuring the

mRNA levels of certain genes, Western blot analysis provides direct evidence of proteins of interest being expressed, and allows for the detection of phosphorylation events.

Another interesting experiment that could be designed could involve the production of a pSTAT3S727-EGFP plasmid, and subsequent transfection into cells for live cell imaging of the protein moving into and out of the mitochondria during differentiation. Combined with this experiment, more robust co-localisation experiments could be set up using mitochondrial markers reported to interact with STAT3, such as GRIM-19. High resolution confocal microscopy would be of great value in this type of experiment. An immunogold electron microscopy experiment would help determine the exact localisation of STAT3 within the mitochondria during differentiation.

Pull down assays of STAT3 against mitochondrial samples followed by mass spectroscopy could be done to identify interacting proteins. Following identification of potential mitochondrial STAT3 interacting proteins Yeast-two-hybrid experiments could be carried out to confirm interactions. Further biophysical experiments using Surface Plasmon Resonance (SPR) spectroscopy to determine the kinetics of each interaction could then be carried out.

This study was one of the first in the investigation of the role mitochondrial STAT3 plays in differentiation. Previous works have focussed mainly on canonical STAT3, ROS or mitochondria during differentiation. Recent evidence of mitochondrial STAT3 and its role in ROS regulation led to the hypothesis that mitochondrial STAT3 may play an indirect role in regulating differentiation. This hypothesis, based on data presented here, may have some validity and with further experimentation could be definitively proven in future work.

Chapter 7: References

References

Aflatoonian, B., & Moore, H. (2005). Human primordial germ cells and embryonic germ cells, and their use in cell therapy. *Current opinion in biotechnology*, *16*(5), 530–5. doi:10.1016/j.copbio.2005.08.008

Alberts, B., Johnson, A., Lewis, J., Raff, M., Roberts, K., & Walter, P. (2002). Molecular Biology of the Cell. Garland Science.

Alison, M. R., & Islam, S. (2009). Attributes of adult stem cells. *The Journal of pathology*, *217*(2), 144–60. doi:10.1002/path.2498

Alitalo, K., Kuismanen, E., Myllylä, R., Kiistala, U., Asko-Seljavaara, S., & Vaheri, a. (1982). Extracellular matrix proteins of human epidermal keratinocytes and feeder 3T3 cells. *The Journal of cell biology*, *94*(3), 497–505.

Andersson, C. X., Sopasakis, V. R., Wallerstedt, E., & Smith, U. (2007). Insulin antagonizes interleukin-6 signaling and is anti-inflammatory in 3T3-L1 adipocytes. *The Journal of biological chemistry*, *282*(13), 9430–5. doi:10.1074/jbc.M609980200

Angell, J. E., Lindner, D. J., Shapiro, P. S., Hofmann, E. R., & Kalvakolanu, D. V. (2000). Identification of GRIM-19, a novel cell death-regulatory gene induced by the interferon-beta and retinoic acid combination, using a genetic approach. *The Journal of biological chemistry*, *275*(43), 33416–26. doi:10.1074/jbc.M003929200

Aonuma, Y., Kondo, Y., Hirano-Iwata, A., Nishikawa, A., Shinohara, Y., Iwata, H., … Niwano, M. (2013). Label-free and real time monitoring of adipocyte differentiation by surface infrared spectroscopy. *Sensors and Actuators B: Chemical*, *176*, 1176–1182. doi:10.1016/j.snb.2012.10.030

Araki, R., Uda, M., Hoki, Y., Sunayama, M., Nakamura, M., Ando, S., … Abe, M. (2013). Negligible immunogenicity of terminally differentiated cells derived from induced pluripotent or embryonic stem cells. *Nature*, *494*(7435), 100–4. doi:10.1038/nature11807

Arsenijevic, T., Grégoire, F., Delforge, V., Delporte, C., & Perret, J. (2012). Murine 3T3-L1 adipocyte cell differentiation model: validated reference genes for qPCR gene expression analysis. *PloS one*, *7*(5), e37517. doi:10.1371/journal.pone.0037517

Bagnaninchi, P. O., & Drummond, N. (2011). Real-time label-free monitoring of adipose-derived stem cell differentiation with electric cell-substrate impedance sensing. *Proceedings of the National Academy of Sciences of the United States of America*, *108*(16), 6462–7. doi:10.1073/pnas.1018260108

Baker, M. (2011). Stem cells in culture: defining the substrate. *Nature Methods*, *8*(4), 293–297. doi:10.1038/nmeth0411-293

Battista, S., Guarnieri, D., Borselli, C., Zeppetelli, S., Borzacchiello, A., Mayol, L., … Netti, P. a. (2005). The effect of matrix composition of 3D constructs on embryonic stem cell differentiation. *Biomaterials*, *26*(31), 6194–207. doi:10.1016/j.biomaterials.2005.04.003

Boengler, K., Hilfiker-Kleiner, D., Heusch, G., & Schulz, R. (2010). Inhibition of permeability transition pore opening by mitochondrial STAT3 and its role in myocardial

ischemia/reperfusion. *Basic research in cardiology*, *105*(6), 771–85. doi:10.1007/s00395-010-0124-1

Bone, H., Krause, D., Ph, D., & Niklason, L. E. (2009). Influence of Culture Medium on Smooth Muscle Cell. *Tissue Engineering*, *15*(2), 319–330.

Boveris, a, Cadenas, E., & Stoppani, a O. (1976). Role of ubiquinone in the mitochondrial generation of hydrogen peroxide. *The Biochemical journal*, *156*(2), 435–44.

Brookes, P. S. (2005). Mitochondrial H(+) leak and ROS generation: an odd couple. *Free radical biology & medicine*, *38*(1), 12–23. doi:10.1016/j.freeradbiomed.2004.10.016

Buettner, C., Muse, E. D., Cheng, A., Chen, L., Pocai, A., Su, K., … Rossetti, L. (2008). Leptin controls adipose tissue lipogenesis via central, STAT3– independent mechanisms. *Nature medicine*, *14*(6), 667–675. doi:10.1038/nm1775.Leptin

Buettner, C., Pocai, A., Muse, E. D., Etgen, A., Myers, M., & Rossetti, L. (2006). Critical role of STAT3 in leptin's metabolic actions. *Cell metabolism*, *4*(1), 49–60. doi:10.1016/j.cmet.2006.04.014.Critical

Campos, S. P., Wang, Y., & Baumann, H. (1996). Insulin modulates STAT3 protein activation and gene transcription in hepatic cells. *The Journal of biological chemistry*, *271*(40), 24418–24.

Cao, Z, Umek, R. M., & McKnight, S. L. (1991). Regulated expression of three C/EBP isoforms during adipose conversion of 3T3-L1 cells. *Genes & Development*, *5*(9), 1538–1552. doi:10.1101/gad.5.9.1538

Cao, Zhenhui, Yang, H., Kong, L., Gu, D., He, Z., Xu, Z., … Lin, Q. (2012). Growth arrest induction of 3T3-L1 preadipocytes by serum starvation and their differentiation by the hormonal adipogenic cocktail. *Journal of Cell and Animal Biology*, *6*(5), 57–65. doi:10.5897/JCAB11.074

Ceresa, B. P., Horvath, C. M., & Pessin, J. E. (1997). Signal Transducer and Activator of Transcription-3 Serine Phosphorylation by Insulin Is Mediated by a Ras /, *138*(10), 4131–4137.

Chem, J. B., Rubin, S., & Hirsch, A. (1978). Development of hormone receptors and hormonal responsiveness in vitro . Insulin receptors and insulin sensitivity in the preadipocyte and adipocyte forms of Development of Hormone Responsiveness in Vitro.

Chen, S., Choo, A., Chin, A., & Oh, S. K. W. (2006). TGF-beta2 allows pluripotent human embryonic stem cell proliferation on E6/E7 immortalized mouse embryonic fibroblasts. *Journal of biotechnology*, *122*(3), 341–61. doi:10.1016/j.jbiotec.2005.11.022

Choi, Y.-S., Hoon Jeong, J., Min, H.-K., Jung, H.-J., Hwang, D., Lee, S.-W., & Kim Pak, Y. (2011). Shot-gun proteomic analysis of mitochondrial D-loop DNA binding proteins: identification of mitochondrial histones. *Molecular bioSystems*, *7*(5), 1523–36. doi:10.1039/c0mb00277a

Christy, R. J., Yang, V. W., Ntambi, J. M., Geiman, D. E., Landschulz, W. H., Friedman, a D., … Lane, M. D. (1989). Differentiation-induced gene expression in 3T3-L1 preadipocytes: CCAAT/enhancer binding protein interacts with and activates the promoters of two adipocyte-specific genes. *Genes & development*, *3*(9), 1323–35. doi:10.1101/gad.3.9.1323

Chung, J., Uchida, E., Grammer, T. C., & Blenis, J. (1997a). STAT3 serine phosphorylation by ERK-dependent and -independent pathways negatively modulates its tyrosine phosphorylation. *Molecular and cellular biology*, *17*(11), 6508–16.

Chung, J., Uchida, E., Grammer, T. C., & Blenis, J. (1997b). STAT3 serine phosphorylation by ERK-dependent and -independent pathways negatively modulates its tyrosine STAT3 Serine Phosphorylation by ERK-Dependent and -Independent Pathways Negatively Modulates Its Tyrosine Phosphorylation. *Molecular and cellular biology*, *17*(11), 6508–6516.

Cornelius, P., Enerback, S., Bjursell, G., Olivecrona, T., & Pekala, P. H. (1988). Regulation of lipoprotein lipase mRNA content in 3T3-L1 cells by tumour necrosis factor. *The Biochemical journal*, *249*(3), 765–9.

Cornelius, P., MacDougald, O. A., & Lane, M. D. (1994). Regulation of adipocyte development. *Annual review of nutrition*, *14*, 99–129. doi:10.1146/annurev.nu.14.070194.000531

Danet, G. H., Pan, Y., Luongo, J. L., Bonnet, D. A., & Simon, M. C. (2003). Expansion of human SCID-repopulating cells under hypoxic conditions. *The Journal of clinical investigation*, *112*(1), 126–35. doi:10.1172/JCI17669

Dayem, A. A., Choi, H.-Y., Kim, J.-H., & Cho, S.-G. (2010). Role of Oxidative Stress in Stem, Cancer, and Cancer Stem Cells. *Cancers*, *2*(2), 859–884. doi:10.3390/cancers2020859

Decker, T., & Kovarik, P. (2000). Serine phosphorylation of STATs. *Oncogene*, *19*(21), 2628–37. doi:10.1038/sj.onc.1203481

Demaria, M., Giorgi, C., Lebiedzinska, M., Esposito, G., D'Angeli, L., Bartoli, A., … Poli, V. (2010). A STAT3-mediated metabolic switch is involved in tumour transformation and STAT3 addiction. *Aging*, *2*(11), 823–42.

Demaria, M., & Poli, V. (2011). From the nucleus to the mitochondria and back. The odyssey of a multitask STAT3. *Cell Cycle*, *10*(19), 3221–3222. doi:10.1038/nrc2734.4.

Deng, J, Hua, K., Lesser, S. S., & Harp, J. B. (2000). Activation of signal transducer and activator of transcription-3 during proliferative phases of 3T3-L1 adipogenesis. *Endocrinology*, *141*(7), 2370–6.

Deng, Jianbei, Hua, K., Caveney, E. J., Takahashi, N., & Harp, J. B. (2006). Protein inhibitor of activated STAT3 inhibits adipogenic gene expression. *Biochemical and biophysical research communications*, *339*(3), 923–31. doi:10.1016/j.bbrc.2005.10.217

Dong, J.-M. (1998). cAMP-induced Morphological Changes Are Counteracted by the Activated RhoA Small GTPase and the Rho Kinase ROKalpha. *Journal of Biological Chemistry*, *273*(35), 22554–22562. doi:10.1074/jbc.273.35.22554

Fan, J. Y., Carpentier, J. L., van Obberghen, E., Grunfeld, C., Gorden, P., & Orci, L. (1983). Morphological changes of the 3T3-L1 fibroblast plasma membrane upon differentiation to the adipocyte form. *Journal of cell science*, *61*, 219–30.

Fuglesteg, B. N., Suleman, N., Tiron, C., Kanhema, T., Lacerda, L., Andreasen, T. V, … Africa, S. (2008). Signal transducer and activator of transcription 3 is involved in the cardioprotective signalling pathway activated by insulin therapy at reperfusion. *Basic research in cardiology*, *103*(5), 444–453. doi:10.1007/s00395-008-0728-x

Fujioka, T., Fujioka, A., & Duman, R. S. (2004). Activation of cAMP signaling facilitates the morphological maturation of newborn neurons in adult hippocampus. *The Journal of neuroscience□: the official journal of the Society for Neuroscience*, *24*(2), 319–28. doi:10.1523/JNEUROSCI.1065.03.2004

Furukawa, S., Fujita, T., Shimabukuro, M., Iwaki, M., Yamada, Y., Nakajima, Y., … Makishima, M. (2004). Increased oxidative stress in obesity and its impact on metabolic syndrome, *114*(12). doi:10.1172/JCI200421625.1752

Gogvadze, V., Zhivotovsky, B., & Orrenius, S. (2010). The Warburg effect and mitochondrial stability in cancer cells. *Molecular aspects of medicine*, *31*(1), 60–74. doi:10.1016/j.mam.2009.12.004

Gough, D. J., Corlett, A., Schlessinger, K., Wegrzyn, J., Larner, A. C., & Levy, D. E. (2009). Mitochondrial STAT3 supports Ras-dependent oncogenic transformation. *Science (New York, N.Y.)*, *324*(5935), 1713–6. doi:10.1126/science.1171721

Gough, D. J., Koetz, L., & Levy, D. E. (2013). The MEK-ERK Pathway Is Necessary for Serine Phosphorylation of Mitochondrial STAT3 and Ras-Mediated Transformation. *PloS one*, *8*(11), e83395. doi:10.1371/journal.pone.0083395

Green, H, & Kehinde, O. (1975). An established preadipose cell line and its differentiation in culture. II. Factors affecting the adipose conversion. *Cell*, *5*(1), 19–27.

Green, Howard, & Kehinde, O. (1974). Sublines of mouse 3T3 cells that accumulate lipid. *Cell*, *1*(3), 113–116.

Gregoire, F. M., Smas, C. M., & Sul, H. S. (1998). Understanding adipocyte differentiation. *Physiological reviews*, *78*(3), 783–809.

Gwon, S. Y., Ahn, J. Y., Jung, C. H., Moon, B. K., & Ha, T. Y. (2013). Shikonin suppresses ERK 1/2 phosphorylation during the early stages of adipocyte differentiation in 3T3-L1 cells. *BMC complementary and alternative medicine*, *13*(1), 207. doi:10.1186/1472-6882-13-207

Haggstrom, M. (2011). Stem cell treatments.svg - Wikipedia, the free encyclopedia. *Wkikipedia, the free encyclopedia*. Retrieved February 08, 2012, from http://en.wikipedia.org/wiki/File:Stem_cell_treatments.svg#filehistory

Hass, R., Kasper, C., Böhm, S., & Jacobs, R. (2011). Different populations and sources of human mesenchymal stem cells (MSC): A comparison of adult and neonatal tissue-derived MSC. *Cell communication and signaling□: CCS*, *9*(1), 12. doi:10.1186/1478-811X-9-12

Hirst, J., King, M. S., & Pryde, K. R. (2008). The production of reactive oxygen species by complex I. *Biochemical Society transactions*, *36*(Pt 5), 976–80. doi:10.1042/BST0360976

Hodge, D. R., Hurt, E. M., & Farrar, W. L. (2005). The role of IL-6 and STAT3 in inflammation and cancer. *European journal of cancer (Oxford, England□: 1990)*, *41*(16), 2502–12. doi:10.1016/j.ejca.2005.08.016

Hoogenboom, B. W., Suda, K., Engel, A., & Fotiadis, D. (2007). The supramolecular assemblies of voltage-dependent anion channels in the native membrane. *Journal of molecular biology*, *370*(2), 246–55. doi:10.1016/j.jmb.2007.04.073

Houstis, N., Rosen, E. D., & Lander, E. S. (2006). Reactive oxygen species have a causal role in multiple forms of insulin resistance. *Nature*, *440*(7086), 944–8. doi:10.1038/nature04634

Hsie, A., Kawashima, K., O'Niell, J. ., & Shroder, C. (1975). Possible Role of Adenosine Cyclic 3'□: 5-Monophasphate Phosphodiesterase in the Morphological Transformation of Chinese Hamster Ovary Cells Mediatied by N6, O2'-Dibutyryl Adenosine Cyclic 3'□: 5-Monophasphate. *The Journal of biological chemistry*, *250*(3), 984–989.

Huang, G., Lu, H., Hao, A., Ng, D. C. H., Ponniah, S., Guo, K., … Cao, X. (2004). GRIM-19 , a Cell Death Regulatory Protein , Is Essential for Assembly and Function of Mitochondrial Complex I GRIM-19 , a Cell Death Regulatory Protein , Is Essential for Assembly and Function of Mitochondrial Complex I. doi:10.1128/MCB.24.19.8447

Huang, Y., Qiu, J., Dong, S., Redell, M. S., Poli, V., Mancini, M. A., & Tweardy, D. J. (2007). Stat3 isoforms, alpha and beta, demonstrate distinct intracellular dynamics with prolonged nuclear retention of Stat3beta mapping to its unique C-terminal end. *The Journal of biological chemistry*, *282*(48), 34958–67.

Jaiswal, R. K. (2000). Adult Human Mesenchymal Stem Cell Differentiation to the Osteogenic or Adipogenic Lineage Is Regulated by Mitogen-activated Protein Kinase. *Journal of Biological Chemistry*, *275*(13), 9645–9652. doi:10.1074/jbc.275.13.9645

Janderová, L., McNeil, M., Murrell, A. N., Mynatt, R. L., & Smith, S. R. (2003). Human mesenchymal stem cells as an in vitro model for human adipogenesis. *Obesity research*, *11*(1), 65–74. doi:10.1038/oby.2003.11

Jansen, B. J. H., Gilissen, C., Roelofs, H., Schaap-Oziemlak, A., Veltman, J. A., Raymakers, R. A. P., … Adema, G. J. (2010). Functional differences between mesenchymal stem cell populations are reflected by their transcriptome. *Stem cells and development*, *19*(4), 481–90. doi:10.1089/scd.2009.0288

Johnson, G. S., Friedimant, R., & Pastan, I. R. A. (1971). Restoration of Several Morphological Characteristics of Normal Fibroblasts in Sarcoma Cells Treated with Adenosine-3 ': 5 ' -Cyclic Monophosphate and Its Derivatives, *68*(2), 425–429.

Kadye, R., Kramer, A. H., Joos-Vandewalle, J., Parsons, M., Njengele, Z., Hoppe, H., & Prinsloo, E. (2013). Guardian of the Furnace: Mitochondria, TRAP1, ROS and stem cell maintenance. *IUBMB life*, (21), 1–4. doi:10.1002/iub.1234

Katherine B Zanin, M., Donohue, J. M., & Everitt, B. a. (2010). Evidence that core histone H3 is targeted to the mitochondria in Brassica oleracea. *Cell biology international*, *34*(10), 997–1003. doi:10.1042/CBI20090281

Khan, R., Lee, J. E., Yang, Y.-M., Liang, F.-X., & Sehgal, P. B. (2013). Live-cell imaging of the association of STAT6-GFP with mitochondria. *PloS one*, *8*(1), e55426. doi:10.1371/journal.pone.0055426

Kim, M. H., Fields, J., & Field, J. (2008). Translationally regulated C/EBP beta isoform expression upregulates metastatic genes in hormone-independent prostate cancer cells. *The Prostate*, *68*(12), 1362–71. doi:10.1002/pros.20801

Kinoshita, S., Ogawa, W., Okamoto, Y., Takashima, M., Inoue, H., Matsuki, Y., … Kasuga, M. (2008). Role of hepatic STAT3 in the regulation of lipid metabolism. *The Kobe journal of medical sciences*, *54*(4), E200–8.

Kléber, M., & Sommer, L. (2004). Wnt signaling and the regulation of stem cell function. *Current opinion in cell biology*, *16*(6), 681–7. doi:10.1016/j.ceb.2004.08.006

Komiya, Y., & Habas, R. (2008). Wnt signal transduction pathways. *Oraganogenesis*, *4*(2), 68–75.

Kondoh, H, Lleonart, M., Gil, J., Beach, D., & Peters, G. (2005). Glycolysis and cellular immortalization. *Drug Discovery Today: Disease Mechanisms*, *2*(2), 263–267. doi:10.1016/j.ddmec.2005.05.001

Kondoh, Hiroshi. (2008). Cellular life span and the Warburg effect. *Experimental cell research*, *314*(9), 1923–8. doi:10.1016/j.yexcr.2008.03.007

Kondoh, Hiroshi, Lleonart, M. E., Gil, J., Wang, J., Degan, P., Peters, G., … Beach, D. (2005). Glycolytic Enzymes Can Modulate Cellular Life Span. *Cancer Res.*, *65*(1), 177–185.

Kondoh, Hiroshi, Lleonart, M. E., Nakashima, Y., Yokode, M., Tanaka, M., Bernard, D., … Beach, D. (2007). A High Glycolytic Flux Supports the Proliferative Potential of Murine Embryonic Stem Cells. *Antioxidants & Redox Signaling*, *9*(3), 293–299. doi:10.1089/ars.2006.1467

Körbling, M., & Freireich, E. J. (2011). Twenty-five years of peripheral blood stem cell transplantation. *Blood*, *117*(24), 6411–6. doi:10.1182/blood-2010-12-322214

Kramer, A. H., Joos-Vandewalle, J., Edkins, A. L., Frost, C. L., & Prinsloo, E. (2014). Real-time monitoring of 3T3-L1 preadipocyte differentiation using a commercially available electric cell-substrate impedance sensor system. *Biochemical and biophysical research communications*, 1–6. doi:10.1016/j.bbrc.2013.12.123

Krieger-Brauer, H. I., & Kather, H. (1995). The stimulus-sensitive H2O2-generating system present in human fat-cell plasma membranes is multireceptor-linked and under antagonistic control by hormones and cytokines. *The Biochemical journal*, *307 (Pt 2*, 543–8.

Kuri-harcuch, W., & Green, H. (1978). Adipose conversion of 3T3 cells depends on a serum factor. *Proceedings of the National Academy of Sciences*, *75*(12), 6107–6109.

Kustermann, S., Boess, F., Buness, A., Schmitz, M., Watzele, M., Weiser, T., … Roth, A. (2013). A label-free, impedance-based real time assay to identify drug-induced toxicities and differentiate cytostatic from cytotoxic effects. *Toxicology in vitro : an international journal published in association with BIBRA*, *27*(5), 1589–95. doi:10.1016/j.tiv.2012.08.019

Kwon, Y., Kon, W., Lee, S., Kim, K., & Young, E. (2012). Monitoring of adipogenic differentiation at the single-cell level using atomic force microscopic analysis. *Spectroscopy*, *26*(2011), 329–335. doi:10.3233/SPE-2012-0566

Laemmli, U. K. (1970). Cleavage of Structural Proteins during the Assembly of the Head of Bacteriophage T4. *Nature*, *227*(5259), 680–685. doi:10.1038/227680a0

Le Belle, J., Orozco, N., Paucar, A., Saxe, J., Mottahedeh, J., Pyle, A., … Kornblum, H. (2011). Proliferative Neural Stem Cells Have High Endogenous ROS Levels that Regulate Self-Renewal

and Neurogenesis in a PI3K/ Akt-Dependant Manner. *Cell stem cell*, *8*(1), 59–71. doi:10.1016/j.stem.2010.11.028.Proliferative

Lee, H., Lee, Y. J., Choi, H., Ko, E. H., & Kim, J. -w. (2009). Reactive Oxygen Species Facilitate Adipocyte Differentiation by Accelerating Mitotic Clonal Expansion. *Journal of Biological Chemistry*, *284*(16), 10601–10609. doi:10.1074/jbc.M808742200

Lee, R., Jung, I., Park, M., Ha, H., & Yoo, K. H. (2013). Real-time monitoring of adipocyte differentiation using a capacitance sensor array. *Lab on a chip*, *13*(17), 3410–6. doi:10.1039/c3lc50453k

Lee, R., Kim, J., Kim, S. Y., Jang, S. M., Lee, S.-M., Choi, I.-H., … Yoo, K.-H. (2012). Capacitance-based assay for real-time monitoring of endocytosis and cell viability. *Lab on a chip*, *12*(13), 2377–84. doi:10.1039/c2lc21236f

Lee, Y.-H., Chen, S.-Y., Wiesner, R. J., & Huang, Y.-F. (2004). Simple flow cytometric method used to assess lipid accumulation in fat cells. *Journal of lipid research*, *45*(6), 1162–7. doi:10.1194/jlr.D300028-JLR200

Li, Q., Lau, A., Morris, T. J., Guo, L., Fordyce, C. B., & Stanley, E. F. (2004). A syntaxin 1, Galpha(o), and N-type calcium channel complex at a presynaptic nerve terminal: analysis by quantitative immunocolocalization. *The Journal of neuroscience : the official journal of the Society for Neuroscience*, *24*(16), 4070–81. doi:10.1523/JNEUROSCI.0346-04.2004

Lim, C. P., & Cao, X. (2001). Regulation of Stat3 activation by MEK kinase 1. *The Journal of biological chemistry*, *276*(24), 21004–11. doi:10.1074/jbc.M007592200

Limame, R., Wouters, A., Pauwels, B., Fransen, E., Peeters, M., Lardon, F., … Pauwels, P. (2012). Comparative analysis of dynamic cell viability, migration and invasion assessments by novel real-time technology and classic endpoint assays. *PloS one*, *7*(10), e46536. doi:10.1371/journal.pone.0046536

Liras, A. (2010). Future research and therapeutic applications of human stem cells: general, regulatory, and bioethical aspects. *Journal of translational medicine*, *8*(1), 131. doi:10.1186/1479-5876-8-131

Liu, L., McBride, K. M., & Reich, N. C. (2005). STAT3 nuclear import is independent of tyrosine phosphorylation and mediated by importin-alpha3. *Proceedings of the National Academy of Sciences of the United States of America*, *102*(23), 8150–5. doi:10.1073/pnas.0501643102

Liu, Y., Fiskum, G., & Schubert, D. (2002). Generation of reactive oxygen species by the mitochondrial electron transport chain. *Journal of neurochemistry*, *80*(5), 780–7.

Lu, B., Malcuit, C., Wang, S., Girman, S., Francis, P., Lemieux, L., … Lund, R. (2009). Long-term safety and function of RPE from human embryonic stem cells in preclinical models of macular degeneration. *Stem cells (Dayton, Ohio)*, *27*(9), 2126–35. doi:10.1002/stem.149

Lufei, C., Ma, J., Huang, G., Zhang, T., Novotny-Diermayr, V., Ong, C. T., & Cao, X. (2003). GRIM-19, a death-regulatory gene product, suppresses Stat3 activity via functional interaction. *The EMBO journal*, *22*(6), 1325–35. doi:10.1093/emboj/cdg135

Lyu, B. N., Ismailov, S. B., Ismailov, B., & Lyu, M. B. (2008). Mitochondrial concept of leukemogenesis: key role of oxygen-peroxide effects. *Theoretical biology & medical modelling*, *5*(1), 23. doi:10.1186/1742-4682-5-23

MacDougald, O. A., & Lane, M. D. (1995). Transcriptional Regulation of Gene Expression During Adipocyte Differentiation. *Annual review of biochemistry*, *64*, 345–373.

Martin, G. R. (1981). Isolation of a Pluripotent Cell Line from Early Mouse Embryos Cultured in Medium Conditioned by Teratocarcinoma Stem Cells. *Proceedings of the National Academy of Sciences*, *78*(12), 7634–7638. doi:10.1073/pnas.78.12.7634

Matsuda, T., Nakamura, T., Nakao, K., Arai, T., Katsuki, M., Heike, T., & Yokota, T. (1999). STAT3 activation is sufficient to maintain an undifferentiated state of mouse embryonic stem cells. *The EMBO journal*, *18*(15), 4261–9. doi:10.1093/emboj/18.15.4261

Mattiasson, G. (2004). Flow cytometric analysis of isolated liver mitochondria to detect changes relevant to cell death. *Cytometry. Part A : the journal of the International Society for Analytical Cytology*, *60*(2), 145–54. doi:10.1002/cyto.a.20024

Mazzini, L., Mareschi, K., Ferrero, I., Miglioretti, M., Stecco, A., Servo, S., … Fagioli, F. (2012). Mesenchymal stromal cell transplantation in amyotrophic lateral sclerosis: a long-term safety study. *Cytotherapy*, *14*(1), 56–60. doi:10.3109/14653249.2011.613929

Mazzini, L., Mareschi, K., Ferrero, I., Vassallo, E., Oliveri, G., Nasuelli, N., … Fagioli, F. (2008). Stem cell treatment in Amyotrophic Lateral Sclerosis. *Journal of the neurological sciences*, *265*(1-2), 78–83. doi:10.1016/j.jns.2007.05.016

McBride, H. M., Neuspiel, M., & Wasiak, S. (2006). Mitochondria: more than just a powerhouse. *Current biology : CB*, *16*(14), R551–60. doi:10.1016/j.cub.2006.06.054

McLennan, H. R., & Degli Esposti, M. (2000). The contribution of mitochondrial respiratory complexes to the production of reactive oxygen species. *Journal of bioenergetics and biomembranes*, *32*(2), 153–62.

Mehra, A., Macdonald, I., & Pillay, T. S. (2007). Variability in 3T3-L1 adipocyte differentiation depending on cell culture dish. *Analytical biochemistry*, *362*(2), 281–3. doi:10.1016/j.ab.2006.12.016

Menendez, J. A., Joven, J., Cufí, S., Corominas-Faja, B., Oliveras-Ferraros, C., Cuyàs, E., … Vazquez-Martin, A. (2013). The Warburg effect version 2.0: metabolic reprogramming of cancer stem cells. *Cell cycle (Georgetown, Tex.)*, *12*(8), 1166–79. doi:10.4161/cc.24479

Mitalipov, S., & Wolf, D. P. (2008). Methods in stem cell research. *Methods (San Diego, Calif.)*, *45*(2), 99–100. doi:10.1016/j.ymeth.2008.06.002

Moody, B., Haslauer, C. M., Kirk, E., Kannan, A., Loboa, E. G., & McCarty, G. S. (2010). In Situ Monitoring of Adipogenesis with Human-Adipose-Derived Stem Cells Using Surface-Enhanced Raman Spectroscopy. *Appl. Spectrosc.*, *64*(11), 1227–1233.

Mukhopadhyay, S., Shah, M., Xu, F., Patel, K., Tuder, R. M., & Sehgal, P. B. (2008). Cytoplasmic provenance of STAT3 and PY-STAT3 in the endolysosomal compartments in pulmonary arterial endothelial and smooth muscle cells : implications in pulmonary arterial hypertension, *10595*, 449–468. doi:10.1152/ajplung.00377.2007.

Nesti, C., Pasquali, L., Vaglini, F., Siciliano, G., & Murri, L. (2007). The role of mitochondria in stem cell biology. *Bioscience reports*, *27*(1-3), 165–71. doi:10.1007/s10540-007-9044-1

Ng, I. H. W., Ng, D. C. H., Jans, D. a, & Bogoyevitch, M. a. (2012). Selective STAT3-α or -β expression reveals spliceform-specific phosphorylation kinetics, nuclear retention and distinct gene expression outcomes. *The Biochemical journal*, *447*(1), 125–36. doi:10.1042/BJ20120941

Novak, U., Ji, H., Kanagasundaram, V., Simpson, R., & Paradiso, L. (1998). STAT3 forms stable homodimers in the presence of divalent cations prior to activation. *Biochemical and biophysical research communications*, *247*(3), 558–63.

Ntambi, J. M., & Kim, Y. (2000). Adipocyte Differentiation and Gene Expression. *American Society for Nutritional Sciences*, 3122–3126.

Nunez, R. (2001). DNA measurement and cell cycle analysis by flow cytometry. *Current issues in molecular biology*, *3*(3), 67–70.

Otto, T. C., & Lane, M. D. (2005). Adipose development: from stem cell to adipocyte. *Critical reviews in biochemistry and molecular biology*, *40*(4), 229–42. doi:10.1080/10409230591008189

Pardo, R., Enguix, N., Lasheras, J., Feliu, J. E., Kralli, A., & Villena, J. a. (2011). Rosiglitazone-induced mitochondrial biogenesis in white adipose tissue is independent of peroxisome proliferator-activated receptor γ coactivator-1α. *PloS one*, *6*(11), e26989. doi:10.1371/journal.pone.0026989

Parker, G. C., Acsadi, G., & Brenner, C. a. (2009). Mitochondria: determinants of stem cell fate? *Stem cells and development*, *18*(6), 803–6. doi:10.1089/scd.2009.1806.edi

Parmar, K., Mauch, P., Vergilio, J.-A., Sackstein, R., & Down, J. D. (2007). Distribution of hematopoietic stem cells in the bone marrow according to regional hypoxia. *Proceedings of the National Academy of Sciences of the United States of America*, *104*(13), 5431–6. doi:10.1073/pnas.0701152104

Patel, Y. M., & Lane, M. D. (2000). Mitotic clonal expansion during preadipocyte differentiation: calpain-mediated turnover of p27. *The Journal of biological chemistry*, *275*(23), 17653–60. doi:10.1074/jbc.M910445199

Pethig, R. (1984). Dielectric Properties of Biological Materials: Biophysical and Medical Applications. *IEEE Transactions on Electrical Insulation*, *EI-19*(5), 453–474. doi:10.1109/TEI.1984.298769

Pranada, A. L., Metz, S., Herrmann, A., Heinrich, P. C., & Müller-Newen, G. (2004). Real time analysis of STAT3 nucleocytoplasmic shuttling. *The Journal of biological chemistry*, *279*(15), 15114–23. doi:10.1074/jbc.M312530200

Prinsloo, E., Kramer, A. H., Edkins, A. L., & Blatch, G. L. (2012). STAT3 interacts directly with Hsp90. *IUBMB life*. doi:10.1002/iub.607

Prowse, A. B. J., McQuade, L. R., Bryant, K. J., Marcal, H., & Gray, P. P. (2007). Identification of potential pluripotency determinants for human embryonic stem cells following proteomic analysis of human and mouse fibroblast conditioned media. *Journal of proteome research*, *6*(9), 3796–807. doi:10.1021/pr0702262

Qian, S.-W., Li, X., Zhang, Y.-Y., Huang, H.-Y., Liu, Y., Sun, X., & Tang, Q.-Q. (2010). Characterization of adipocyte differentiation from human mesenchymal stem cells in bone marrow. *BMC developmental biology*, *10*, 47. doi:10.1186/1471-213X-10-47

Ramirez-Zacarias, J. L., Castro-Munozledo, F., & Kuri-Harcuch, W. (1992). Quantification of adipose conversion and triglycerides by staining intracytoplasmic lipids with Oil red O. *Histochemistry*, *97*, 493–497.

Raz, R., Lee, C. K., Cannizzaro, L. a, d'Eustachio, P., & Levy, D. E. (1999). Essential role of STAT3 for embryonic stem cell pluripotency. *Proceedings of the National Academy of Sciences of the United States of America*, *96*(6), 2846–51.

Reed, S. a, & Johnson, S. E. (2014). Expression of scleraxis and tenascin C in equine adipose and umbilical cord blood derived stem cells is dependent upon substrata and FGF supplementation. *Cytotechnology*, *66*(1), 27–35. doi:10.1007/s10616-012-9533-3

Reich, N. C. (2009). STAT3 revs up the powerhouse. *Science signaling*, *2*(90), pe61. doi:10.1126/scisignal.290pe61

Reya, T, Morrison, S. J., Clarke, M. F., & Weissman, I. L. (2001). Stem cells, cancer, and cancer stem cells. *Nature*, *414*(6859), 105–11. doi:10.1038/35102167

Reya, Tannishtha, & Clevers, H. (2005). Wnt signalling in stem cells and cancer. *Nature*, *434*(7035), 843–50. doi:10.1038/nature03319

Ruckenstuhl, C., Büttner, S., Carmona-Gutierrez, D., Eisenberg, T., Kroemer, G., Sigrist, S. J., … Madeo, F. (2009). The Warburg effect suppresses oxidative stress induced apoptosis in a yeast model for cancer. *PloS one*, *4*(2), e4592. doi:10.1371/journal.pone.0004592

Russell, T. R. (1976). Conversion of 3T3 fibroblasts into adipose cells: Triggering of, *73*(12), 4516–4520.

Saretzki, G., Armstrong, L., Leake, A., Lako, M., & von Zglinicki, T. (2004). Stress defense in murine embryonic stem cells is superior to that of various differentiated murine cells. *Stem cells (Dayton, Ohio)*, *22*(6), 962–71. doi:10.1634/stemcells.22-6-962

Saretzki, G., Armstrong, L., Leake, A., Lako, M., von Zglinicki, T., & Zglinicki, V. (2004). Stress defence in murine embryonic stem cell is superior to that of various differentiated murinr cells. *Stem cells*, *22*(6), 962–971. doi:10.1634/stemcells.22-6-962

Sato, Noboru, Meijer, L., Skaltsounis, L., Greengard, P., & Brivanlou, A. H. (2004). Maintenance of pluripotency in human and mouse embryonic stem cells through activation of Wnt signaling by a pharmacological GSK-3-specific inhibitor. *Nature medicine*, *10*(1), 55–63. doi:10.1038/nm979

Sato, Noriko, Yamamoto, T., Sekine, Y., Yumioka, T., Junicho, A., Fuse, H., & Matsuda, T. (2003). Involvement of heat-shock protein 90 in the interleukin-6-mediated signaling pathway through STAT3. *Biochemical and Biophysical Research Communications*, *300*(4), 847–852. doi:10.1016/S0006-291X(02)02941-8

Sauer, H., Wartenberg, M., & Hescheler, J. (2001). Reactive oxygen species as intracellular messengers during cell growth and differentiation. *Cellular physiology and biochemistry : international journal of experimental cellular physiology, biochemistry, and pharmacology*, *11*(4), 173–86.

Scadden, D. T. (2006). The stem-cell niche as an entity of action. *Nature*, *441*(7097), 1075–1079. doi:10.1038/nature04957

Schell, J. C., & Rutter, J. (2013). The long and winding road to the mitochondrial pyruvate carrier. *Cancer & metabolism*, *1*(1), 6. doi:10.1186/2049-3002-1-6

Schwartz, S. D., Hubschman, J.-P., Heilwell, G., Franco-Cardenas, V., Pan, C. K., Ostrick, R. M., … Lanza, R. (2012). Embryonic stem cell trials for macular degeneration: a preliminary report. *Lancet*, *379*(9817), 713–20. doi:10.1016/S0140-6736(12)60028-2

Scott, M. a, Nguyen, V. T., Levi, B., & James, A. W. (2011). Current methods of adipogenic differentiation of mesenchymal stem cells. *Stem cells and development*, *20*(10), 1793–804. doi:10.1089/scd.2011.0040

Sebolt-Leopold, J. S., & Herrera, R. (2004). Targeting the mitogen-activated protein kinase cascade to treat cancer. *Nature reviews. Cancer*, *4*(12), 937–47. doi:10.1038/nrc1503

Shah, M., Patel, K., Fried, V. a, & Sehgal, P. B. (2002). Interactions of STAT3 with caveolin-1 and heat shock protein 90 in plasma membrane raft and cytosolic complexes. Preservation of cytokine signaling during fever. *The Journal of biological chemistry*, *277*(47), 45662–9. doi:10.1074/jbc.M205935200

St John, J. C., Amaral, A., Bowles, E., Oliveira, J. F., Lloyd, R., Freitas, M., … Ramalho-Santos, J. (2006). The analysis of mitochondria and mitochondrial DNA in human embryonic stem cells. *Methods in molecular biology (Clifton, N.J.)*, *331*, 347–74. doi:10.1385/1-59745-046-4:347

Stankov, M. V, Schmidt, R. E., & Behrens, G. M. N. (2009). Impact of stimulatory pathways on adipogenesis and HIV-therapy associated lipoatrophy. *Experimental biology and medicine (Maywood, N.J.)*, *234*(12), 1484–92. doi:10.3181/0907-RM-205

Stephans, J. ., Morrison, R. F., & Pilch, P. . (1996). The Expression and Regulation of STATs during 3T3-L1 Adipocyte Differentiation. *Journal of Biological Chemistry*, *271*(18), 10441–10444. doi:10.1074/jbc.271.18.10441

Sullivan, G. J., Bai, Y., Fletcher, J., & Wilmut, I. (2010). Induced pluripotent stem cells: epigenetic memories and practical implications. *Molecular human reproduction*, *16*(12), 880–5. doi:10.1093/molehr/gaq091

Szczepanek, K., Chen, Q., Derecka, M., Salloum, F. N., Zhang, Q., Szelag, M., … Larner, A. C. (2011). Mitochondrial-targeted Signal transducer and activator of transcription 3 (STAT3) protects against ischemia-induced changes in the electron transport chain and the generation of reactive oxygen species. *The Journal of biological chemistry*, *286*(34), 29610–20. doi:10.1074/jbc.M111.226209

Szczepanek, K., Chen, Q., Larner, A. C., & Lesnefsky, E. J. (2012). Cytoprotection by the modulation of mitochondrial electron transport chain: the emerging role of mitochondrial STAT3. *Mitochondrion*, *12*(2), 180–9. doi:10.1016/j.mito.2011.08.011

Takahashi, Kazutoshi, & Yamanaka, S. (2006). Induction of pluripotent stem cells from mouse embryonic and adult fibroblast cultures by defined factors. *Cell*, *126*(4), 663–676.

Takahashi, Kazutoshi;, Tanabe, K., Ohnuki, M., Megumi;, N., Ichisaka, T., Tomoda, K., & Yamanaka, S. (2007). Induction of Pluripotent Stem Cells from Adult Human Fibroblasts by Defined Factors. *Cell*, *131*(5), 861–872.

Takeda, K., Noguchi, K., Shi, W., Tanaka, T., Matsumoto, M., Yoshida, N., … Akira, S. (1997). Targeted disruption of the mouse Stat3 gene leads to early embryonic lethality. *Proceedings of the National Academy of Sciences of the United States of America*, *94*(8), 3801–4.

Tammineni, P., Anugula, C., Mohammed, F., Anjaneyulu, M., Larner, A. C., & Sepuri, N. B. V. (2013). The import of the transcription factor STAT3 into mitochondria depends on GRIM-19, a component of the electron transport chain. *The Journal of biological chemistry*, *288*(7), 4723–32. doi:10.1074/jbc.M112.378984

Tang, Q. Q., & Lane, M. D. (1999). Activation and centromeric localization of CCAAT/enhancer-binding proteins during the mitotic clonal expansion of adipocyte differentiation. *Genes & development*, *13*(17), 2231–41.

Tang, Q.-Q., Grønborg, M., Huang, H., Kim, J.-W., Otto, T. C., Pandey, A., & Lane, M. D. (2005). Sequential phosphorylation of CCAAT enhancer-binding protein beta by MAPK and glycogen synthase kinase 3beta is required for adipogenesis. *Proceedings of the National Academy of Sciences of the United States of America*, *102*(28), 9766–71. doi:10.1073/pnas.0503891102

Tang, Q.-Q., Otto, T. C., & Lane, M. D. (2003). Mitotic clonal expansion: a synchronous process required for adipogenesis. *Proceedings of the National Academy of Sciences of the United States of America*, *100*(1), 44–9. doi:10.1073/pnas.0137044100

Tang, Y.-W., & Stratton, C. W. (Eds.). (2013). *Advanced Techniques in Diagnostic Microbiology*. Boston, MA: Springer US. doi:10.1007/978-1-4614-3970-7

Thiede, M. (2009). Stem Cell Applications and Opportunities in Drug Discovery - Drug Discovery World. *Drug Discovery World*. Retrieved January 31, 2012, from http://rjcoms.com/therapeutics/302312/stem_cell_applications_and_opportunities_in_drug_discovery.html

Thomson, J. A. . K., Golos, T. G., Durning, M., Harris, C. P., R A Becker, A., & Hearn, J. P. (1995). Isolation of a Primate Embryonic Stem Cell Line. *Proceedings of the National Academy of Sciences*, *92*(17), 7844–7848. doi:10.1073/pnas.92.17.7844

Thomson, J., Itskovitz-Eldo, J., Shapiro, S., Waknitz, M., Sqiergiel, J., Marshell, V., & Jones, J. (1998). Embryonic Stem Cell Lines Derived from Human Blastocysts. *Science*, *282*(5391), 1145–1147. doi:10.1126/science.282.5391.1145

Timofeeva, O. a, Chasovskikh, S., Lonskaya, I., Tarasova, N. I., Khavrutskii, L., Tarasov, S. G., … Dritschilo, A. (2012). Mechanisms of unphosphorylated STAT3 transcription factor binding to DNA. *The Journal of biological chemistry*, *287*(17), 14192–200. doi:10.1074/jbc.M111.323899

Tirado, M., Grosse, C., Schraderm, W., & Kaatza, U. (2002). Broad frequency range dielectric spectroscopy of aqueous suspensions of phospholipid vesicles. *Journal of Non-Crystalline Solids*, *305*, 373–378.

Tormos, K. V, Anso, E., Hamanaka, R. B., Eisenbart, J., Joseph, J., Kalyanaraman, B., & Chandel, N. S. (2011). Mitochondrial complex III ROS regulate adipocyte differentiation. *Cell metabolism*, *14*(4), 537–44. doi:10.1016/j.cmet.2011.08.007

Tremain, N., Korkko, J., Ibberson, D., Kopen, G. C., DiGirolamo, C., & Phinney, D. G. (2001). MicroSAGE analysis of 2,353 expressed genes in a single cell-derived colony of undifferentiated human mesenchymal stem cells reveals mRNAs of multiple cell lineages. *Stem cells (Dayton, Ohio)*, *19*(5), 408–18. doi:10.1634/stemcells.19-5-408

Vieira, H. L. a, Alves, P. M., & Vercelli, A. (2011). Modulation of neuronal stem cell differentiation by hypoxia and reactive oxygen species. *Progress in neurobiology*, *93*(3), 444–55. doi:10.1016/j.pneurobio.2011.01.007

Villa-Diaz, L. G., Pacut, C., Slawny, N. a, Ding, J., O'Shea, K. S., & Smith, G. D. (2009). Analysis of the factors that limit the ability of feeder cells to maintain the undifferentiated state of human embryonic stem cells. *Stem cells and development*, *18*(4), 641–51. doi:10.1089/scd.2008.0010

Wang, D., Zhou, Y., Lei, W., Zhang, K., Shi, J., Hu, Y., … Song, J. (2010). Signal transducer and activator of transcription 3 (STAT3) regulates adipocyte differentiation via peroxisome-proliferator-activated receptor gamma (PPARgamma). *Biology of the cell / under the auspices of the European Cell Biology Organization*, *102*(1), 1–12. doi:10.1042/BC20090070

Wang, K., Zhang, T., Dong, Q., Nice, E. C., Huang, C., & Wei, Y. (2013). Redox homeostasis: the linchpin in stem cell self-renewal and differentiation. *Cell death & disease*, *4*(3), e537. doi:10.1038/cddis.2013.50

Wegrzyn, J., Potla, R., Chwae, Y.-J., Sepuri, N. B. V, Zhang, Q., Koeck, T., … Larner, A. C. (2009). Function of mitochondrial Stat3 in cellular respiration. *Science (New York, N.Y.)*, *323*(5915), 793–7. doi:10.1126/science.1164551

Weissman, I. L. (2000). Stem cells: units of development, units of regeneration, and units in evolution. *Cell*, *100*(1), 157–68.

Wen, Z., & Darnell, J. E. (1997). Mapping of Stat3 serine phosphorylation to a single residue (727) and evidence that serine phosphorylation has no influence on DNA binding of Stat1 and Stat3. *Nucleic acids research*, *25*(11), 2062–7.

Wilson-fritch, L., Burkart, A., Bell, G., Leszyk, J., Nicoloro, S., Czech, M., … Mendelson, K. (2003). Mitochondrial Biogenesis and Remodeling during Adipogenesis and in Response to the Insulin Sensitizer Rosiglitazone. doi:10.1128/MCB.23.3.1085

Xu, F., Mukhopadhyay, S., & Sehgal, P. B. (2007). Live cell imaging of interleukin-6-induced targeting of "transcription factor" STAT3 to sequestering endosomes in the cytoplasm. *American journal of physiology. Cell physiology*, *293*(4), C1374–82. doi:10.1152/ajpcell.00220.2007

Yang, H. N., Park, J. S., Woo, D. G., Jeon, S. Y., Do, H.-J., Lim, H.-Y., … Park, K.-H. (2011). C/EBP-α and C/EBP-β-mediated adipogenesis of human mesenchymal stem cells (hMSCs) using PLGA nanoparticles complexed with poly(ethyleneimmine). *Biomaterials*, *32*(25), 5924–33. doi:10.1016/j.biomaterials.2011.04.072

Yang, H.-B., Song, W., Chen, L.-Y., Li, Q.-F., Shi, S.-L., Kong, H.-Y., & Chen, P. (2014). Differential expression and regulation of prohibitin during curcumin-induced apoptosis of immortalized human epidermal HaCaT cells. *International journal of molecular medicine*, *33*(3), 507–14. doi:10.3892/ijmm.2014.1621

Young, H. E., & Black, A. C. (2004). Adult stem cells. *The anatomical record. Part A, Discoveries in molecular, cellular, and evolutionary biology*, *276*(1), 75–102. doi:10.1002/ar.a.10134

Yu, J., Vodyanik, M. a, Smuga-Otto, K., Antosiewicz-Bourget, J., Frane, J. L., Tian, S., … Thomson, J. a. (2007). Induced pluripotent stem cell lines derived from human somatic cells. *Science (New York, N.Y.)*, *318*(5858), 1917–20. doi:10.1126/science.1151526

Zebisch, K., Voigt, V., Wabitsch, M., & Brandsch, M. (2012). Protocol for effective differentiation of 3T3-L1 cells to adipocytes. *Analytical biochemistry*, *425*(1), 88–90. doi:10.1016/j.ab.2012.03.005

Zhang, J., Yang, J., Roy, S. K., Tininini, S., Hu, J., Bromberg, J. F., … Kalvakolanu, D. V. (2003). The cell death regulator GRIM-19 is an inhibitor of signal transducer and activator of transcription 3. *Proceedings of the National Academy of Sciences of the United States of America*, *100*(16), 9342–7. doi:10.1073/pnas.1633516100

Zhang, K., Guo, W., Yang, Y., & Wu, J. (2011). JAK2/STAT3 pathway is involved in the early stage of adipogenesis through regulating C/EBPβ transcription. *Journal of cellular biochemistry*, *112*(2), 488–97. doi:10.1002/jcb.22936

Zhang, L., Seitz, L. C., Abramczyk, A. M., Liu, L., & Chan, C. (2011). cAMP initiates early phase neuron-like morphology changes and late phase neural differentiation in mesenchymal stem cells. *Cellular and molecular life sciences : CMLS*, *68*(5), 863–76. doi:10.1007/s00018-010-0497-1

Zhang, Q., Raje, V., Yakovlev, V. a, Yacoub, A., Szczepanek, K., Meier, J., … Larner, A. C. (2013a). Mitochondrial-Localized Stat3 Promotes Breast Cancer Growth via Phosphorylation of Serine 727. *The Journal of biological chemistry*, 0–18. doi:10.1074/jbc.M113.505057

Zhang, Y., Marsboom, G., Toth, P. T., & Rehman, J. (2013). Mitochondrial respiration regulates adipogenic differentiation of human mesenchymal stem cells. *PloS one*, *8*(10), e77077. doi:10.1371/journal.pone.0077077

Zhong, Z., Wen, Z., & Darnell, J. E. (1994). Stat3: a STAT family member activated by tyrosine phosphorylation in response to epidermal growth factor and interleukin-6. *Science (New York, N.Y.)*, *264*(5155), 95–8.

Zhou, P., Qian, L., D'Aurelio, M., Cho, S., Wang, G., Manfredi, G., … Iadecola, C. (2012). Prohibitin reduces mitochondrial free radical production and protects brain cells from different injury modalities. *The Journal of neuroscience : the official journal of the Society for Neuroscience*, *32*(2), 583–92. doi:10.1523/JNEUROSCI.2849-11.2012

Chapter 8: Appendix

A1. Mycoplasma detection protocols

*Mycoplasma*s were tested for using immunofluorescent microscopy and amplification of a fragment of the 16S rRNA gene.

A1.1 Detection via PCR

Isolation of DNA by boiling cells

- A T25 flask of cells was trypsinized (approximately 280 000 cells)
- Trypsinization was then inhibited by adding media
- Cells were transferred to an Eppendorf tube in TE buffer
- Centrifuged @ 2000 rpm for 2 minutes.
- Cells were resuspended in 50 µl of TE buffer
- Samples were then boiled in a kettle for 15 minutes to lyse the cells
- Samples was then used in the PCR reaction as template DNA.

The size of the PCR product of *Mycoplasma* contaminated cells is approximately 270 bp.

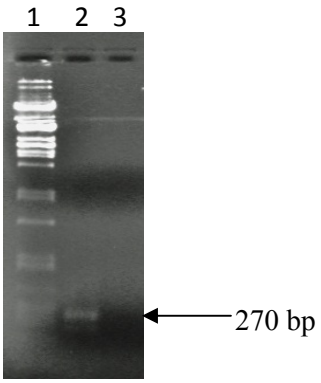

Figure A1.1.1: *Mycoplasma* contamination PCR test. Lane1: Marker; Lane 2: positive PCR test for *Mycoplasma;* Lane3: Negative test for *Mycoplasma*.

A1.2 Detection via immunofluorescent microscopy

- Seed cells and grow on sterile glass cover slips overnight at 37 °C
- Remove media, and wash with PBS
- Fix cells with ice cold methanol
- Dip cover slip into Hoechst 33342 (1:1000 dilution in sterile water) for 15 seconds
- Leave cover slip to dry on paper towel
- Mount cover slip onto glass slide with mounting medium and seal with nail varnish

Negative detection:

Clean blue nuclei without any other speckled staining.

Positive detection:

Blue specks (nuclear staining) around and on top of the area on the cytoplasm (Figure A1).

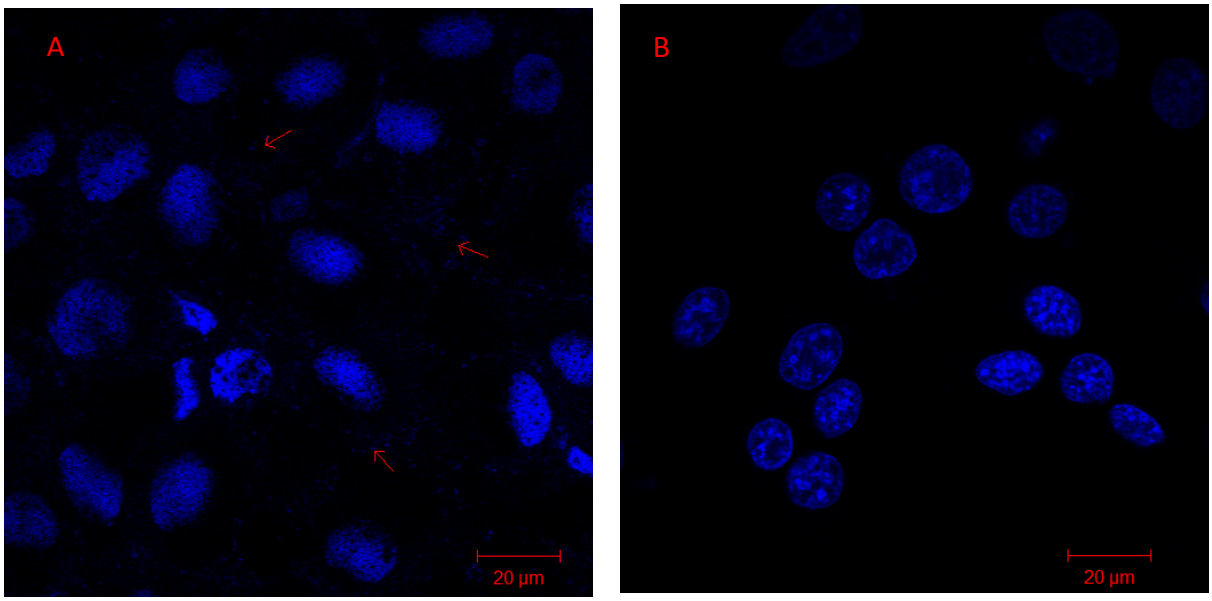

Figure A1.2.1: *Mycoplasma* detection by immunefluorescence analysis. (A) Positive *Mycoplasma* detection (blue specks). **(B)** Negative *Mycoplasma* detection

A2. Determination of IC50 values of S31-201 and PD0325901 using the ACEA xCELLigence RTCA SP System

3T3-L1 cells were seeded onto the xCELLigence systme as previously described and allowed to equilibrate for a minimum of 48 hours. Quadruplicate sets of wells were then treated with PD0325901 at final concentration of either 10, 20, 30, 40, 50 or 60 nM. Cells were incubated in the presence of the inhibitor for 4 days. Using the xCELLigence RTCE software, IC50 values were determined as illustrated in Figure A2.1

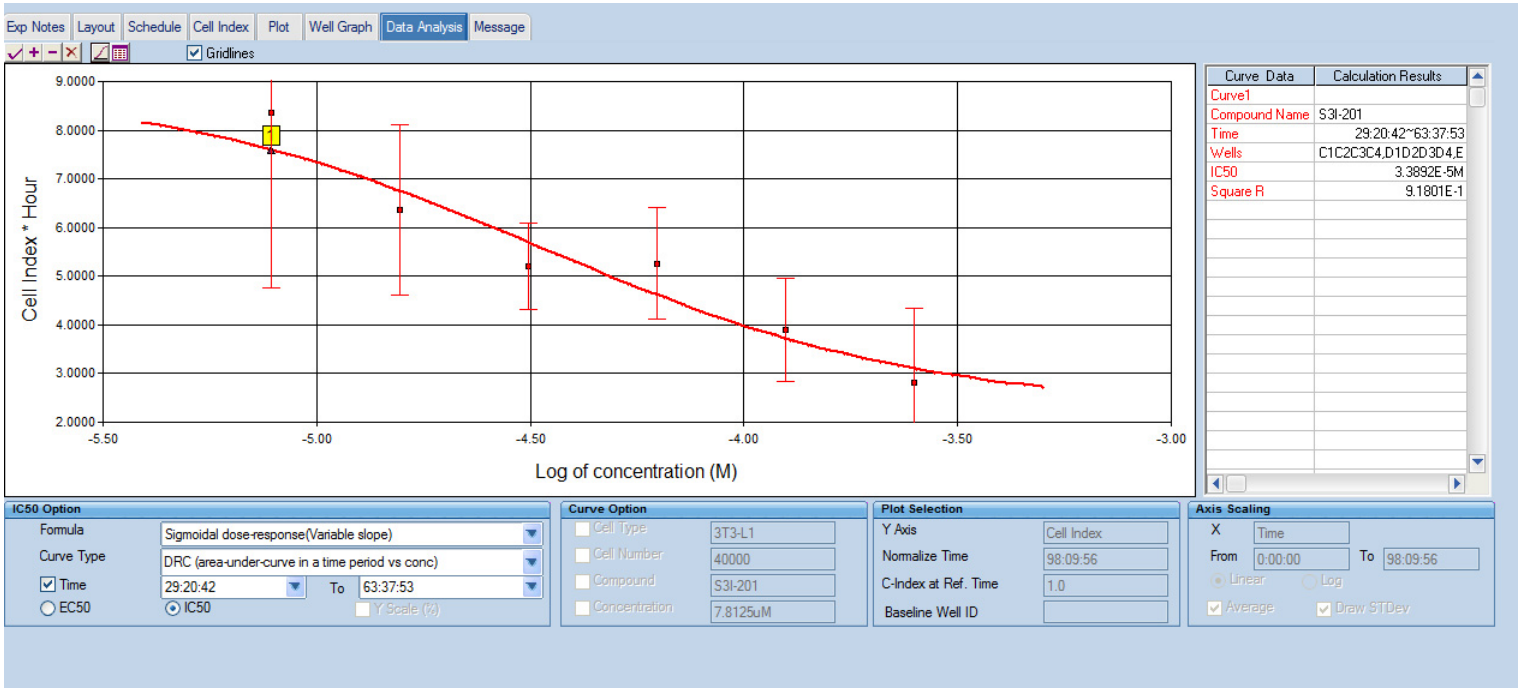

Figure A2.1: Screenshot of the xCELLigence RTCA software used to determine the IC50 value of PD0325901 in 3T3-L1 preadipocytes

A similar experiment was set up to determine the IC50 value of S31-201 in 3T3-L1 preadipocytes. 3T3-L1 cells were seeded onto the xCELLigence systme as previously described and allowed to equilibrate for a minimum of 48 hours. Quadruplicate sets of wells were then treated with S31-201 at final concentration of either 7.81, 15.62. 31.25, 62.50. 125

or 250 µM. Cells were incubated in the presence of the inhibitor for 4 days. Using the xCELLigence RTCE software, IC50 values were determined as illustrated in Figure A2.2

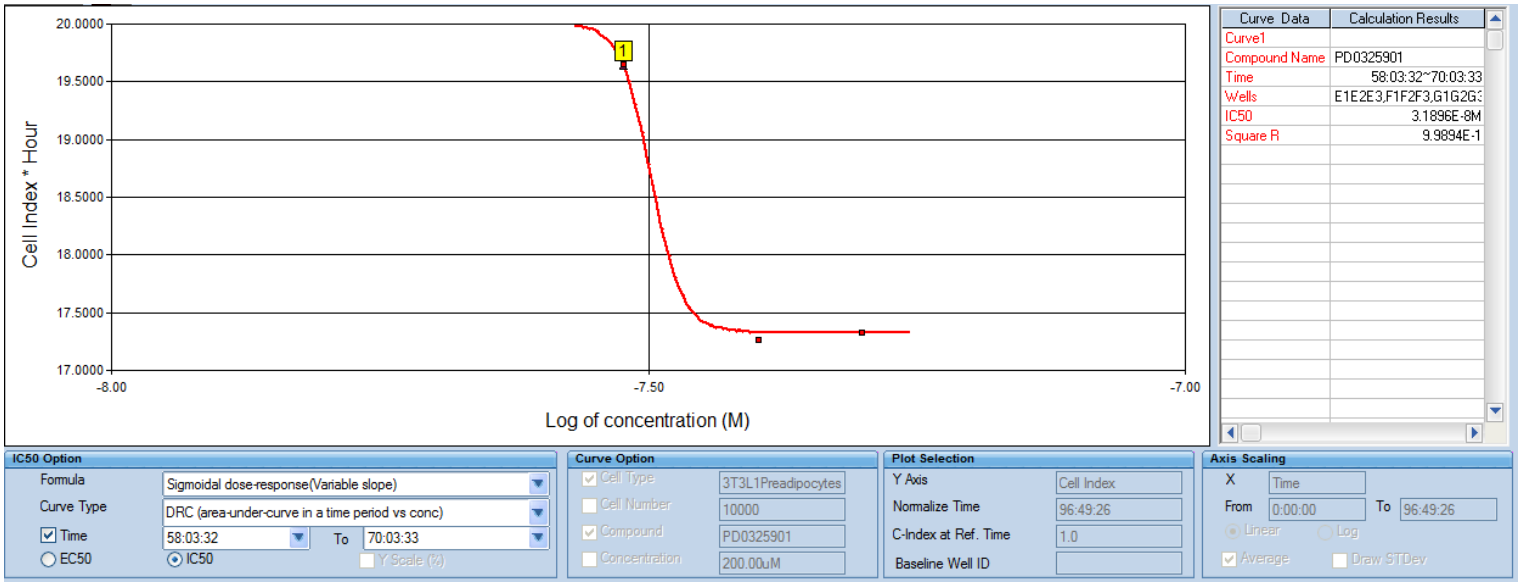

Figure A2.2: Screenshot of the xCELLigence RTCA software used to determine the IC50 value of S31-201 in 3T3-L1 preadipocytse

A3: Kramer A.H, Joos-Vandewalle J., Edkins AL., Frost CL., Prinsloo E., Real-time monitoring of 3T3-L1 preadipocyte differentiation using a commercially available electric cell-substrate impedance sensor system., Biochem. Biophys. Res. Commun. (2014) 1–6.

Biochemical and Biophysical Research Communications 443 (2014) 1245–1250

Contents lists available at ScienceDirect

Biochemical and Biophysical Research Communications

journal homepage: www.elsevier.com/locate/ybbrc

Real-time monitoring of 3T3-L1 preadipocyte differentiation using a commercially available electric cell-substrate impedance sensor system

Adam H. Kramer [a,1], Julia Joos-Vandewalle [a,1], Adrienne L. Edkins [a], Carminita L. Frost [b], Earl Prinsloo [a,*]

[a] Biomedical Biotechnology Research Unit, Department of Biochemistry, Microbiology and Biotechnology, PO Box 94, Rhodes University, Grahamstown 6140, South Africa
[b] Department of Biochemistry and Microbiology, PO Box 77000, Nelson Mandela Metropolitan University, Port Elizabeth 6031, South Africa

ARTICLE INFO

Article history:
Received 18 December 2013
Available online 3 January 2014

Keywords:
3T3-L1 cells
Adipogenesis
Real-time analysis
Impedance

ABSTRACT

Real-time analysis offers multiple benefits over traditional end point assays. Here, we present a method of monitoring the optimisation of the growth and differentiation of murine 3T3-L1 preadipocytes to adipocytes using the commercially available ACEA xCELLigence Real-Time Cell Analyser Single Plate (RTCA SP) system. Our findings indicate that the ACEA xCELLigence RTCA SP can reproducibly monitor the primary morphological changes in pre- and post-confluent 3T3-L1 fibroblasts induced to differentiate using insulin, dexamethasone, 3-isobutyl-1-methylxanthine and rosiglitazone; and may be a viable primary method of screening compounds for adipogenic factors.

1. Introduction

Label-free live cell monitoring provides an unhindered real-time view of whole cell biology. Real-time monitoring of adipogenesis using electric cell substrate impedance and capacitance based biosensor platforms have been reported for adipogenic human mesenchymal stem cells [1] and the mouse preadipocyte 3T3-L1 model [2], respectively.

In the capacitance based sensor developed by Lee et al. [2] cells were placed between two electrodes and the change in the dielectric constant (ε) was measured. This value is directly proportional to capacitance and is dependent on cell size, cell membrane potential and cellular content [3] making capacitance based sensors ideal to measure the differentiation of cells where gross cellular accumulation or novel biogenesis occurs; case in point, lipid accumulation during adipogenesis. However, lipid accumulation is but one property that can be measured to monitor adipogenesis. The morphology of cells dramatically changes during differentiation processes [4]. These changes in morphology can be measured in real-time using Electric Cell-Substrate Impedance Sensors (ECIS). These impedance based systems measure alternating current impedance differences between a smaller sensing and a larger counter current electrode; adherent cells remain viable and are cultured on the gold sensing electrode thereby passively blocking the current. The electrical impedance which results is registered by the sensor. Impedance is therefore affected by the shape, adhesion, or mobility of the adherent cells [5,6]. Both impedance based and capacitance based biosensors provide insights on what is happening to cells, and ideally an instrument that measures both these parameters would be advantageous.

The 3T3-L1 murine preadipocyte model is viewed as the gold standard to monitor unipotent cell differentiation to mature adipocytes, typically via supplementation with a cocktail of insulin, dexamethasone and 3-isobutyl-1-methylxanthine (INS/DEX/IBMX). The inclusion of the insulin sensitizer, rosiglitazone, has been reported to enhance differentiation [7]. Adipogenesis is typically gauged by end point monitoring by the formation of lipid droplets using Oil Red O staining. As 3T3-L1 differentiation has been shown to be sensitive to cell culture plastics and differentiation cocktail recipes [8], optimization of differentiation protocols through the use of end point assays can be laborious and inaccurate; real-time analysis offers defined benefits for the development of optimal, efficient differentiation protocols. This ultimately leads to more accurate results as a profile of cell growth, arrest or death [9] at any point during the differentiation process can be monitored.

When induced to differentiate, growth-arrested post confluent 3T3-L1 preadipocytes synchronously re-enter the cell cycle and undergo mitotic clonal expansion (MCE), mitotically dividing two to four times before differentiation. The DNA replication process

Abbreviations: INS, insulin; DEX, dexamethasone; IBMX, 3-isobutyl-1-methylxanthine; RTCA, Real-time Cell Analyser; ROSI, rosiglitazone.

* Corresponding author. Fax: +27 466223984.
E-mail address: e.prinsloo@ru.ac.za (E. Prinsloo).

[1] These authors contributed equally to this work.

0006-291X/$ - see front matter © 2013 Elsevier Inc. All rights reserved.
http://dx.doi.org/10.1016/j.bbrc.2013.12.123

during growth is hypothesized to be required to make the promoter/enhancer elements available for the transcription of genes important for adipocyte differentiation [10].

The development of commercial real-time biosensors such as the ACEA xCELLigence Real-time Cell Analyser (RTCA) has revolutionised label-free cell biological analysis, giving more reliable medium to high throughput data regarding, amongst others, cell proliferation, migration [11], compound toxicity [9] and viral cytopathic effects [12]. Here we report the use of the ACEA xCELLigence RTCA Single Plate (SP) system to monitor the primary events of 3T3-L1 differentiation.

Based on published recommendations [7,8] we evaluated the ability of the ACEA xCELLigence RTCA SP to monitor growth and differentiation of 3T3-L1 preadipocytes in real-time in a 96 well assay format. The proprietary 96 well E-plates used in the experiment are designed with gold microelectrode arrays at the base of each well that measure electrical impedance at given time points (Z_i) in relation to a background reading (Z_0) to calculate arbitrary cell index (*CI*) units as:

$$CI = \frac{Z_i - Z_0}{15}$$

The xCELLigence monitoring software records the *CI* values which can be used to calculate theoretical doubling time (as cell density increases, so does *CI*) however as these values are affected by cell properties such as shape, adhesion, and mobility of cells, the system can be used to monitor morphological changes.

2. Methods

2.1. Reagents

Antibodies used in this study included: rabbit polyclonal anti-C/EBPβ IgG (sc-150), goat anti-rabbit IgG-horse radish peroxidase (HRP) (sc-2301) from Santa Cruz Biotechnology, Inc (USA), and AlexFluor® 488 goat anti-rabbit IgG (H + L) from Life Technologies (USA). Hoechst 33342 was provided by Invitrogen (USA), Trypsin/ethylenediaminetetraacetic acid (EDTA), propidium ioide, Dulbecco's Modified Eagles Medium (DMEM), L-glutamine, penicillin/streptomycin/amphotericin B (PSA), dexamethasone (DEX), 3-Isobutyl-1-methylxanthine (IBMX), Rosiglitazone (ROSI), Triton-X and Oil Red O were purchased from Sigma–Aldrich (USA). Fluorescence mounting medium was provided by Dako (USA). Foetal Calf Serum (FCS) was sourced from BioWest (France), insulin (INS) from Novo Nordisk (Denmark) and Clarity Western ECL Substrate from BioRad (USA). Unless stated otherwise, all reagents were of the highest grade and purity available.

2.2. Cell culture

Murine preadipocyte 3T3-L1 cells were routinely maintained in a basal media (DMEM supplemented with 5% (v/v) FCS, 1% (v/v) L-glutamine and 1% (v/v) PSA) in a humidified incubator at 37 °C, in a 5% CO_2 atmosphere and sub-cultured as necessary by routine trypsinization. Cell viability was determined by trypan blue staining. 3T3-L1 preadipocytes were freshly split 24 h prior to experimentation.

2.3. Differentiation of 3T3-L1 preadipocytes

Differentiation of 3T3-L1 cells was based on the protocol by Zebisch et al. [7]. Cells were grown to confluence (Day-2) and maintained in normal growth medium for a further 2 days. Two days post-confluence (Day 0), cells were washed with phosphate buffered saline (PBS, pH 7.4, 16 mM Na_2HPO_4, 2 mM KH_2PO_4, 137 mM NaCl, 3 mM KCl) and fed using adipocyte differentiation media. Differentiation media was composed of basal media supplemented with 10 μg/mL INS, 0.25 μM DEX, 0.5 mM IBMX and 2 μM ROSI. Two days post induction, media was aspirated and cells washed with PBS. Cells were supplemented with maintenance media containing 10 μg/mL INS for days 3–4 and then basal media.

2.4. Real time analysis using the xCELLigence system

The xCELLigence RTCA SP system was initialized, as per manufacturer's instructions, prior to commencement of the experiment by filling all 96 wells of the E-plate with the basal media (100 μL) and equilibrated at room temperature for 30 min. The plate was placed into the single plate (SP) station cradle (housed in a humidified incubator at 37 °C with a 5% CO_2 atmosphere) to establish a background reading. Cells were enumerated by trypan blue staining and plated at 1×10^4 cells per well in 50 μL aliquots in quadruplicate. Cells were allowed to settle for 30 min outside the incubator prior to returning the E-plate to the SP station. Growth was monitored by electrical impedance measurements using the RTCA SP as arbitrary *CI*. Cells were treated with either full differentiation media (as described above) or individual components of differentiation media (at the specified concentrations, as above) at 24, 48 or 60 h post-seeding. Standard differentiation media components, i.e. INS/DEX/IBMX/ROSI were added at 4x strength in 50 μl to account for dilution effects in predetermined wells. Duplicate clear plastic 96 well plates were prepared in the same manner to allow for comparative end-point Oil Red O staining and microscopy.

2.5. Oil Red O Staining

Following the xCELLigence experiment, plates were stained with Oil Red O as described by Ramirez-Zacarias et al. [13] with slight modifications. A working solution was prepared from a filtered 0.5% (w/v) stock solution with distilled water to a final concentration of 0.3% (w/v). Briefly, medium was discarded and cells were washed in PBS. Cells were then incubated for 5 min in 10% (v/v) formalin at room temperature after which fresh formalin was added and incubated at room temperature for a further hour. The plate was wrapped in parafilm and tinfoil to prevent drying. The formalin was removed and wells were washed with 60% (v/v) isopropanol. Wells were allowed to dry completely before the addition of Oil Red O working solution. The plate was incubated at room temperature for 10 min before removing the stain and washing repeatedly with sterile distilled water. Cells were viewed at 20× magnification (UOP BSZ500X Inverted microscope) under brightfield conditions, ScopePhoto 3.1 (ScopeTek) was used to capture images.

2.6. Cell cycle analysis

Pre-confluent and 2 days post confluent 3T3-L1 cells (as judged by light microscopy) were collected via trypsinization. Cells were stained with propidium iodide in the presence of RNAse as specified by Nunez [14]. After doublet discrimination gating to exclude cell aggregates, DNA content as a measure of PI fluorescence was detected by excitation with the blue laser at 488 nm and emission detected in the 610/20 channel flow cytometry using a Becton Dickson FACS Aria II flow cytometer. Cell cycle analysis was performed using FCSExpress 4 (De Novo Software) using built in cell cycle models.

2.7. Immunofluorescence staining

Cells were grown on borosilicate glass coverslips in 6 well culture plates (Nunclon™, Nunc). Following differentiation

treatments, cells were subjected to immunofluorescence staining. Medium was aspirated, and the cells were washed with PBS (3 × 10 min), before fixation for 30 min using a 4% (v/v) formaldehyde solution. Following fixation, cells were washed with PBS. Cells were then permeabilized for 5 min with 0.1% Triton X-100 (v/v) solution and washed with PBS (3 × 10 min). Coverslips were blocked for a minimum of 1 h at room temperature using a 1% (w/v) BSA/PBS solution. Coverslips were incubated with rabbit anti-C/EBPβ (1:500 dilution in 1% BSA/PBS) overnight at 4 °C. Thereafter the antibody solution was aspirated and coverslips washed with 1% BSA/PBS solution. Coverslips were incubated with AlexFluor® 488 goat anti-rabbit IgG (1:2000 dilution in 1% BSA/PBS) in the dark at room temperature for an hour before and finally washed with a 1% BSA/PBS solution (3 × 10 min). Hoechst 33342 solution (1:1000 in water) was used to stain nuclear material. The cover slips were dried before mounting with fluorescence mounting medium. Fluorophore labelled secondary antibody only staining was used as a control. Images were captured using the Zeiss AxioVert.A1 FL-LED Fluorescence Microscope and analysed using Zen Blue Microscope Software (Zeiss).

2.8. Western blot analysis

Cells were harvested and enumerated by trypan blue staining. Equal numbers of cells were lysed in Laemmli sample buffer supplemented with 5% (v/v) β-mercaptethanol (BioRad) at 95 °C for 10 min. Following SDS–PAGE electrophoresis [15] and transfer onto PVDF filter membranes (BioRad), membranes were blocked for 1 h at room temperature with 5% (w/v) skim milk in a TBS-Tween 20 (0.8% (w/v) NaCl, 0.24% (w/v) 1% (w/v) Tween-20) Tris, pH 7.6) buffer. Blocking was followed by an overnight incubation at 4 °C in rabbit anti-C/EBPβ (1:1000). The membrane was washed with TBS-T (3 × 15 min) and incubated with anti-rabbit-HRP (1:5000) for 1 h at room temperature. After washing, the membrane was developed with Clarity Western ECL Substrate according to the manufacturer's instructions. Images were captured using the UVTec UVIPro System.

Unless noted otherwise all experiments were performed in triplicate ($n = 3$).

3. Results and discussion

3.1. Confirmation of adipogenic initiation

CCAAT/enhanced binding protein β plays a significant role during adipogenesis [10,16]. C/EBPβ localization and levels were monitored by fluorescence microscopy and Western blot analysis to confirm adipogenic initiation upon stimulation with IBMX, dexamethasone, insulin and rosiglitazone (Fig. 1).

It is important to note that C/EBPβ has two major isoforms. It has been shown that isoform expression is differentially regulated at the translational level [17,18]. Isoforms have an expected relative mass of 38 and 18 kDa. Uninduced preadipocytes were shown to have minimal levels of the transcription factor, with a faint band of the larger isoform being observed in the uninduced lysate (Fig. 1A, Day 0 – Lane 1). Western blot analysis indicated that expression of C/EBPβ increased upon differentiation with maximum levels being observed in the first 24 h of differentiation, as observed Day 1 (Fig. 1A). These levels were shown to remain relatively constant for 4 days post induction (Fig. 1A, Days 2–5 – Lanes 3–6), and thereafter slowly started to diminish with minimal levels observed on Day 6 (Fig. 1A, Lane 7) of the sample set.

As expected, prior to the induction of differentiation the localization of C/EBPβ was cytoplasmic, with minimal nuclear staining on the Day 0 (Fig. 1B). The intensity of fluorescence signal in uninduced cells was particularly low. This low signal was expected as the levels of C/EBPβ in preadipocytes is expected to be minimal, as confirmed by Western blot analysis (Fig. 1A, Day 0). C/EBPβ localized to the nucleus (Fig. 1B, Day 1) as expected upon the induction of differentiation. This strong nuclear localization persisted for 48 h post-induction as highlighted in Days 1 and 2, Fig. 1B (red arrows). This nuclear staining was reduced 72 h post-induction. Punctate cytoplasmic structures (Fig. 1B, white arrow) were observed and the majority of cells had lost the nuclear C/EBPβ localization phenotype. Through days 4–6 post-induction the nuclear localization of C/EBPβ became less distinct (Fig. S1).

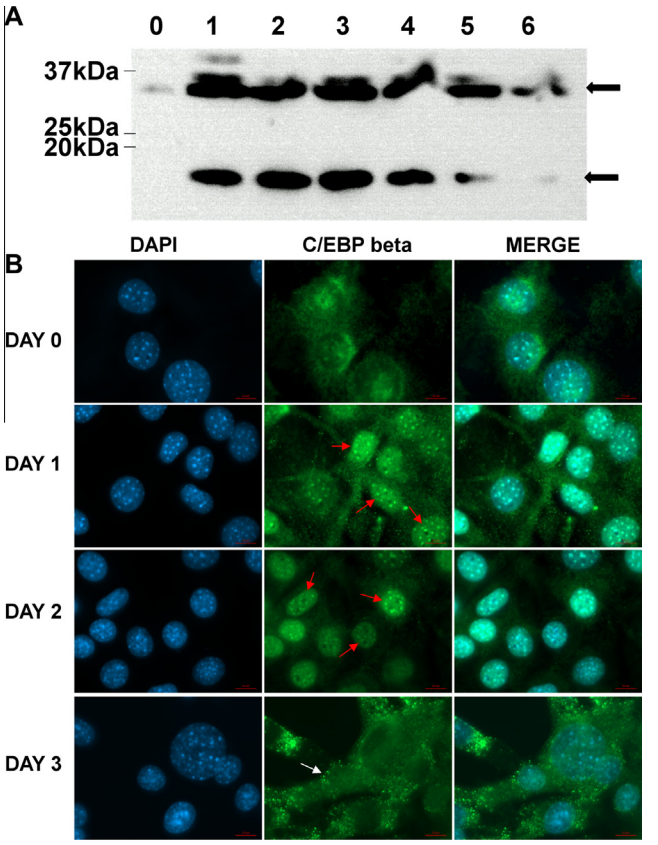

Fig. 1. Expression and localization of C/EBPβ during 3T3-L1 adipocyte differentiation. (A) Western blot analysis of C/EBPβ expression pre- (Day 0) and post- (Days 1–6) induction of adipocyte differentiation. (B) Immunofluorescence analysis of the localization of C/EBPβ through days 1–3 of 3T3-L1 adipocyte differentiation. Red arrows highlight nuclear localized of C/EBPβ during Days 1 and 2 post-induction, the white arrow highlights punctate structures observed on Day 3. Scale bars = 10 μm. (For interpretation of the references to colour in this figure legend, the reader is referred to the web version of this article.)

These results indicate that differentiation of the preadipocytes into adipocytes was occurring in the same manner as reported in literature. Tang and Lane [18] showed that the expression of C/EBPβ occurs rapidly after the induction of differentiation with maximum levels being reached 4 h after induction and maintained for a further 48 h. Levels of C/EBPβ then slowly start to decrease.

3.2. Real time monitoring of differentiation

The ability of the xCELLigence system to measure the adipogenic events following induction of differentiation was investigated. The requirement of cytostaticity (G_0) prior to induction of differentiation is well documented [19–21], and is typically achieved by growing cells to post-confluence. Despite the requirement of post-confluent cells for efficient differentiation it was hypothesized that the xCELLigence system would be able to

measure the morphological changes that accompany the induction of differentiation regardless of the general cell cycle state of the cells.

Cells were seeded at the same density in three separate experiments and induced to differentiate before reaching confluence, 24 h post-seeding (Fig. 2A), upon confluence, 48 h post-seeding (Fig. 2B) and once post-confluent, 60 h post seeding (Fig. 2C) as judged by the gradient of the *CI* curves and calculated doubling times. Analysis of cell cycle distribution by flow cytometry confirmed that pre-confluent cells were actively dividing, with a population found to be in the S phase of the cell cycle (~40%) while post-confluent cells had reached cytostaticity with the majority of the population (>90%) in $G_{0/1}$ as shown in the cell cycle analysis (Fig. 2D and E). Despite the reported requirement for cells to be cytostatic prior to induction of differentiation, the xCELLigence system was able to detect similar *CI* profiles for cells induced to differentiate regardless of their position in the cell cycle.

Mitotic clonal expansion, as it involves active cell growth, should be able to be monitored using the xCELLigence system. However, as shown in Fig. 2, the *CI* curves of cells induced to differentiate rapidly drop as opposed to the expected increase in *CI* values as a result of dividing cells. This dramatic drop was found to be reproducible and is thought to be a characteristic primary event in the *CI* curves of 3T3-L1 cells induced to differentiate. A similar *CI* curve of 3T3-L1 differentiation using the xCELLigence system was achieved by Melloni et al. [22]. The drop in the *CI* values upon induction of differentiation was speculated to be caused by a dramatic change in morphology. Cell death was ruled out as a cause for the drop in *CI* values as *CI* values did not decrease to 0 and cell viability was confirmed by microscopic analysis.

To confirm that these *CI* profiles were not artefacts of a single component of the differentiation cocktail and in fact as a result of the induction of differentiation, cells were individually treated with each of the components making up the differentiation cocktail. Each component plays a role in activation of the factors required for adipogenesis: Insulin acts through the insulin-like growth factor receptor (IGF-1). Activation of IGF-1 results in an increase of cyclic adenosine monophosphate (cAMP). Levels of cAMP are further increased through the activation of glucocorticoid pathways by glucocorticoids such as dexamethasone. The cAMP phosphodiesterase inhibitor, IBMX is used to further increase levels of cAMP. Cyclic AMP and IBMX decrease levels of Specificity protein 1 (Sp1), a transcription factor which represses the C/EBPα promoter [21]. To improve efficiency of differentiation, the insulin sensitizer and peroxisome proliferator-activated receptor γ (PPARγ) (another key adipogenic factor) agonist, rosiglitazone, has been included in the cocktail [7].

Cells treated with DMSO (0.3%), solvent controls (Fig. 3A), had minimal effect on the *CI* curve and growth of 3T3-L1 cells, while samples treated with full differentiation media resulted in the expected drop in the *CI* curve, as illustrated in Fig 3B. Both insulin (Fig. 3C) treatment and dexamethasone (Fig. 3D) treatment resulted in significantly altered *CI* profiles, while treatment with rosiglitazone (Fig. 3F) had no measurable effect, Treatment with IBMX (Fig. 3E) resulted in a *CI* profile similar to cells treated with the full differentiation cocktail. Interestingly, individual treatment of the cells with insulin, dexamethasone or IBMX resulted in an increased nuclear C/EBPβ localization (Fig. S2) however only IBMX treated cells resulted in a reduction of *CI* values comparable, but not identical, to the full differentiation *CI* profile as shown in Fig. 3G. This characteristic drop in *CI* values was unexpected, as upon induction of differentiation, cells are reported to re-enter the cell cycle and undergo active growth [10]. As the xCELLigence system is an impedance based sensor the dramatic reduction in *CI* values were hypothesized to be as a result of a morphological change in the cells. To illustrate that preadipocytes and differentiated adipocytes (Fig. 3H) are completely different cell phenotypes, in terms of cell type, cell size, cell shape and cell property, both preadipocytes and

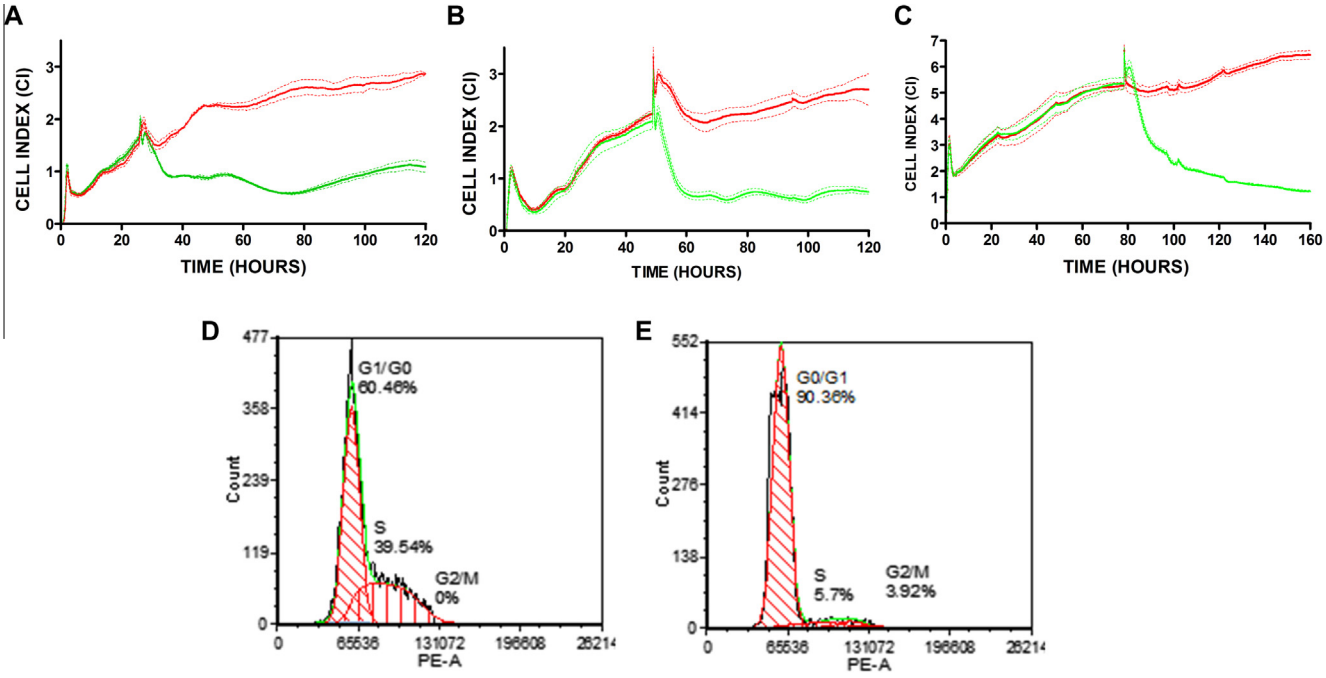

Fig. 2. The effect of confluency on the ability to detect differentiation events. (A–C): *CI* versus time curves of 3T3-L1 preadipocytes induced to differentiate at (A) pre-confluent (doubling time of 14.6 ± 0.58 h), (B) confluent (doubling time of 44.8 ± 0.6 h) and (C) post-confluent (doubling time of 283.6 ± 10.23 h) points as judged by the doubling times calculated 20 h pre-induction. Red curves indicate uninduced samples while green curves indicate samples induced to differentiate at points indicated by red vertical lines. Curves were plotted as an average of quadruplicate treatments. (D) Cell cycle analysis of pre-confluent and (E) post-confluent 3T3-L1 cells, as judged by light microscopy. Error bars show standard deviation ($n = 3$). (For interpretation of the references to colour in this figure legend, the reader is referred to the web version of this article.)

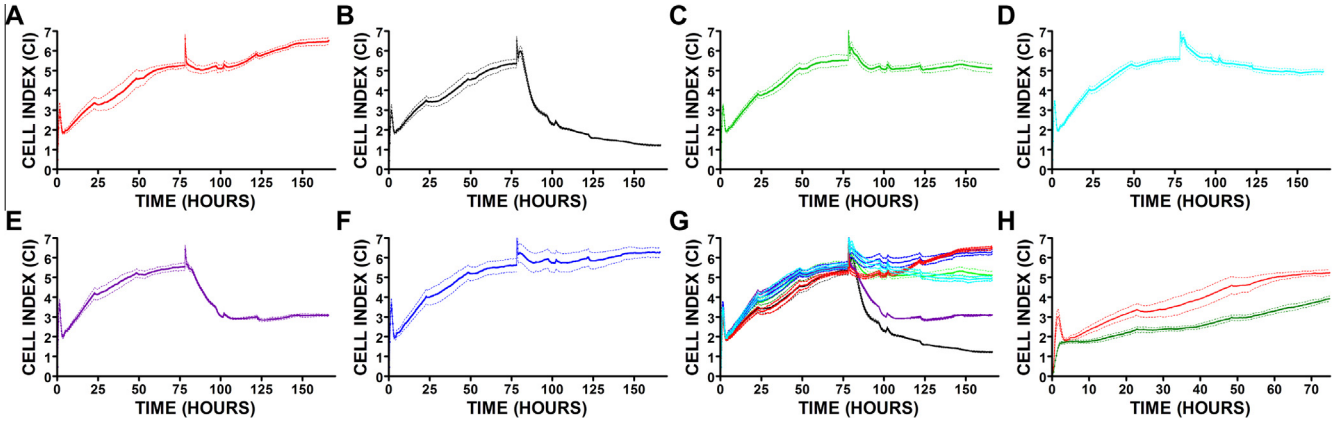

Fig. 3. Effects of individual components of differentiation cocktail on 3T3-L1 growth *CI* curves. Cells were treated at the same time with: (A) DMSO (control), (B) Differentiation cocktail (INS/DEX/IBMX/ROSI), (C) Insulin, (D) Dexamethasone, (E) IBMX, and (F) Rosiglitazone. (H) Preadipocytes (red) and differentiated adipocytes (green) were seeded at the same density to compare the resulting *CI* growth curves. All curves were plotted as an average of quadruplicate treatments. Error bars show standard deviation ($n = 3$). (For interpretation of the references to colour in this figure legend, the reader is referred to the web version of this article.)

14 days old differentiated adipocytes were plated at the same density onto the xCELLigence system and growth monitored and compared. As expected, the 2 cell types had different *CI* profiles as shown in Fig. 3H. Interestingly, adipocytes had lost the distinctive *CI* peak directly after plating the cells. This peak was routinely observed when plating preadipocytes on the system. Differentiated adipocytes had much lower *CI* values, and, as analysed using the xCELLigence software, grow much more slowly. Doubling time was calculated between 5 and 22 h post-seeding as illustrated in Fig. 3H. Adipocytes were found to have a doubling time of 37 ± 1.06 h while that of the preadipocyte progenitors were found to have a doubling time of 21.6 ± 3.28 h. Lower *CI* values further indicate that adipocytes are not as adherent as their fibroblast-like progenitors.

Fully differentiated 3T3-L1 cells (Fig. 4A) are typically rounded and have large lipid droplets, distinct from 3T3-L1 preadipocytes (Fig. 4B). However, microscopic analysis confirmed cells had adopted a spindle like morphology upon treatment with either full differentiation cocktail (Fig. 4C) or IBMX (Fig. 4F). This spindle shaped morphology was observed for approximately 48 h post induction, following which the cells become more characteristically rounded and accumulate lipid droplets. This morphological change seems to be a characteristic primary event in 3T3-L1 differentiation and may be a useful measurement for the screening of pro- or anti-adipogenic compounds. The individual treatment with insulin (Fig 4D) had minimal effect on the accumulation of lipid droplets, while treatment with dexamethasone (Fig. 4E), IBMX (Fig. 4F) or rosiglitazone (Fig. 4G) resulted in an increase in the accumulation of lipids. However, this was not measured by the xCELLigence system. This is expected as the system measures impedance and is therefore only able to measure changes as a result of cell size, morphology and membrane potential and not changes as a result of composition of cells.

We speculate, based on the *CI* curves resulting from the treatment of 3T3-L1 cells that IBMX is critical in allowing the induction of efficient differentiation and measurable associated primary morphological changes. As an aside, it has been reported that increased levels of cAMP lead to a spindle, fibroblast morphology in Chinese Hamster Ovary (CHO) cells [23]. We have utilized the ACEA xCELLigence RTCA SP system to successfully monitor the primary morphological changes that occur during 3T3-L1 adipocyte differentiation and successfully identified the instigating compound, IBMX, which causes this morphological change. In contrast, and in a sense in combination, to already established end point

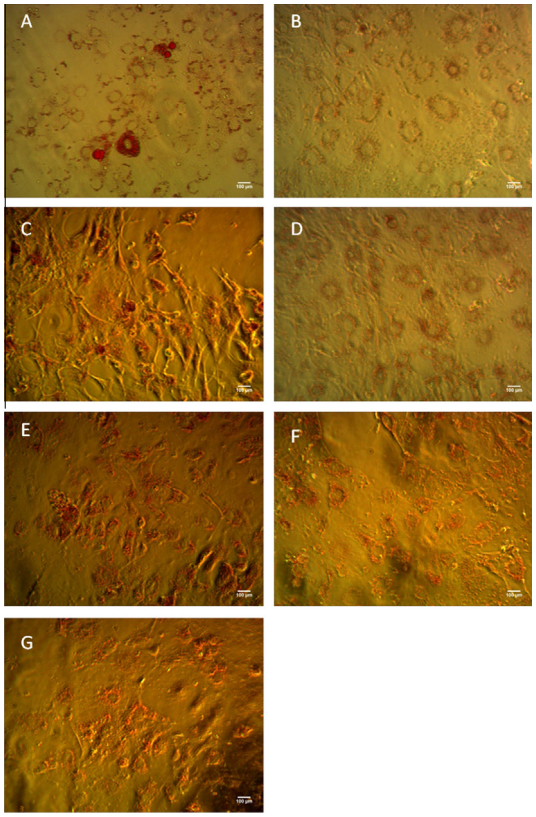

Fig. 4. Oil Red O staining of xCELLigence samples. (A) Terminally differentiated 3T3-L1 adipocytes. Preadipocytes treated with: (B) DMSO (control), (C) Differentiation cocktail, (D) Insulin, (E) Dexamethasone, (F) IBMX, or (G) Rosiglitazone Media. Scale bars = 100 μm, 200× magnification.

assays such as Oil Red O staining, immunofluorescence microscopy and Western blot analysis, real-time label-free monitoring provides a powerful non-invasive tool to streamline development of differentiation protocols.

By defining distinct *CI* profiles for cells with the potential to differentiate and undergo morphological shifts, impedance based real-time cell analysis can be used as an initial medium to high throughput screen for chemical morphogens which may have pro- or anti-differentiation activities.

Acknowledgments

The authors acknowledge the National Research Foundation (NRF), Department of Science and Technology (DST), the Medical Research Council (MRC), the Kresge Foundation and Rhodes University for funding and www.somersault1824.com for their Library of Science Illustrations. The ACEA xCELLigence RTCA SP was purchased under the NRF/DST National Nanotechnology Equipment Programme. AHK is a recipient of a NRF Scarce Skills Scholarship and JJVW is a recipient of a MRC Scholarship.

Appendix A. Supplementary data

Supplementary data associated with this article can be found, in the online version, at http://dx.doi.org/10.1016/j.bbrc.2013.12.123.

References

[1] P.O. Bagnaninchi, N. Drummond, Real-time label-free monitoring of adipose-derived stem cell differentiation with electric cell-substrate impedance sensing, Proc. Natl. Acad. Sci. USA 108 (2011) 6462–6467.
[2] R. Lee, I. Jung, M. Park, H. Ha, K.H. Yoo, Real-time monitoring of adipocyte differentiation using a capacitance sensor array, Lab Chip 13 (2013) 3410–3416.
[3] R. Lee, J. Kim, S.Y. Kim, S.M. Jang, S.-M. Lee, I.-H. Choi, et al., Capacitance-based assay for real-time monitoring of endocytosis and cell viability, Lab Chip 12 (2012) 2377–2384.
[4] J.Y. Fan, J.L. Carpentier, E. van Obberghen, C. Grunfeld, P. Gorden, L. Orci, Morphological changes of the 3T3-L1 fibroblast plasma membrane upon differentiation to the adipocyte form, J. Cell Sci. 61 (1983) 219–230.
[5] R. Pethig, Dielectric properties of biological materials: biophysical and medical applications, IEEE Trans. Electr. Insul. EI-19 (1984) 453–474.
[6] M. Tirado, C. Grosse, W. Schraderm, U. Kaatza, Broad frequency range dielectric spectroscopy of aqueous suspensions of phospholipid vesicles, J. Non Cryst. Solids 305 (2002) 373–378.
[7] K. Zebisch, V. Voigt, M. Wabitsch, M. Brandsch, Protocol for effective differentiation of 3T3-L1 cells to adipocytes, Anal. Biochem. 425 (2012) 88–90.
[8] A. Mehra, I. Macdonald, T.S. Pillay, Variability in 3T3-L1 adipocyte differentiation depending on cell culture dish, Anal. Biochem. 362 (2007) 281–283.
[9] S. Kustermann, F. Boess, A. Buness, M. Schmitz, M. Watzele, T. Weiser, et al., A label-free, impedance-based real time assay to identify drug-induced toxicities and differentiate cytostatic from cytotoxic effects, Toxicol. In Vitro 27 (2013) 1589–1595.
[10] P. Cornelius, O.A. MacDougald, M.D. Lane, Regulation of adipocyte development, Annu. Rev. Nutr. 14 (1994) 99–129.
[11] R. Limame, A. Wouters, B. Pauwels, E. Fransen, M. Peeters, F. Lardon, et al., Comparative analysis of dynamic cell viability, migration and invasion assessments by novel real-time technology and classic endpoint assays, PLoS ONE 7 (2012) e46536.
[12] Y.-W. Tang, C.W. Stratton (Eds.), Advanced Techniques in Diagnostic Microbiology, Springer, US, Boston, MA, 2013.
[13] J.L. Ramirez-Zacarias, F. Castro-Munozledo, W. Kuri-Harcuch, Quantification od adipose conversion and triglycerides by staining intracytoplasmic lipids with Oil red O, Histochemistry 97 (1992) 493–497.
[14] R. Nunez, DNA measurement and cell cycle analysis by flow cytometry, Curr. Issues Mol. Biol. 3 (2001) 67–70.
[15] U.K. Laemmli, Cleavage of structural proteins during the assembly of the head of bacteriophage T4, Nature 227 (1970) 680–685.
[16] Q.-Q. Tang, T.C. Otto, M.D. Lane, Mitotic clonal expansion: a synchronous process required for adipogenesis, Proc. Natl. Acad. Sci. USA 100 (2003) 44–49.
[17] M.H. Kim, J. Fields, J. Field, Translationally regulated C/EBP beta isoform expression upregulates metastatic genes in hormone-independent prostate cancer cells, Prostate 68 (2008) 1362–1371.
[18] Q.Q. Tang, M.D. Lane, Activation and centromeric localization of CCAAT/enhancer-binding proteins during the mitotic clonal expansion of adipocyte differentiation, Genes Dev. 13 (1999) 2231–2241.
[19] Z. Cao, H. Yang, L. Kong, D. Gu, Z. He, Z. Xu, et al., Growth arrest induction of 3T3-L1 preadipocytes by serum starvation and their differentiation by the hormonal adipogenic cocktail, J. Cell Anim. Biol. 6 (2012) 57–65.
[20] Y.M. Patel, M.D. Lane, Mitotic clonal expansion during preadipocyte differentiation: calpain-mediated turnover of p27, J. Biol. Chem. 275 (2000) 17653–17660.
[21] J.M. Ntambi, Y. Kim, Adipocyte differentiation and gene expression, Am. Soc. Nutr. Sci. (2000) 3122–3126.
[22] E. Melloni, G. Zauli, C. Celeghini, I. Volpi, P. Secchiero, Release of a specific set of proinflammatory adipokines by differentiating 3T3-L1 cells, Nutrition 29 (2013) 332–337.
[23] A. Hsie, K. Kawashima, J. O'Niell, C. Shroder, Possible role of adenosine cyclic 3′: 5-monophasphate phosphodiesterase in the morphological transformation of chinese hamster ovary cells mediatied by N6, O2′-dibutyryl adenosine cyclic 3′: 5-monophasphate, J. Biol. Chem. 250 (1975) 984–989.